Assessment of system behaviour of prestressed concrete girder bridges using staggered 2D Non-Linear Finite Element Approach

Sneha Kasturi Rangan

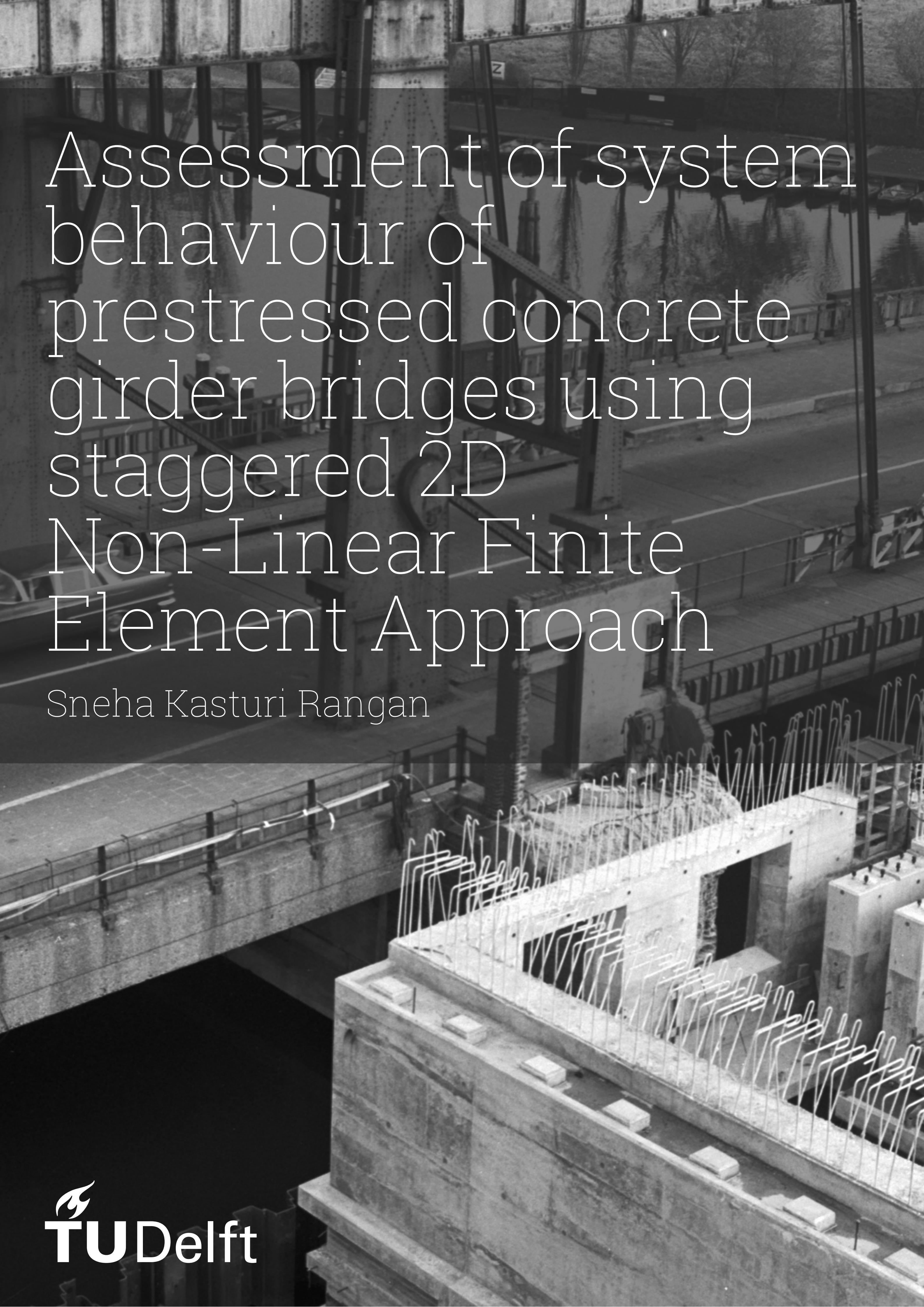

TU Delft

Assessment of system behaviour of prestressed concrete girder bridges using staggered 2D Non-Linear Finite Element Approach

by

Sneha Kasturi Rangan

Student Number
5771285

Graduation committee

Prof.dr.ir. M.A.N. (Max) Hendriks
Chairperson, Delft University of Technology

Dr.ir. E.O.L. (Eva) Lantsoght
Supervisor, Universidad San Francisco de Quito

Ir. N.W. (Niels) Kostense
Supervisor, Delft University of Technology

Ir. J. (Jasper) Doorgeest
Supervisor, Rijkswaterstaat

Date: July 13, 2024

TU Delft

Acknowledgement

It is a bittersweet feeling to write this acknowledgment as it marks the conclusion of my master's studies at TU Delft. My time in the Netherlands has been truly wonderful, and my journey at TU Delft has been fun, challenging and deeply memorable. I feel grateful to have met such loving and inspiring people from all around the world.

First and foremost, I would like to thank my chair Max Hendriks for being the most supportive and encouraging throughout my thesis. His office door was always open for me to seek help, and I deeply appreciate the effort he made to accommodate me in his busy schedule and address all my doubts. I will cherish all our conversations.
I am grateful to Niels Kostense for his valuable assistance in finite element modeling, particularly in resolving the challenges I faced in my thesis. Thank you for sharing your insights and experience with me.
I extend my thanks to Eva Lantsoght for her expertise in theoretical aspects of bridge testing, her help in improving my writing skills and for being very supportive. Finally, thanks to Jasper Doorgeest who made me think from a different perspective and readily answering my doubts.

A heartfelt thanks to my friends who made the Netherlands feel like a second home. I will never forget our wonderful times together: from watching movies and playing Mario Kart during lecture breaks, to purposeless walks amidst deadlines, countless coffee and lunch breaks, study sessions, dinners, and travels. I will dearly miss our time together.

The most important people to thank are my parents for always believing in me and supporting me endlessly. I wouldn't have made it this far without your love and support.
அம்மா அப்பா நீங்கள் எனக்காக செய்த அனைத்திற்கும் நன்றி.

Sneha Kasturi Rangan
Delft, July 2024

Contents

Abstract

There are about 70 prestressed concrete T-beam girder bridges built between 1953 and 1970 in the Netherlands. Ensuring the safety of these existing bridges under current traffic conditions is imperative. Upon initial assessment of these existing prestressed concrete T-girder bridges, half of them didn't meet the safety requirement specified by the design code even though they didn't show any sign of distress during inspection. This is because the system behaviour of the T-girder bridges (i.e.) load transfer mechanisms such as CMA (compressive Membrane Action) and load redistribution were not considered, which could potentially increase the calculated strength capacity of these existing bridges. Therefore, a computationally efficient method for evaluating these bridges is needed. This research addresses the challenge of accurately predicting the strength capacity of prestressed concrete T-girder bridges using a computationally efficient approach.

The study involves modelling the 2D bridge deck in the horizontal plane using orthotropic plate elements and 2D individual girders in the vertical plane with non-linear material properties. The 2D bridge model was compared with a 3D linear bridge deck model, showing a variation in bending moment between 10% to 13%, sufficient for studying load effects. The 2D individual girder model built was validated using experimental data of the disconnected T-beam test of the Vecht Bridge, incorporating a quasi-Newton solution method with the Broyden-Fletcher-Goldfarb-Shanno (BFGS) algorithm. The predicted load versus deflection curve from the 2D non-linear individual girder model closely followed the load versus deflection curve obtained from the experimental test results.

To combine the 2D bridge deck model with the 2D non-linear individual girder model, an equivalent loading technique was developed by numerically solving the shear force distribution of the critical girder in the 2D bridge deck model. The staggered 2D Non-Linear Finite Element Approach developed utilising the equivalent loading technique accurately predicted the ultimate failure load of the connected T-beams (system behavior) within 10% of experimental values, despite neglecting the effect of end crossbeams.

The 2D bridge deck model without considering crossbeam effects showed conservative stiffness estimates. Crossbeam inclusion in the model indicated significant improvements in stiffness, load distribution and redistribution.

The 3D non-linear finite element model predicted 87% to 95% of the failure load of the connected T-beam tests [10]. The 2D non-linear individual girder model using the staggered non-linear approach predicted up to 96.5% of the ultimate failure load of the connected T-beam test, achieving this with a run time of approximately 18 to 21 minutes. Overall, the staggered 2D Non-Linear Finite Element Approach developed shows promise for preliminary bridge safety assessments offering a balance between computational efficiency and accurate prediction of strength capacity.

1
Introduction

1.1. Background

Many of the bridges made of prefabricated prestressed concrete beams were built shortly after WWII. Consequently, the bridges built in the early period are reaching their end of theoretical service life. The main question to answer is whether these bridges are structurally safe to withstand today's traffic conditions. The road traffic has seen significant increases in both numbers and axle loads since these bridges were built. These changes have prompted revisions to the design codes in the Netherlands over the last 80 years [16]. Even if the bridges don't show any signs of distress, it is important to assess the conditions to current needs such as increased traffic demands and deficiencies related to shear resistance.
In the Netherlands, there are about 70 prestressed T-beam bridges with cast-in situ decks built between 1953-1977 that are still present in service today [10], see Figure 1.1 for the typical cross-section of prestressed T-beam concrete bridges.

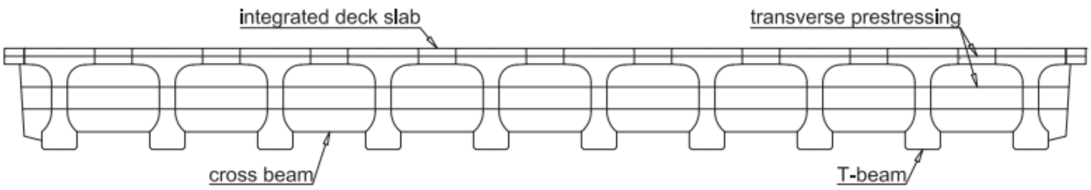

Figure 1.1: Typical cross-section of pre-stressed concrete T-beam bridge [10]

There's an increasing need to use an accurate technique to assess the existing bridges. There is also a discrepancy in checking the safety of the bridge since the system behaviour of the bridge is not taken into account. Consequently, the loading capacity of the prestressed T-beam bridge is severely underestimated. From research [3], it is observed that integrated deck slabs with transverse prestressing can withstand higher load capacities due to the effect of arching action, also known as Compressive Membrane Action (CMA). Arching action or CMA is activated when a load is applied directly to the T-beam or when the slab begins to bend after cracking has initiated in the concrete. The horizontal movement (lateral direction) of the slab is restricted by adjacent T-beams, and longitudinal movement is restricted by crossbeams, inducing compressive membrane forces. This results in the deck slab not being the governing section for failure, but rather the T-beam. Arching action substantially increases the strength capacity of prestressed concrete T-beam bridges, a phenomenon referred to as the system behavior in prestressed concrete T-beam bridges. This thesis focuses on assessing the load-carrying capacity of prestressed concrete girder bridges by considering system behavior like compressive membrane action (CMA), and load distribution and redistribution between connected T-girders using a simplified 2D Non-Linear Finite Element Approach.

1.2. Research Questions

The main research question that will be answered in this thesis:

"How can we use a simplified 2D Non–Linear Finite Element Approach using a 2D individual girder model and a 2D bridge deck model to verify the capacity of prestressed concrete girder bridges that represent a full bridge system; avoiding computationally costly 3D Finite Element models?"

To answer the main question, the following sub-questions are answered in the process:

1. How can we model the integrated deck slab in the 2D horizontal plane? How can we incorporate the change in stiffness in longitudinal and transverse direction due to the presence of cross beams and integrated slab deck?
2. How can we model an individual T-beam girder, with material Non-linearity in the 2D vertical plane?
3. How can we connect the 2D bridge deck in the horizontal plane and 2D single beam girder in the vertical plane in such a way that the resistance of a single T-beam correlates to the system behaviour of connected T-beams?

1.3. Research scope

The focus of this research is to develop a simple 2D Non-Linear Finite Element Approach to predict the strength capacity of existing prestressed concrete T-girder bridges, taking into account system behavior. For this purpose, two Finite Element Models are built: 2D linear bridge deck model in the horizontal plane and 2D non-linear individual girder model in the vertical plane. The 2D bridge deck is purely for studying the load effects. Subsequently, an equivalent loading that can be applied on the non-linear individual girder which can predict the full strength capacity of the bridge is studied in this thesis.
Although a 3D non-linear Finite Element model is available that can accurately predict the strength capacity of bridges, including the effect of system behavior, it is computationally time-consuming and not feasible for practical use. Currently, a Live Load Distribution Factor (LLDF) is available that can be applied to individual girders to estimate the full capacity of the bridge. However, this approach provides a very conservative estimate of the load effect and is based on linear analysis. Therefore, there is a need to develop an equivalent loading method that incorporates material non-linearity to accurately predict the bridge's load capacity.
This thesis is limited to assessing the load-carrying capacity of existing prestressed concrete T-girder bridges. The study focuses on the most common layout of the crossbeams—bridges with four cross-beams (two end cross-beams and two intermediate cross-beams), including the Vecht bridge, which is used as a case study. The emphasis is on creating a simplified 2D Non-Linear Finite Element Analysis to determine the equivalent loading that integrates the bridge deck and individual girder by comparing results from both experimental tests and a 3D Non-Linear Finite Element model of the case study.

1.4. Research Methodology

The goal is to investigate the system behaviour of existing T-beam bridge resistance by utilising a 2D non-linear finite element model approach. The research of this thesis builds upon a case study of a multi-span T-beam bridge named 'Vecht Bridge' built in the Netherlands in 1962, for validation purposes.
The case study progresses as follows: initially, two separate models—an individual T-beam girder and an integrated deck slab—are built in the vertical and horizontal planes, respectively. The 2D bridge deck model is a linear model. Variations in stiffness in the longitudinal and transverse directions, due to the presence of crossbeams and variations in concrete properties, are incorporated as geometrical orthotropy. This 2D bridge model is then compared with an available 3D linear model [10] to ensure that the behavior of the 2D bridge deck model aligns with that of the 3D linear bridge deck model. To improve the accuracy of the 2D bridge deck model, the element type and the element size are varied.

The individual girder model, built in the vertical plane, incorporates material non-linearity. The material properties used are based on tests conducted on the Vecht Bridge [10]. The constitutive model and solution method are the same as those used for the 3D non-linear analysis of the Vecht Bridge. Only the element type and size are optimised to get the improvised model of the individual girder that are comparable to the experimental results of the case study. Then, the improved models of the 2D non-linear individual girder model and 2D linear bridge deck model are correlated by developing an equivalent method that can be applied on the individual girder which can determine the full load capacity including the system behaviour of the prestressed concrete girder bridge.
Finally, the validation of the 2D Non-Linear Finite Element Model approach is done by comparing the real-time experimental data obtained from the Vecht bridge [11].

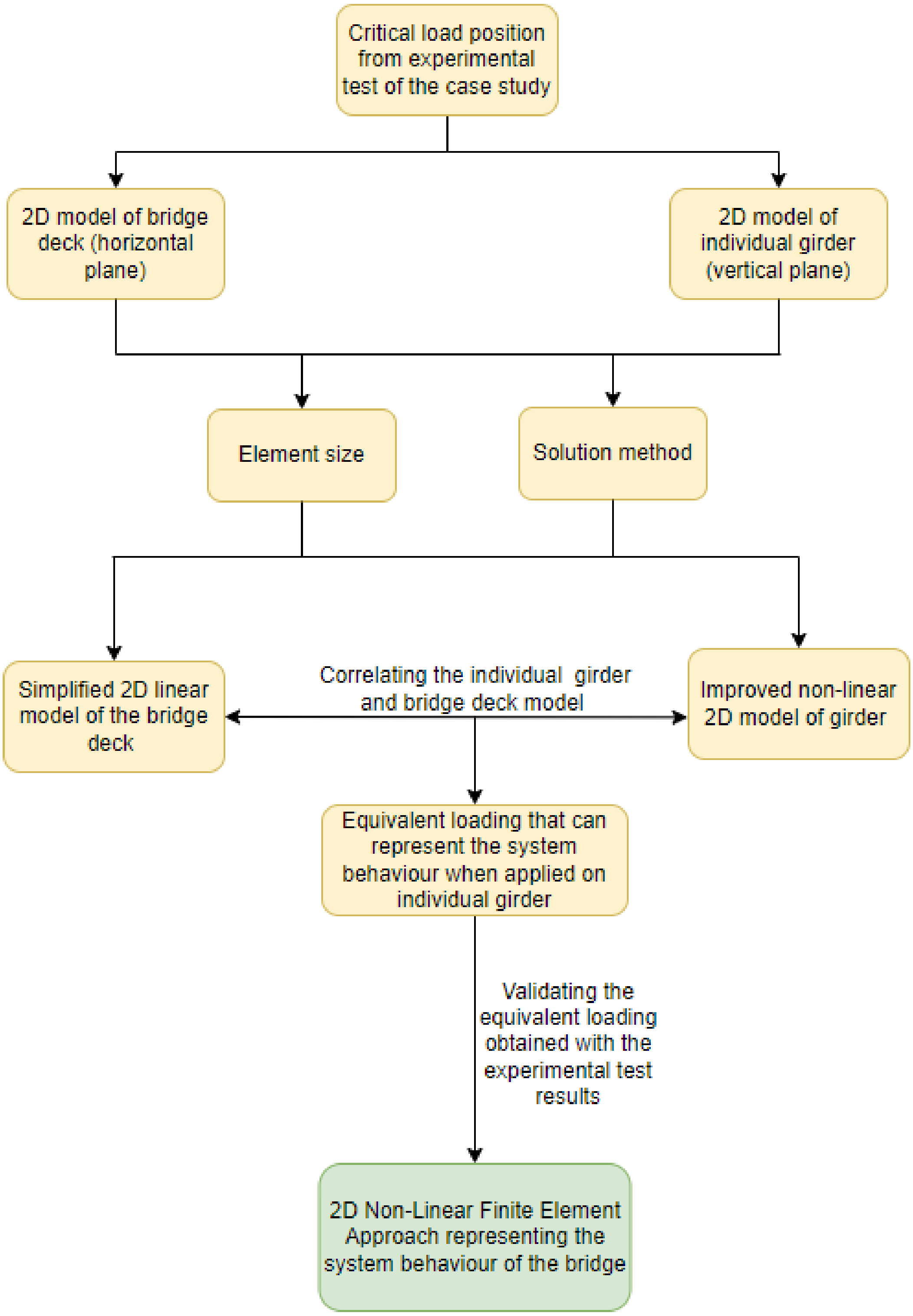

Figure 1.2: Theoretical framework

1.5. Thesis outline

The outline of this master's thesis is described briefly in this section to guide the reader. This thesis contains seven chapters. The second chapter 'Literature Study' describes the strategies for assessing the existing bridges analytically, numerically, and experimentally. It then proceeds toward how an existing bridge can be analysed numerically by extensively describing about the modeling strategies. As the modeling strategies are more relevant for this thesis. Finally, the research gap that this master's thesis aims to fill is mentioned at the end.

In Chapter 3, the case study, a typical T-beam bridge called the Vecht bridge is introduced. The description of the geometry of the whole bridge is described in this section. The geometry, reinforcement and prestressing layout of the T-beam, cross-beam and integrated deck slab is explained in detail in this section as well. The results from the material investigation and the full-collapse test of the Vecht bridge is reported in this chapter. The critical load positions that were obtained from the experimental and numerical results study are addressed here as well.

Chapter 4 is exclusively about developing a 2D Nonlinear analysis approach. Modeling of an individual T-beam girder in the vertical plane and the integrated deck slab in the horizontal plane is described step by step. The results from the non-linear analysis of the individual T-beam girder and integrated deck slab are also discussed.

Chapter 5 covers the system behavior of the girder bridges. The methodology followed to combine the two models - individual T-girder and integrated deck slab is explained here. Finally, 2D Non-Linear Finite Element Approach to find the system behavior of the prestressed T-beam concrete bridge is presented int this chapter.

In Chapter 6 the results from the Non-linear analysis of individual girder, integrated deck slab and the combination of both these models are compared with the already available numerical and experimental results from the case study are discussed.

Finally, Chapter 7 summarises all the conclusions and also gives recommendations for future research needed in this area.

2
Literature review

This chapter covers the literature review regarding the numerical assessment of the shear capacity of prestressed concrete T-beam bridges. Firstly, various assessment strategies of existing bridges are explained. Secondly, the modelling strategies (numerical assessment) are elaborated in detail. The Linear Finite Element method used for analysing the bridge is introduced. Then, the modelling approach of an individual girder (non-linear) and bridge deck is presented in this section. Also, the methods of correlating the two models - individual girder and bridge deck using equivalent loading technique is introduced here. The research gap related to shear deficiencies, system behaviour, non-linear analysis and equivalent loading technique used are summarised.

2.1. Assessment Strategies of Existing Bridges

The current assessment of existing bridge structures is based on the safety conditions required for new bridge structures. This assessment primarily checks the loads for the Ultimate Limit State (ULS) and not for the Service Limit State (SLS). Consequently, the initial assessment of existing prestressed concrete T-beam bridges indicates that half of the bridges do not comply with the code requirements for existing structures in the Ultimate Limit State, as per NEN 8700 and RTD 1006 [7]. However, this does not necessarily qualify the bridge as unsafe, since load transfer mechanisms such as Compressive Membrane Action or arching action are not considered [3].

The shear resistance of concrete calculated using the current code (NEN-EN 1992-1-1 [7]), is substantially reduced (depending on the combination of parameters) compared to the older code (pre-1974) [17]. The older code approach in calculating shear resulted in very low shear reinforcement and overestimated shear resistance. Additionally, the current detailing for stirrups differs from older engineering practices. This discrepancy means that even if sufficient shear reinforcement is present in prestressed concrete girder bridges, it is in some cases unclear how to account for it in the assessment of existing structures.

It is also known that the strength of concrete increases over time, often exceeding the 28-day compressive strength used in design calculations. Therefore, if an existing bridge underperforms in terms of strength capacity according to the current code, several refinement options are available as outlined by RBK [22] and NEN 8700 [18].

From referring to Figure 2.1 the following steps can be taken to refine the assessment of the existing bridges. The refinements are divided into analytical, numerical and experimental methods. From the analytical method, the deficit bridge can be assessed by reducing the design load by lowering the safety level and limiting the remaining lifespan to 30 years (this corresponds to a minimum reliability index of β_{rel} = 3.3). Another analytical option is that the design traffic load can be reduced by fixing the traffic lane which can reduce the critical sectional forces. If the bridge still remains deficit, an on-site material investigation can be conducted which is sometimes proven to increase the design value of compressive strength of concrete. This increase in concrete strength is advantageous for an increase in shear strength. Also, Code modification recommended by the Dutch Ministry of Infrastructure and Water Management (Rijkswaterstaat) to the Eurocode for flexural shear formula can be used. For prestressed beams with sufficient and properly detailed stirrups, Equation 2.1

allows using a prescribed fixed strut angle of θ = 30◦. Note that the additional terms for variable height box girders are not included in Equation 2.1 as it is not relevant here.

$$V_{\text{Rd}} = V_{\text{Rd,s}} + V_{\text{Rd,c}} \tag{2.1}$$

Where the term $V_{Rd,c}$ (i.e.) the resistance offered by the concrete is added to the resistance offered by the stirrups $V_{Rd,s}$ to get the total flexural shear resistance. Generally, for inverted T-beam bridges built before 1974; the amount of shear reinforcement doesn't comply with the code (i.e). is less than the typical values required for shear reinforcements, or the detailing of the stirrup is not proper. The equation 2.1 cannot be used in the above situation and only $V_{Rd,c}$ is used for the capacity.

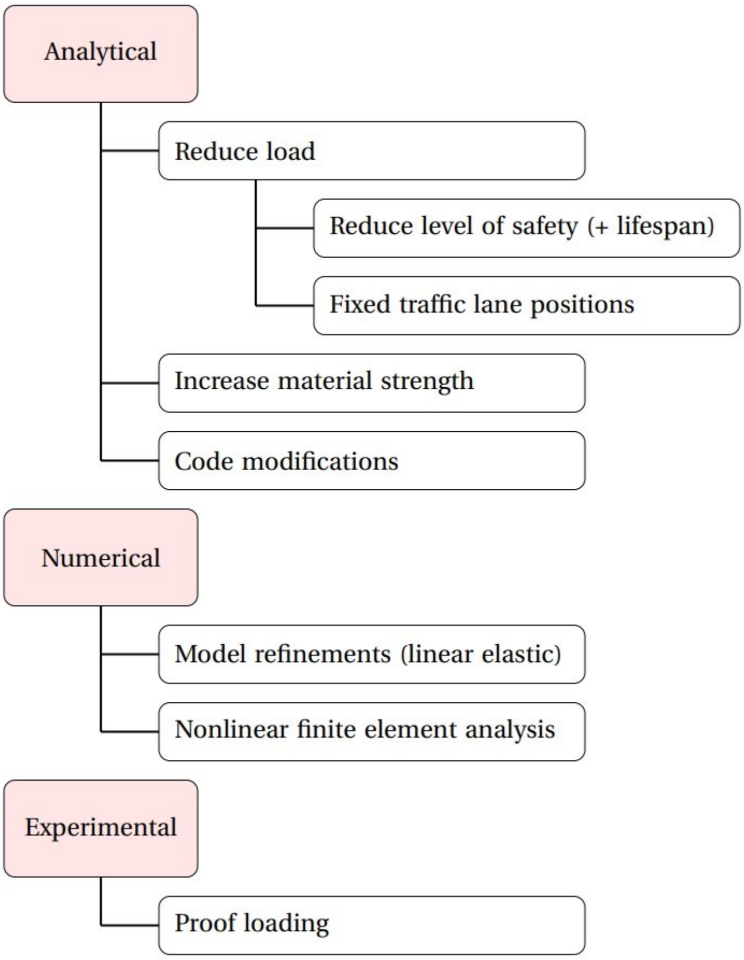

Figure 2.1: Methods of structural assessment refinements for existing concrete bridges (according to RBK [22] and NEN 8700 [18] ((Reprinted from [10]))

Apart from analytical options, there are numerical methods for structural assessment of bridges. Linear finite element analysis can be used for assessing the bridge capacity. The linear elastic finite element model can also be improved by using advanced elements like shell or solid elements. Also, implementing the exact positions, dimensions and stiffness of the supports in the linear finite element model can be done.
Another numerical method to use is non-linear finite element analysis when the analytical and linear elastic models don't yield acceptable results. A two-step procedure is followed for prestressed concrete bridges. Firstly, the load position that yields the maximum shear force on the bridge deck is determined using a linear elastic model. Secondly, the shear resistance is analysed (in an individual girder) using the non-linear finite element model. The Non-Linear often includes a sensitivity analysis. As a last resort, if uncertainties are present – missing records, presence of structural damage like

corrosion and cracking, or analytical/ numerical assessment concludes the bridge's load-carrying capacity is deficient; experimental assessment (proof loading) can be done on the bridge deck [1].

2.2. Modelling strategies

2.2.1. Linear Finite Element Method for analysing bridge

Finite element analysis (FEA) of a bridge can be performed using 1D beam elements, 2D plate elements, or 3D solid elements. For instance, the maximum bending moment and shear force obtained from a 3D finite element model using solid elements are smaller compared to those from a 1D model using beam elements, according to AASHTO specifications. This indicates that a 3D structural model achieves better load distribution, behaving as a single unit, unlike a 1D model [19]. This study focused on assessing the long-term performance of a prestressed concrete T-shaped beam using 1D, 2D, and 3D elements. The 3D model simulated a more realistic behavior of a T-beam but required approximately 4 days to analyze, whereas the 2D and 1D models took about 1 day and 4 hours, respectively [6]. The 2D model was more accurate than the 1D models and less computationally intensive than the 3D models. Additionally, numerical results from the 2D model were in good agreement with experimental measurements for load/mid-span displacement and crack opening of the reinforced concrete trough bridge. The damage pattern obtained closely matched the experimental results [20].
However, conventional FEA typically uses linear analysis of bridge models with 1D, 2D, or 3D elements. Linear FEA provides conservative results and lacks accuracy. To better account for the material behavior of concrete, including cracking, lateral tensile and compressive stresses, and load reversals, a non-linear FEA approach is recommended [14]. Despite this, there is currently no standardised fully validated model approach for non-linear finite element analysis of existing bridge structures.

2.2.2. Non-Linear Finite Element Analysis on girder level in vertical plane

The modelling of pre-stressed beams in Non-Linear Finite Element Analysis has been a subject of study in recent decades. Especially studying the behaviour of beams after the cracking of concrete is of importance. A Non-Linear Finite Element Analysis is necessary to consider the contribution of concrete after cracking as the stiffness changes [9]. Other non-linearities that can be accounted are slipping of reinforcement bars, concrete-concrete interfaces, concrete-reinforcement interaction, strength degradation due to lateral cracking, strength increase due to lateral confinement, the effect of cyclic loading, effect of high strain rates and deterioration mechanisms. Also, the type of constitutive model used influences the final results therefore an appropriate model should be opted. The constitutive model for concrete should be chosen in such a way that it represents the realistic behaviour of the material in the structure. It is preferred to use exponential-type softening diagrams such as Hordijk or exponential softening since the cracks are more localised. Also, to reduce the mesh size sensitivity during compressive strain localisation, the stress-strain diagram with fracture energy-based softening is recommended [14]. It is necessary to incorporate the effects that can cause significant variation in the material models while assessing the bridge structures. The constitutive models used for non-linear analysis of the individual girder follow the guidelines laid out by the Rijkswaterstaat Ministry of Infrastructure and Water Management regarding NLFEA of Concrete Structures [14] and the literature [10].
The Non-Linear Finite Element Method is a powerful numerical tool to simulate realistic loading effects for the capacity control of critical sections and could be very useful for designing/assessing bridges.

2.2.3. Finite Element Analysis on bridge deck in horizontal plane

The bridge deck can withstand higher loads due to Compressive Membrane Action. The load-carrying mechanisms include Compressive Membrane Action (CMA) in the bridge deck, arch action in the beam (longitudinal direction) or transverse load redistribution to the adjacent beams in the Ultimate Limit State [10]. CMA can significantly influence the flexural and punching shear strength of the bridge deck but it is usually neglected in the design as well as assessment stage. Also, due to CMA, bridge decks have a larger shear capacity than assumed in the initial design stage [3]. Hence, quantifying such mechanisms is important to know about the realistic resistance of the bridge. In Eurocode, the load-carrying mechanisms are not considered which could influence the resistance of

the structure. The following conclusions were drawn from the full-size field test conducted on the Vecht bridge – a large discrepancy between experimental loading and analytically found resistance (almost a factor of 2) for beams tested allowing load distribution to adjacent beams. Also, for the edge beam tested individually, the experimental loads were much higher than the resistance found analytically [11]. Therefore, there's a need for further investigation of the load distribution. However, a 3D model of bridge for studying the load distribution is computationally costly. The 2D bridge deck model of the bridge can be built using three methods.
Many plate structures in bridges cannot be designed using isotropic plate elements. This is due to the fact that stiffeners may be present and can be different in the orthogonal directions. There are three ways to consider the shape orthotropy in the 2D Finite Element Models refer to Figure 2.2. In model 1, it is designed using a spatial assemblage of isotropic volume elements, but the input is very strenuous/ complicated and the output is very extensive and complex.
In model 2, the shape orthotropy is introduced using isotropic membrane-bending elements. The plane isotropic elements can represent both membrane action and bending quite accurately. However, the output consists of a combination of normal force, shear force, bending moment and/or twisting moment of total beam cross-sections; it can be difficult to interpret the result of an individual element.
In model 3, the shape orthotropy in the Finite Element model is incorporated using orthotopic plate elements. The structure is modeled using a flat plate with orthotopic element properties. This model is preferred when the stiffeners occur at regular intervals (in this case, the stiffeners are the T-girders). However, the centre line of the top plate is connected to the centre line of stiffeners as opposed to reality. After Finite Element analysis, the starting and membrane forces in the top plate can be computed [4]. The method 2 is used for building the 2D bridge deck model in the horizontal plane due to its simplicity in attaining the combination of normal forces, shear forces and bending moments of the total section.

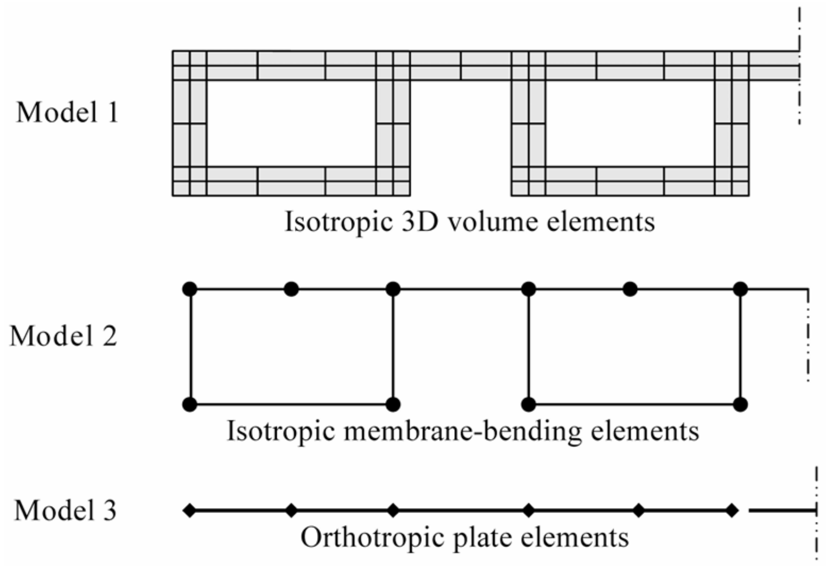

Figure 2.2: Three different levels of FE model for the same structure [4]

2.2.4. Combining the 2D Finite Element Models of the bridge deck and individual girder

To simplify the design of the bridges in general, the concept of equivalent loading/Load Distribution Factor is introduced. This concept helps assess how designed girders distribute loads when live loads are placed at various locations on the bridge. This method simplifies designing multiple girders in three-dimensional plane to designing just one girder in two-dimensional plane. For this purpose, AASHTO recommendations provided an empirical formula for calculating Live Load Distribution Factor (LLDF) [2]. This Live Load Distribution Factor (LLDF) recommended by AASHTO majorly takes into account the beam spacing and a constant that depends on the the type of bridge. It was inferred from a study that there was a deficiency in calculating shear in interior girders for box-girder bridges as there were not enough field measurements to support the load distribution factors provided by AASHTO for spread box girder bridges and other types of bridges [15]. A study was also conducted to develop the Load Distribution Factor for shear consisting of 30 bridges with varying girder spacing, moment of inertia and span length. It was observed that the shear distribution factor was underestimated using AASHTO LRFD. It was inferred that the LLDF majorly depended on the spacing between girders [24].

The concrete slab and I-girder of prestressed concrete girder bridges were modelled using shell and beam elements respectively and the Load Distribution Factor for shear is obtained from the FEM according to AASHTO. It was found that the FEM model accurately predicted the strain compared with the field test of seven bridges. In addition, an analytical formula was also proposed using a parametric study and the one with the lowest sum of squares error (SSE) was chosen. The proposed equation showed good accordance with both the FEM model and field test results [24]. There is potential to develop an analytical formula that can predict accurate load distribution factors for connecting the individual girder and bridge deck model.

The diaphragms (cross-beams) play an important role in the load distribution of prestressed concrete bridges. But, the diaphragm action is not included in both live-load distribution and capacity of by AASHTO. Theoretically, full diaphragm stiffness can be achieved by post-tensioning the diaphragm across the bridge width. However, modelling the effects of the intermediate diaphragm on load distributions in the Finite Element Model needs more verification/study [5].

The Load and Resistance Factor Design (LRFD) methodology recommended by the American Association of State Highway and Transportation Officials (AASHTO) is based on the assumption of linear elastic behaviour of concrete [2]. This approach is suitable for both the Service Limit State and the Ultimate Limit State, which assume linear elastic behavior of concrete. However, this linear assumption does not hold true for existing bridge structures, particularly when the concrete is cracked, leading to a non-linear load redistribution [23].

Given this discrepancy, it is imperative to develop an accurate equivalent loading method that can correlate the bridge deck model to individual girder models while accounting for non-linear load redistribution effect due to cracking of concrete.

2.3. Research Gap

The conventional approach uses a linear finite element model to account for load effects and it usually provides a conservative estimate of the strength capacity of the bridge. On the other hand, a non-linear finite element model has the potential to predict a more realistic capacity of the existing bridges. In previous studies using Non-Linear Finite Element Analysis, the analysis was limited to individual beams and not system behaviour of connected T-girders like Compressive Membrane Action (CMA) and load distribution/redistribution between T-girders. Using a full 3D finite element model to incorporate the system behaviour of the bridge is computationally expensive and is less preferred. Hence, a simplified 2D non-linear finite element model is becoming more common in practice. However, in a 2D non-linear finite element analysis, the system behaviour of the structure (i.e.). redistribution of load is not accounted for, this can significantly increase the capacity (shear capacity) of the bridge. A simplified 2D bridge deck model which can predict both the load distribution and redistribution effect and is comparable to the 3D Finite Element Model is developed. Also, a 2D non-linear individual girder model which can predict the shear capacity of the full bridge system by applying equivalent loading obtained from the 2D bridge deck model is developed.

This thesis aims to develop a staggered 2D Non-Linear Finite Element Model approach using two models - a 2D bridge deck model for studying the load effect and a 2D individual girder model for predicting the strength capacity. This approach combines these two models through an equivalent loading technique, aiming to accurately predict the capacity of both a single girder and the overall system behaviour of prestressed concrete girder bridges.

3

Case Study: Vecht bridge Introduction

3.1. Introduction to case study

The Vecht bridge was built in 1962 nearer to the town Muiden, in the province of Noord Holland, the Netherlands. The Vecht bridge is a prestressed T-beam concrete bridge with cast-in-between decks. It consisted of 9 simply supported spans; of which one was a movable bridge crossing over the Vecht river refer to Figure 3.2. The bridge was initially located in A1 highway and since the highway was rerouted, a new bridge replaced the old bridge refer to Figure 3.1. Due to this, the Vecht bridge was available for testing before complete demolition. With the experimental data from testing the real bridge, the numerical model being developed can be validated. The validated model can be used for predicting the capacity of similar bridges in the Netherlands. Only the already existing bridge will be described explicitly since the tests are conducted only on the existing bridge.

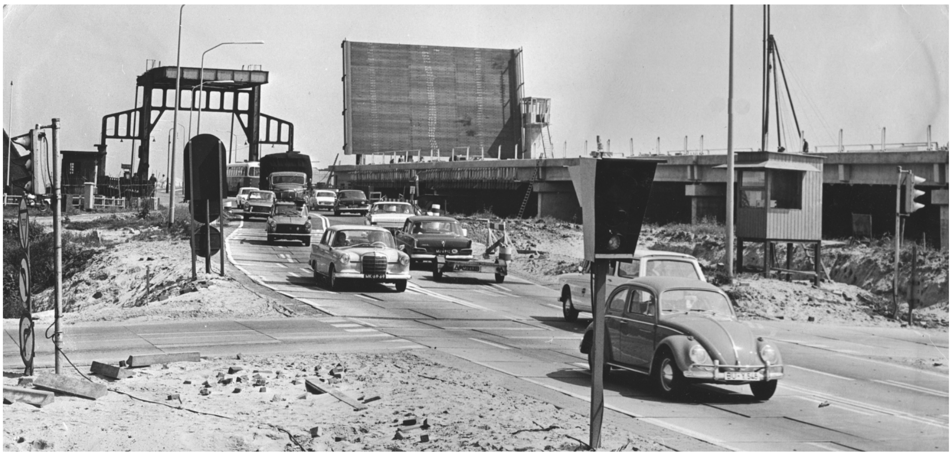

Figure 3.1: Construction of the new Vecht bridge in 1962 (right), existing bridge (left) ([21])

3.2. Description of the Vecht bridge

3.2.1. Geometry of the Vecht bridge

The Vecht Bridge is a simply supported multiple span bridge. The 9 spans had a length of 24 m each and consisted of 15 post-tensioned beams along with cross-beams at 8 m interval. Expansion joints are placed at the piers and abutments. The piers have a centre-to-centre distance of 24.9 m. The centre-to-centre distance between the T-beams 1.225 m, and the total width of deck (including kerb) is 18.40 m (see Figure 3.4). The piers consist of a continuous slender tapered wall and a rectangular beam at the top to accommodate the bearings and support the bridge deck. The foundation of the piers consists of a slab on closely spaced square concrete piles.

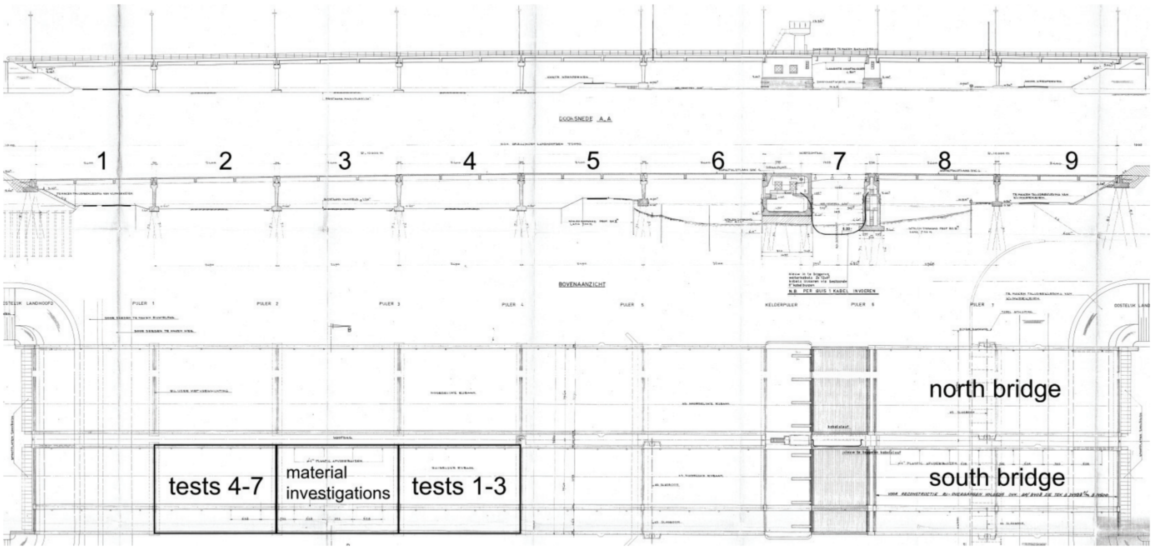

Figure 3.2: Overview of Vecht bridge, span numbering and test locations, side view (top), longitudinal cross-section (middle) and top view (bottom) (Reprinted from [10])

3.2.2. T-beam: geometry, reinforcement and prestressing

The total length of the T-beam is 24700 mm. The end block that is present at the end of the T-beam is prefabricated and it also contains the anchorage zones of the prestressing tendons. The prefabricated end block is connected with the T-beam by a transition piece. The intermediate cross-beams are cast as a part of the T-beam (see Figure 3.3).

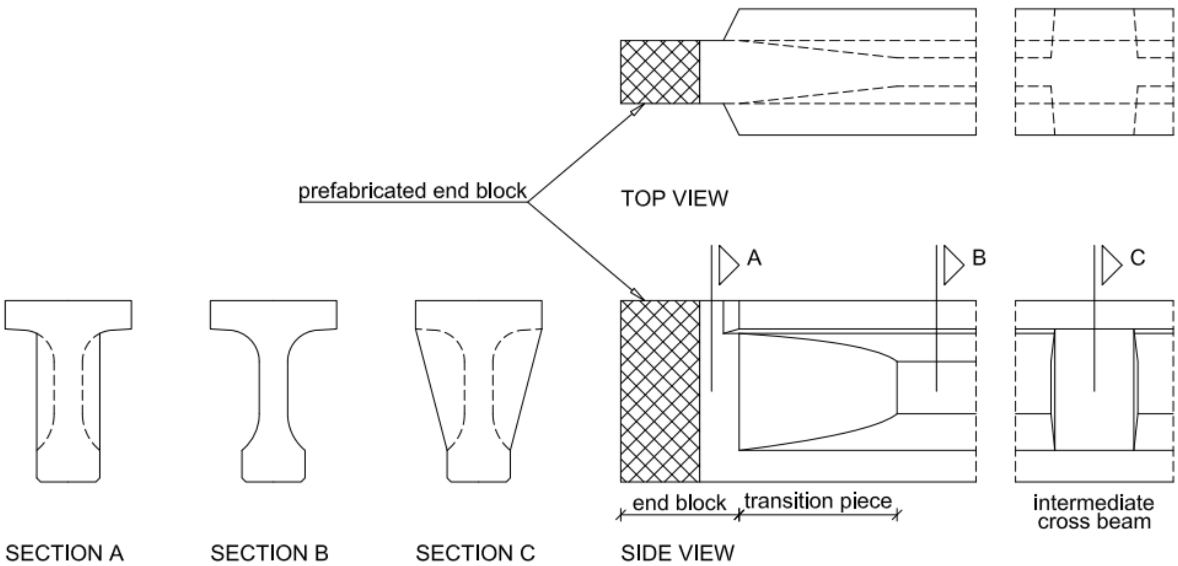

Figure 3.3: Overview of Vecht bridge, span numbering and test locations, side view (top), longitudinal cross-section (middle) and top view (bottom) (Reprinted from [10])

The design of prefabricated prestressed T-beam is shown in Figure 3.4. The T-beam has an end block of thickness 400 mm and it extends up to a length of 750 mm which is then followed by a transition piece of length 1000 mm. The dimensions of the T-beam and the layout of the reinforcements and the tendons are given in Figures 3.6 and 3.7. The T-beam has a total height of 1150 mm and the minimal thickness of the web is 180 mm. The shear reinforcement follow the shape of T-beam, it can also be observed that there's only a minimal amount of shear reinforcement present (i.e.) ⌀ 8 - 500 mm (Figure 3.7). The profile of tendons 1 - 7 is shown in Figure 3.6, the numbering presumably follows the order of post-tensioning of the tendons. It can also be inferred that six tendons are anchored at the end block and the tendon number 7 is anchored in the top flange at a distance of 1902 mm from the support. The end block and intermediate cross-beams contain ⌀ 50 ducts for transverse prestressing tendons. Each tendon consists of 12 ⌀ 7 mm (A_P = 462 mm^2) in ⌀ 42 mm ducts [10].

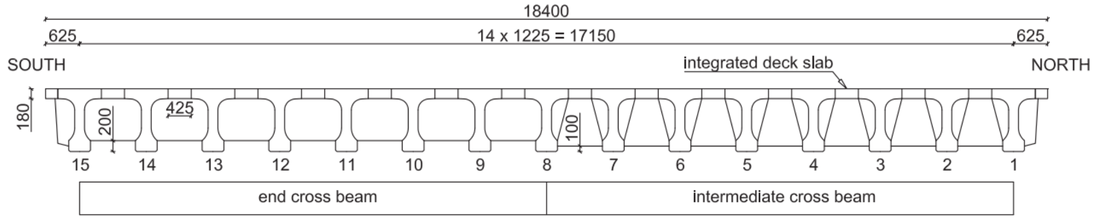

Figure 3.4: Vecht bridge, cross-section deck, T-beam numbering (measurements in mm) (Reprinted from [10])

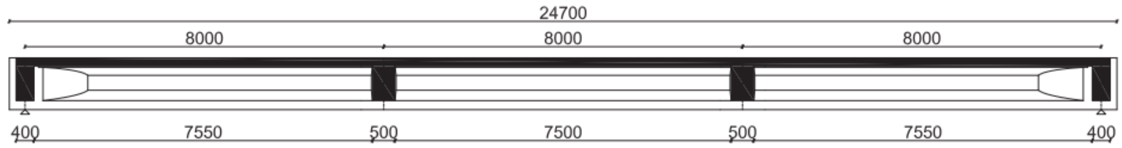

Figure 3.5: Vecht bridge, longitudinal section deck (measurements in mm) (Reprinted from [10])

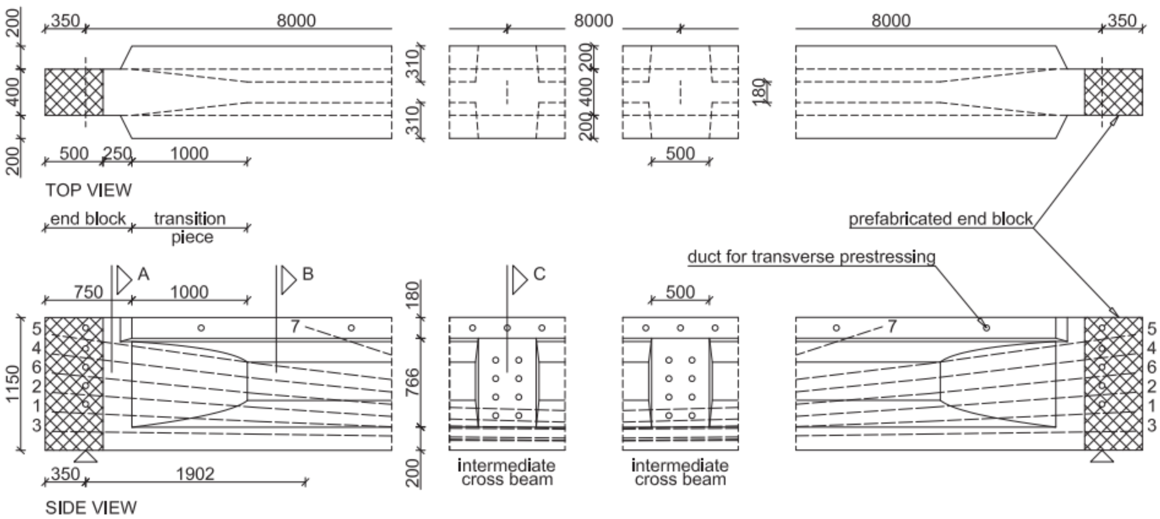

Figure 3.6: Vecht bridge, T-beam dimensions and draped prestressing tendons 1-7 (measurements in mm) (Reprinted from [10])

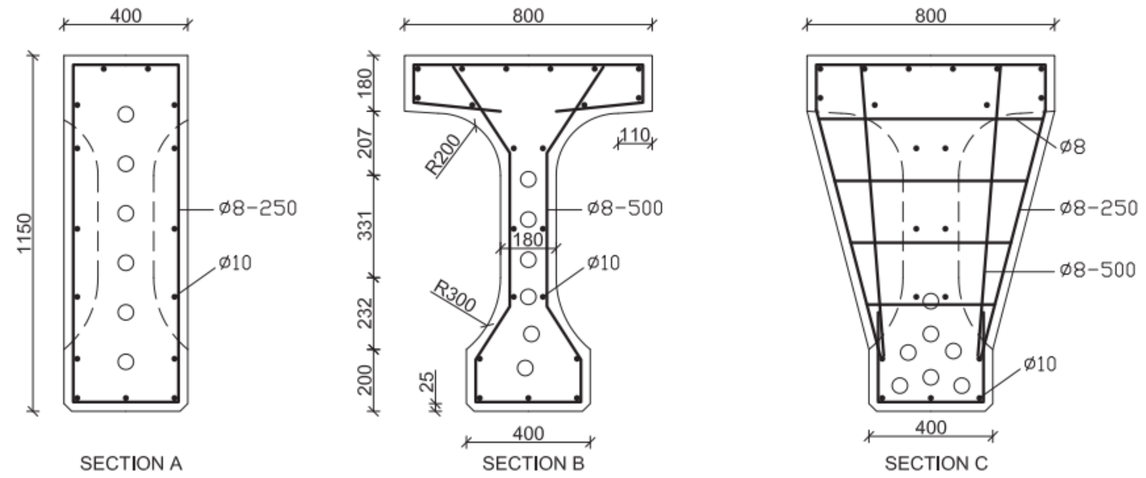

Figure 3.7: Vecht bridge, T-beam dimensions and reinforcement layout (measurements in mm) (Reprinted from [10])

3.2.3. Cross-beam: geometry, reinforcement and prestressing

There are four cross-beams in total, two end cross-beams and two intermediate cross-beams (refer Figure 3.5). The end cross-beams have a thickness of 400 mm and are offset by 200 mm from the end of the T-beam. The end cross-beams contain five transverse prestressing tendons. The intermediate cross-beams have a thickness of 500 mm and have an offset of 100 mm from the bottom of the T-beam refer section 3.2.3. The intermediate cross-beams have a centre-to-centre distance of 8 m. They contain seven prestressing tendons in total (see Figure 3.6).

3.2.4. Integrated deck slab: geometry, reinforcement and prestressing

The integrated deck slab is present in between the T-beams and has a width of 425 mm and a thickness of 180 mm see Figure 3.4. The T-beam and the integrated deck slabs are connected using 35 unevenly spaced transverse prestressing tendons. It can be inferred that the transverse prestressing is more concentrated at the location of intermediate cross-beams. The prestressing system is the Freyssinet system, same as for the T-beam Refer section 3.2.2. The reinforcement layout consists of a longitudinal reinforcement of 4⌀6 and stirrups of ⌀ 6 - 400 mm.

3.3. Material Properties

The material properties are inferred from the experimental test conducted on the Vecht bridge [10]. The average concrete compressive strength of the T-beams, the integrated deck slab, and the kerb; the strength of reinforcing and prestressing steel are found from the investigation done on the south-western approach bridge on the third span see Figure 3.2. The results from the test investigation are summarised in Table 3.1.

Table 3.1: Vecht bridge: concrete compressive strength and density [10]

Location	$f_{cm,cube}$ N/mm^2	$f_{cm}{}^a$ N/mm^2	ρ kg/m^2
T-beam	106.9	87.7	2444
Integrated deck slab	73.5_c	60.3	2367
Kerb	67.6	55.4	2383

$f_{cm}{}^a = 0.82 x f_{cm,cube}$
^{c} based on 21 samples (2 outliers removed)

Table 3.2: Vecht bridge: strength of reinforcement and prestressing steel [10]

Type	f_y N/mm^2	f_u N/mm^2	ϵ_u %
Prestressing wire average	1505.4	1769.5	9.0
Reinforcement average	287.7	351.8	10.0

3.4. Prestressing forces

The tendon layout and the prestressing system is described in Section 3.2.2. The tendon profile of the Vecht bridge is not given in the drawing, hence a third degree polynomial equation is used for solving the tendon profile [10].

$$y = ax^3 + bx^3 + cx + d \tag{3.1}$$

Equation 3.1 is solved in Maple software (refer appendix B) using the following boundary conditions,

1. The coordinates at the anchorage location and half span length.
2. An angle of zero is applied at the half span length due to the symmetry of the tendon.

Note, for tendon 7 the change in tendon profile at the transition point at x = 4.5 m and x = 20.2 m from the centre of support is disregarded as it is negligible. The profile of tendons 1 to 7 is shown in Figure 3.8.

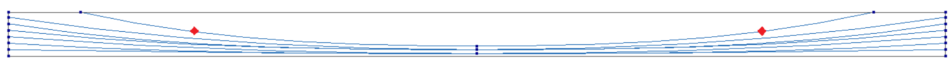

Figure 3.8: Tendon profile of tendon 1 - 7 calculated from third degree polynomial equation (half span length)
The red dot represents the location of the change in tendon 7 profile

The prestressing force at the anchorage point is calculated assuming 20% time-dependent losses; the working prestressing force is then calculated using,

$$N_{\text{pw}} = 0.8\sigma_{\text{pi}} * A_{\text{p}} = 0.8 * 1084 * 462 * 10^{-3} = 400.6kN \tag{3.2}$$

The prestressing force calculated from the above equation is applied at both the anchorage ends of the tendon.

3.5. Results from the full-collapse test of the Vecht bridge

The results from the connected and disconnected T-beam test is eloborated in this section. The data is inferred from the full-collapse test done on the Vecht bridge [10]. The description of the test, failure load, failure model and deflection at failure are elaborated in the section below. The tests listed below will be used for validating the 2D non-linear individual girder model in the vertical plane and the non-linear finite element approach developed for predicting the strength capacity of the connected T-girders (system behaviour).

3.5.1. Disconnected T-beam test

For the disconnected T-beam test 4 - 7, In the disconnected T-beam test 4-7, the integrated deck slab was sawn in the longitudinal direction for testing the individual T-beams refer to Figure 3.9. This setup allows to understand the individual behaviour of the T-girder when a failure load is applied. The details of the disconnected T-beam test is enumerated in Table 3.3 and Table 3.4. The failure mode for all the disconnected T-beam test was flexural shear failure.

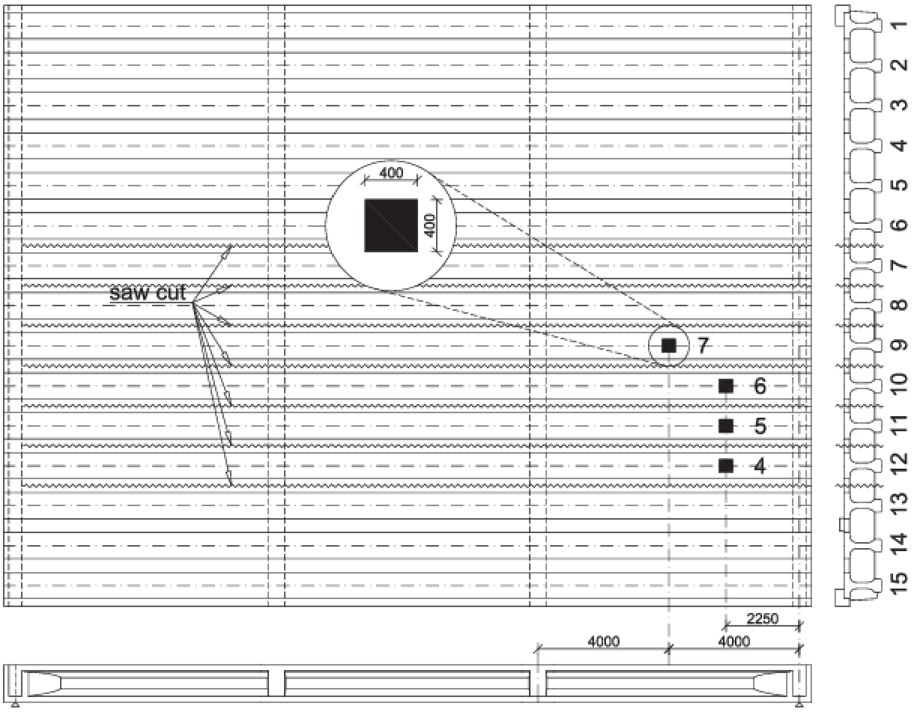

Figure 3.9: Disconnected beam tests 4–7, span 2, southern Vecht bridge (measurements in mm) (Reprinted from [10])

Table 3.3: Overview of disconnected beam tests [10]

test	a mm	beam number	beam type	structural system
4	2250	12	disconnected beam	sawn
5	2250	11	disconnected beam	sawn
6	2250	10	disconnected beam	sawn
7	4000	9	disconnected beam	sawn

Table 3.4: Results of disconnected beam tests [10]

test	δ_u mm	F_u kN	failure mode
4	79	1678	flexural shear T-beam
5	65	1703	flexural shear T-beam
6	74	1774	flexural shear T-beam
7	132	1022	flexural shear T-beam

3.5.2. Connected beam test 1

The load is applied as a concreted surface load of 400 X 400 mm at 4000 mm from the support on the T-girder using a hydraulic jack that is positioned between the concrete deck and the steel bridge for the full-scale collapse test of the Vecht bridge refer Figure 3.10 and Figure 3.11. For more details regarding the full-scale collapse of the Vecht Bridge please refer [11]. This test setup is chosen because the loading is applied at the midpoint between the cross-beams. Also, at least four beams are present between the end of the bridge and the beam being tested, meaning that significant load distribution between the adjacent beams can be achieved. The failure mode of the connected beam test 1 observed was primarily shear failure of the T-girder followed by punching failure of the deck. The details of the connected beam test 1 is enumerated in Table 3.5 and Table 3.6.

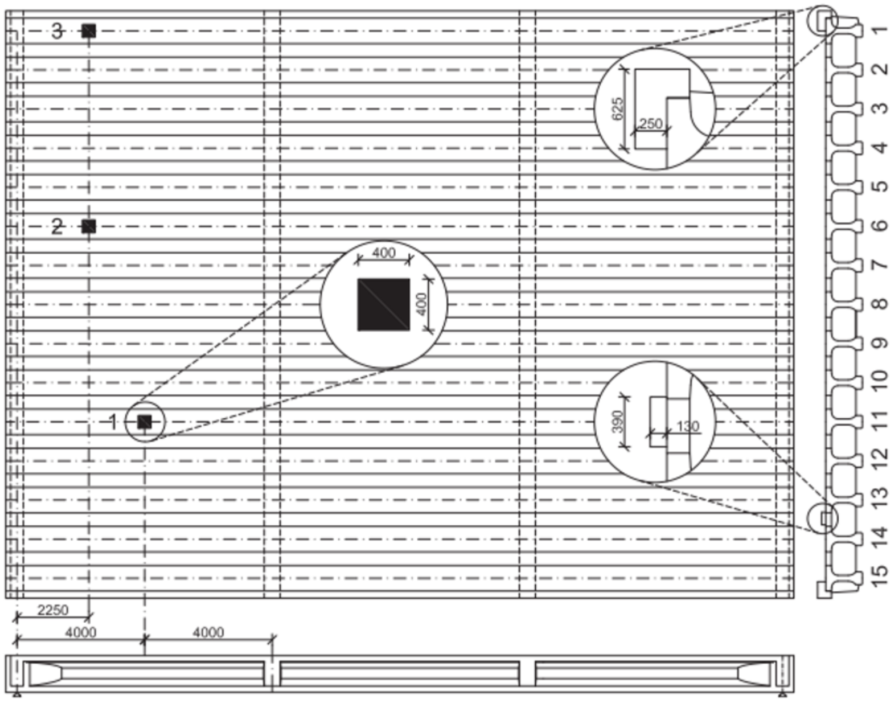

Figure 3.10: Connected beam tests 1–3, span 4, southern Vecht bridge (measurements in mm) (Reprinted from [10])

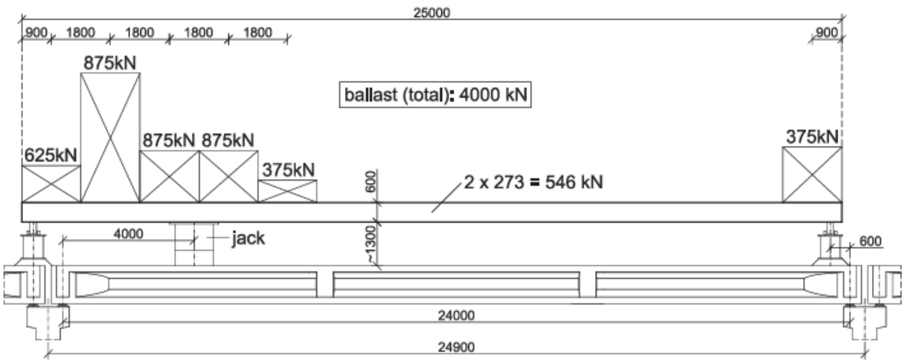

Figure 3.11: Load application according to test setup 1 on 2D bridge deck model (Reprinted from [10])

Table 3.5: Overview of connected beam test 1 [10]

test	a mm	beam number	beam type	structural system
1	4000	11	connected beam	unchanged

Table 3.6: Results of connected beam test 1 [10]

test	δ_u mm	F_u kN	failure mode
1	21	3004	Shear T-beam and secondary punching deck

4

Case Study: Vecht bridge - Developing a 2D Nonlinear analysis approach

In this chapter, an elaborate description of the two Finite Element Models, (i.e.) the bridge deck and individual girder are provided. Modeling aspects like - material properties, constitutive models and element types used for both the bridge deck and individual girder models are explained in this chapter. To analyse the full bridge system, a linear analysis is carried out in the bridge deck model in the horizontal plane and a non-linear analysis is carried out in the individual girder model.

4.1. 2D FEM approach of the bridge deck in horizontal plane

This section gives a detailed overview of the Finite Element Model of the bridge deck. The integrated deck slab is built in the horizontal 2D plane. A linear analysis is performed for the integrated deck slab. The plate structure in the bridges can't be handled as isotropic because the stiffness properties are different and can vary in two orthogonal directions. The variation in stiffness properties is due to the presence of cross-beams and different concrete materials used in the integrated deck slab. The orthotropy of the bridge deck is handled in terms of geometrical orthotropy and not using material orthotropy.

The modeling approach to account for the variation in stiffness and how the orthotropy is approached in the linear bridge deck model is addressed in this section. Further, the material and meshing properties opted are described in this section as well.

The 2D FEM model of the bridge built in the horizontal plane is only for studying the load effects such as load distribution to adjacent T-girders of the loaded T-girder. The corresponding shear force distribution or bending moment distribution of the loaded T-girder is then used for calculating/finding the equivalent distributed load that can be applied to the non-linear individual girder model in the vertical plane.

4.1.1. Constitutive modeling of concrete

As mentioned above, the material property used for the FEM model is defined as linear material property. Because of the prestressing, all components are considered to be uncracked concrete with a mean modulus of elasticity E_{cm}. The modulus of elasticity E_{cm} is based on the concrete class of the corresponding structural element refer Section 3.3. The concrete material properties for T-girders, cross-beams and integrated deck slab is defined as a linear isotropic material (using only Young's modulus and poison ratio) in the 2D FEM model of the bridge deck refer Table 4.1. The material properties used in the FEM model are inferred from the material investigation done on the Vecht bridge [10].

4.1.2. Element types and sizes

For modeling the integrated bridge deck in the horizontal plane, the deck slab is modelled as a flat plate with orthotopic geometrical properties, and the T-girders and crossbeams are modelled as line

Table 4.1: Concrete FEM material properties for integrated bridge deck model

T-beam			
Concrete class	C80/95		
Young's modulus	E_{cm}	42244	N/mm^2
Poisson ratio	ν	0.15	-
Slab and cross-beam			
Concrete class	C55/67		
Young's modulus	E_{cm}	38214	N/mm^2
Poisson ratio	ν	0.15	-

elements (refer Figure 4.1) with orthotopic geometrical properties as an input parameter refer Table 4.2, Table 4.3 and Table 4.4. The geometrical properties are calculated from the cross-section of the T-girder and cross-beam refer to Appendix A. In this model type, the shape of the structure is not recognised but it is defined purely based on the geometric properties. That is the integrated deck slab is modelled using a flat plate and the T-girders and crossbeams are modelled using just a line element refer to Figure 4.1 but with their geometric properties as an input parameter. The integrated deck slab and the T-girder are connected at their centroids. It is worth mentioning that the integrated deck slab connected at the centroid of the T-girder offers stiffness for bending and helps in load distribution amongst the T-girders as well refer to Figure 4.2.
The integrated deck slab is thin, with a thickness of 180 mm, and the shear effects are less pronounced than the bending effects. Therefore, plate bending elements are used to model the integrated deck slab. The plate element used for the bridge deck has a uniform thickness of 180 mm representing the integrated deck slab refer Figure 3.4. Plate bending elements are used to model the bridge deck instead of shell elements (membrane bending elements). This is because shell elements output separate membrane forces and bending moments for each part, rather than combining them into the normal force, shear force, and bending/twisting moments of the entire beam cross-section. For checking with codes, having these combined forces and moments is preferred. Calculating the combination manually, especially for complex geometries in structural components would be excessively strenuous.
Class I - 3D beam elements are used modelling for the T-girders, intermediate cross-beams and end cross-beams as it is compatible with the plate bending elements for the interpolation scheme used. The cross-section type for the class I - 3D beam elements is defined using arbitrary shape parameters with cross-section, Moment of Inertias (I_y^*, I_z^* and I_{yz}^*) and torsional moment of inertia (I_t) refer Table 4.2, Table 4.3 and Table 4.4.

Table 4.2: Orthotropic geometric properties of T-girder with acting width of integrated deck slab

Arbitary parametrs	Values	Units
Cross-section	506020	mm^2
Moment of inertia I_y^*	7.24685e+10	mm^4
Moment of inertia I_z^*	4.36019e+10	mm^4
Moment of inertia I_{yz}^*	-1.6622e+10	mm^4
Torsional moment of inertia It^*	1.1607e+11	mm^4/rad

Table 4.3: Orthotropic geometric properties of T-beam end block with acting width of integrated deck slab

Arbitary parametrs	Values	Units
Cross-section	608500	mm^2
Moment of inertia I_y^*	7.81503e+10	mm^4
Moment of inertia I_z^*	3.27473e+10	mm^4
Moment of inertia I_{yz}^*	0	mm^4
Torsional moment of inertia It^*	1.109e+11	mm^4/rad

The element size used is in accordance with RTD 1016-1 [13], a smooth stress field should be

Table 4.4: Orthotropic geometric properties of T-girder with acting width of integrated deck slab at the location of intermediate cross beam

Arbitary parametrs	Values	Units
Cross-section	762500	mm^2
Moment of inertia I_y^*	8.39622e+10	mm^4
Moment of inertia I_z^*	4.27145e+10	mm^4
Moment of inertia I_{yz}^*	6.58778e+08	mm^4
Torsional moment of inertia It^*	1.2668e+11	mm^4/rad

calculated using the maximum element size chosen. For 2D modeling of beam and slab structure, the maximum element size should be calculated as follows Refer table 4.5.

Table 4.5: Maximum element size for beam and slab structure

Beam structure	Maximum element size
2D modeling	min($l/50, h/6$)
Slab structure	Maximum element size
2D modeling	min($l/50, b/6$)

where h is the depth, l is the span, and b is the width of the beam/slab element. According to table 4.5; the T-beam has a total height of 1150 mm meaning the maximum element size should be 192 mm. The integrated deck slab is considered as part of the top flange of the T-beam due to its acting width, the maximum element size of 180/6 = 30 mm is not chosen. Also, the element size of 30 mm is not feasible. Therefore, the maximum element size of 200 mm should be chosen for the Finite Element Model of the bridge deck to calculate a relatively smooth stress field. That is a relatively dense mesh allows sufficient modelling of stress distribution in compressive zones [14]. The element size of 100 mm was chosen to avoid the formation of triangular elements that can cause stress concentration at a point.

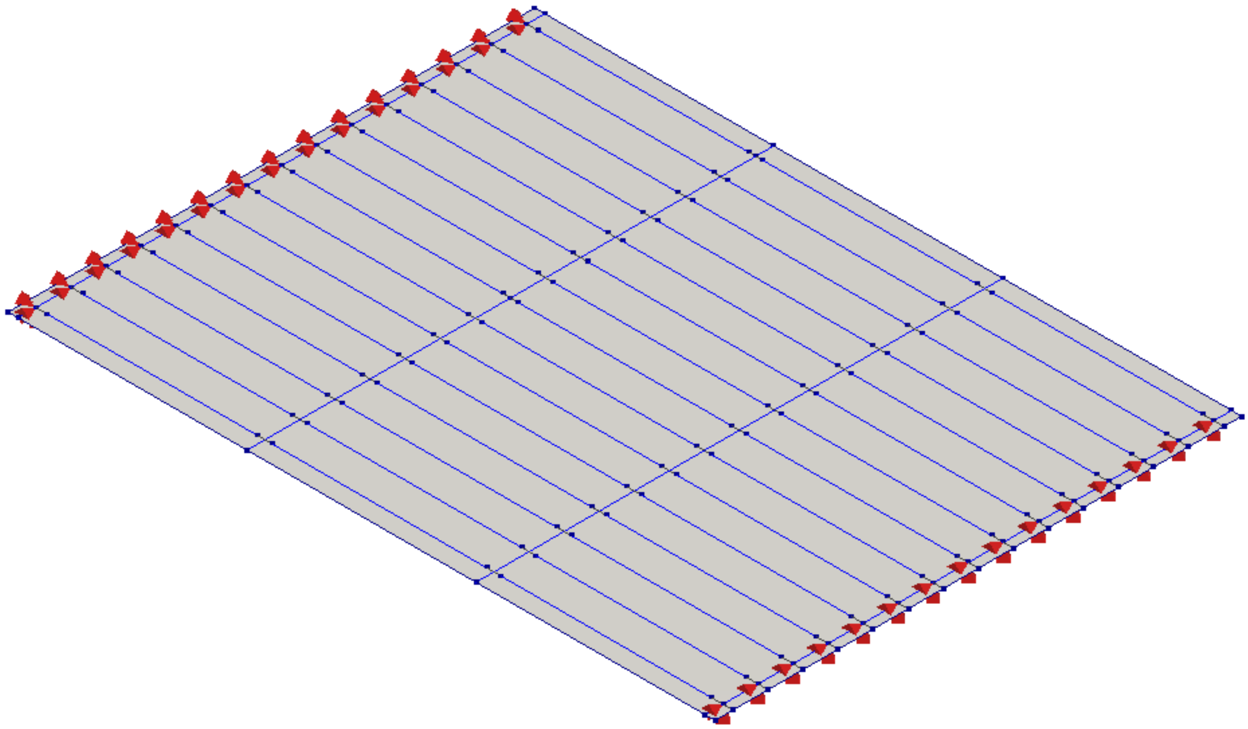

Figure 4.1: Geometry of bridge deck model in the horizontal plane.

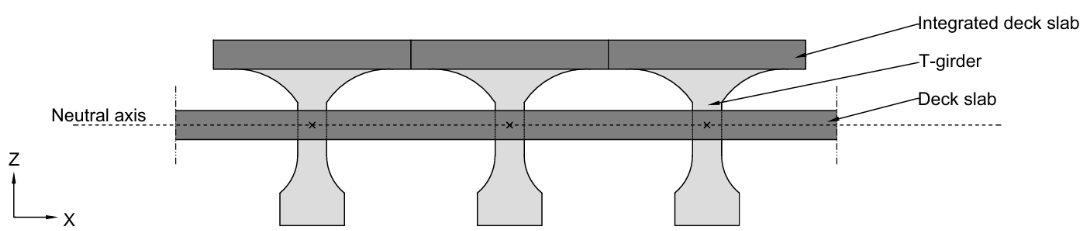

Figure 4.2: Representation of connection of girder with bridge deck in the FEM model.

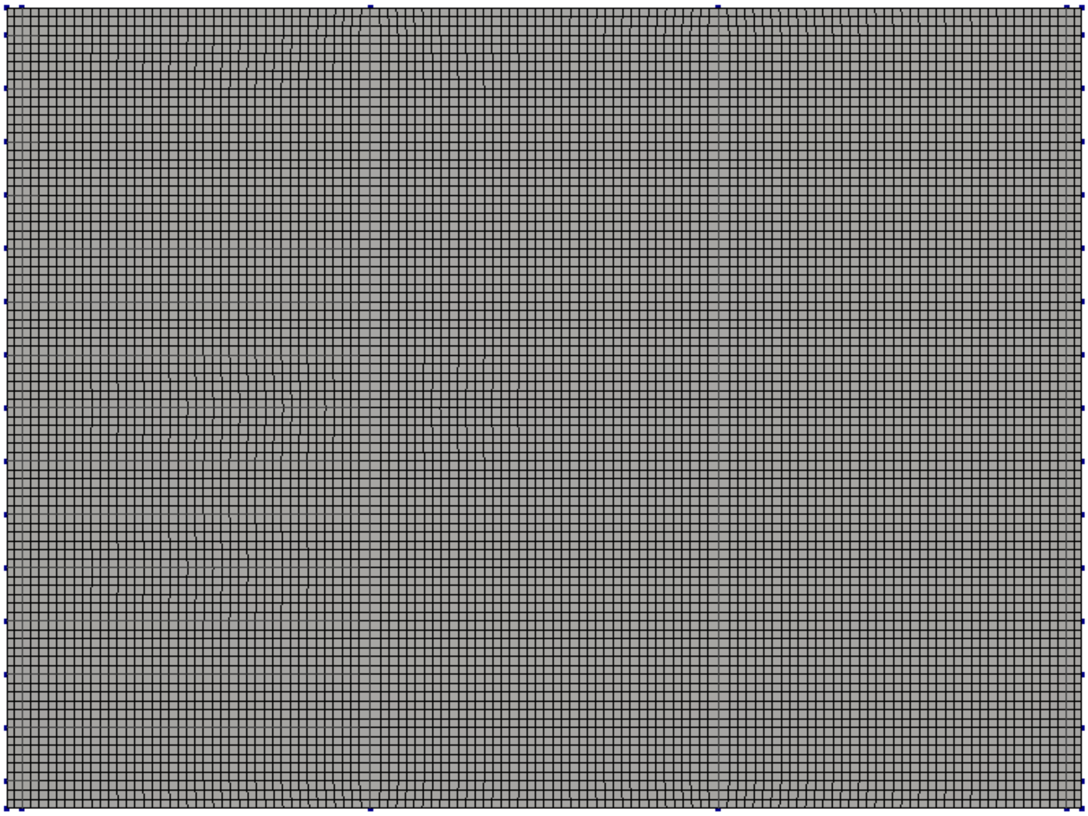

Figure 4.3: Top view of the meshing of bridge deck model in the horizontal plane.

4.2. Results from the bridge deck finite element model

4.2.1. Validation of the 2D bridge deck model based on the linear analysis

To check the validity of the 2D bridge deck model built in the horizontal plane, it is compared with the already available Linear Finite Element model in the 3D plane. The bridge deck model in the 3D plane consists of integrated deck slab and the top flange of T-beams strengthened by ribs (representing remaining T-beams and cross-beams) refer Figure 4.4 and Figure 4.5 [10]. A unity load of F = 1000 KN is placed on T-beam 1 and 8, for the numbering of T-beams refer 4.6 at the intervals in the longitudinal direction at a = 2, 4, 6, 8, 10 and 12 m from the centre of the support refer 4.7. The corresponding cross-section moments obtained from the 2D bridge deck model in the horizontal plane is then compared with the bridge deck model in 3D plane.

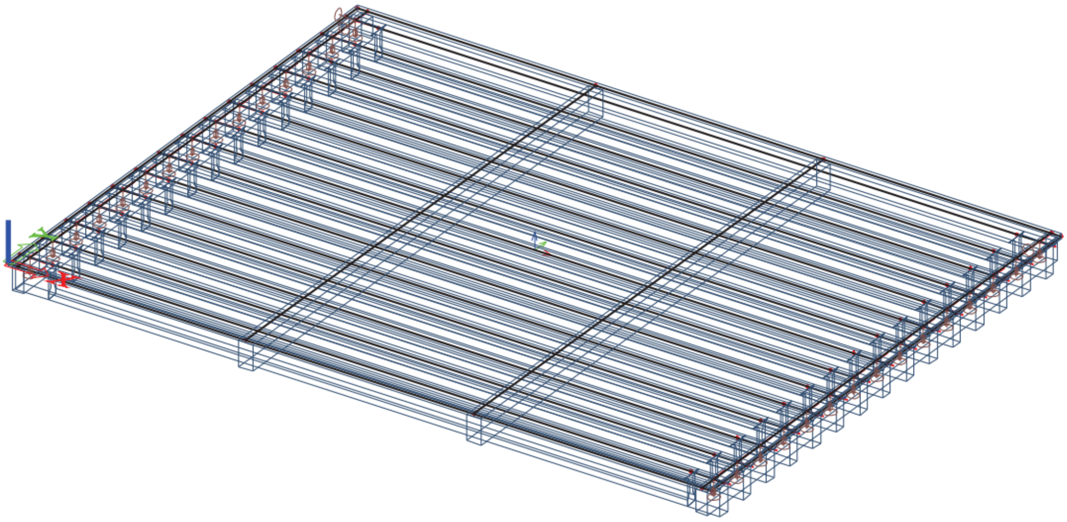

Figure 4.4: Single span linear elastic FEM model, 2D slab strengthened by ribs (Reprinted from [10])

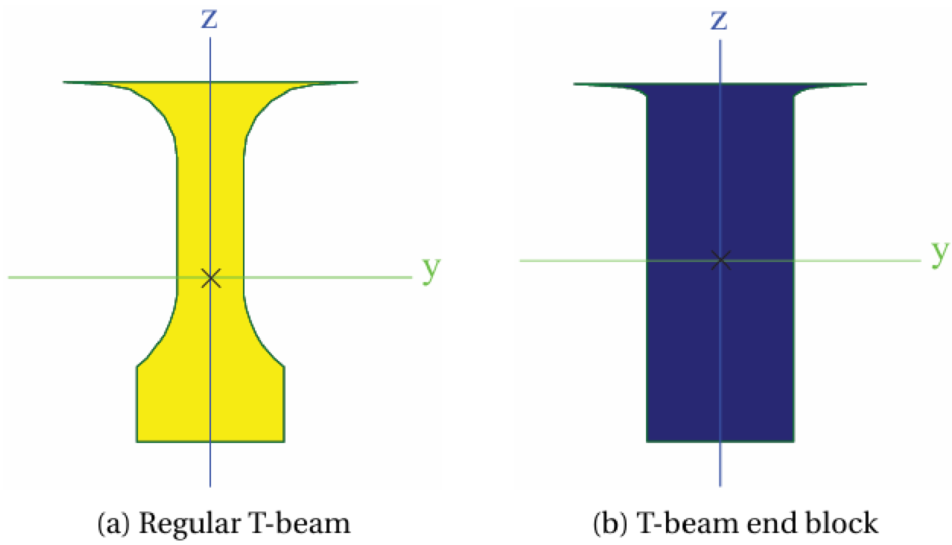

Figure 4.5: Cross-sections of T-beam without top flange (ribs in FEM model) (Reprinted from [10])

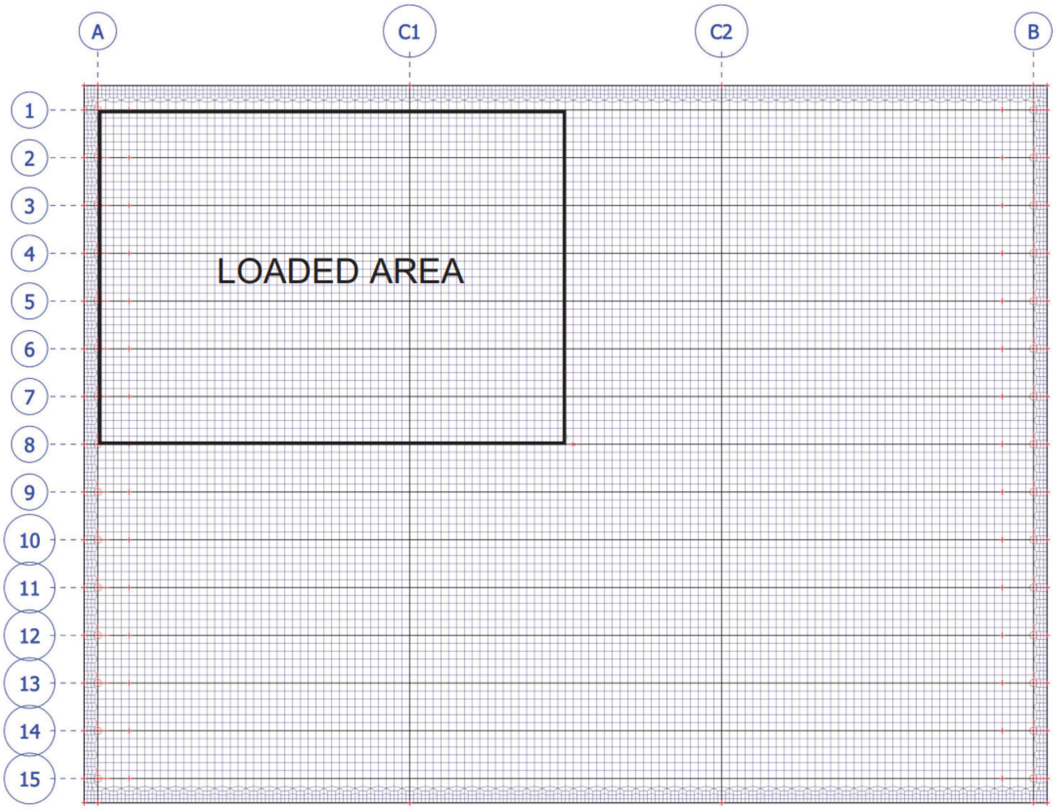

Figure 4.6: Top view of mesh, numbering of T-beams and loaded area (Reprinted from [10])

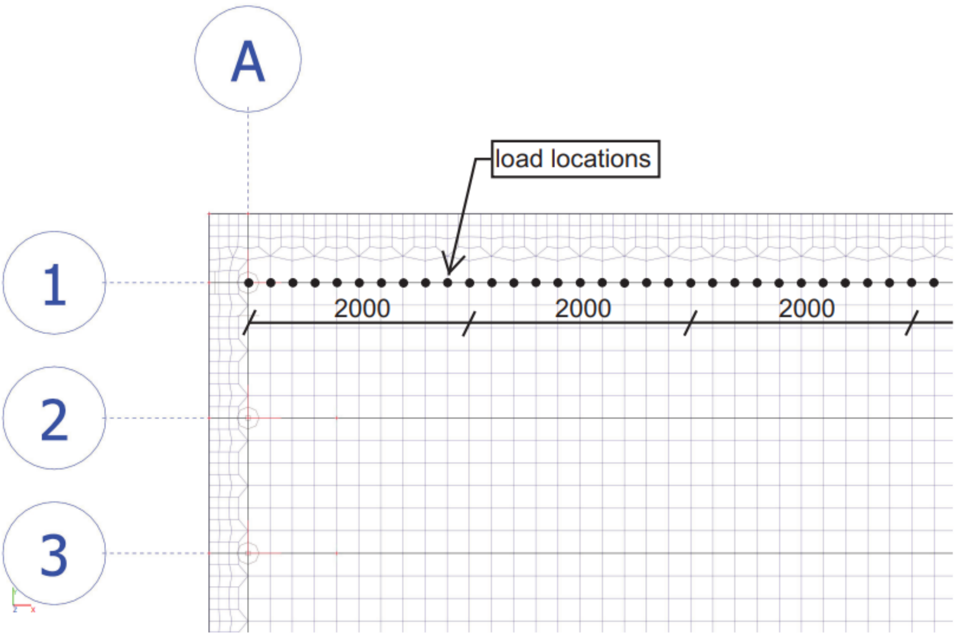

Figure 4.7: Detail of mesh and grid of load locations (grid only shown on T-beam 1) (measurements in mm) (Reprinted from [10])

The cross-section moment from the 2D linear Finite Element Model of the bridge deck in the horizontal plane is compared with the bending moment obtained from the 3D linear model of the bridge deck. From referring to figures 4.8 and 4.9, it was calaculated that the average variation in cross-section moment from the 2D linear bridge deck model in the horizontal plane from the 3D linear model of the bridge was 12.1 %. The average variation of the bending moment from applying unity load at different locations from T-beam 1 is 13.75% and T-beam 8 is 10.45% refer Table 4.6 and Table 4.7. Even though the average variation of the bending moment between 2D bridge deck model and 3D bridge deck model ranges from 10.45% - 13.75%, it is sufficient to study the load effects alone (i.e.) distribution of loads to adjacent beams. It should be duly noted that the variation could be caused due to uncertainty in the stiffness of the elastomeric bearing, cracks that could be present in the structural elements which are unnoticed causing discrepancy in the load distribution effects between FEM models and the real bridge structure. It should be duly noted there will always be a variation in load distribution between FEM models and real bridge structure due to uncertainties in the stiffness of the elastomeric bearing, unnoticed cracks in the structural elements, etc.

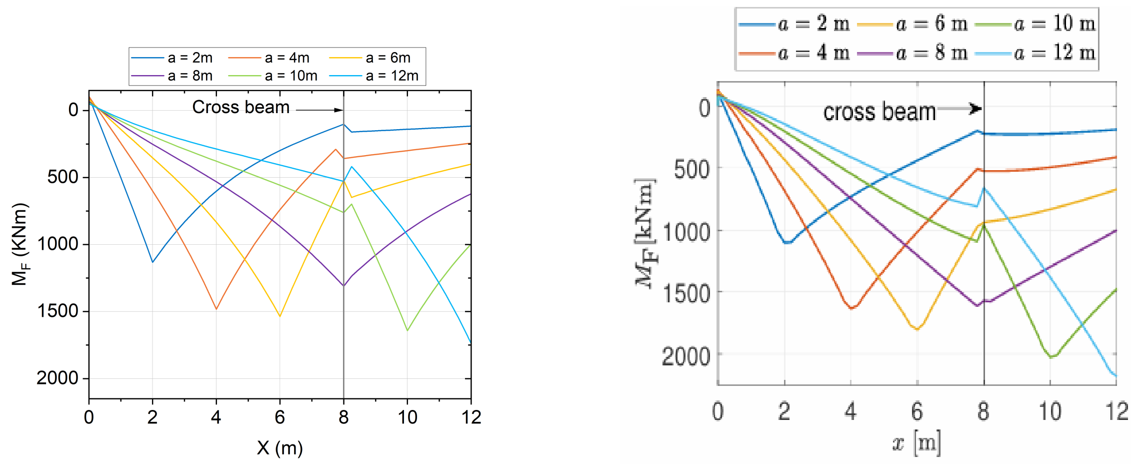

(a) Bending moment M_F, T-beam 1 in 2D horizontal plane bridge deck model

(b) Bending moment M_F, T-beam 1 in 3D linear bridge model (Reprinted from [10])

Figure 4.8: Comparison of bending moment of the 2D linear deck model with 3D linear model obtained from T-beam 1

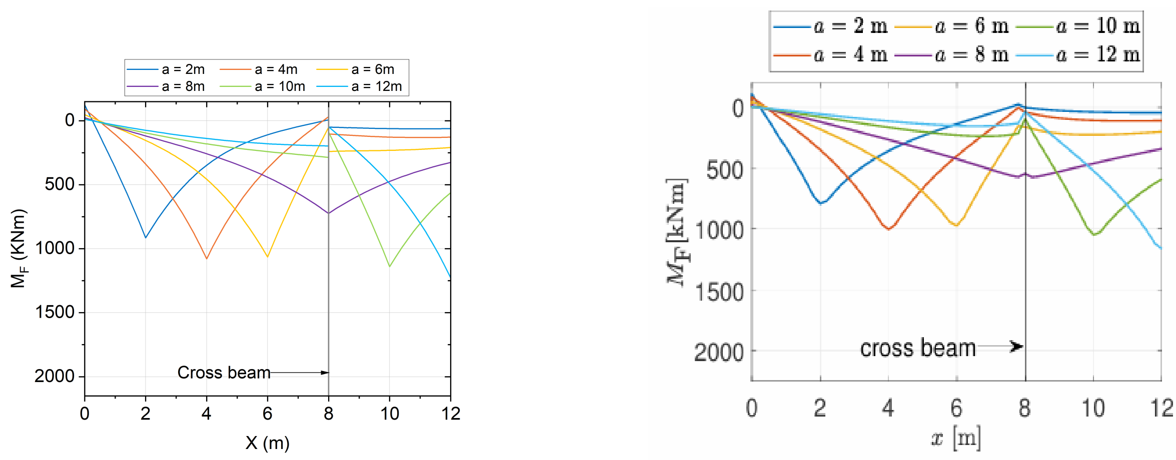

(a) Bending moment M_F, T-beam 8 in 2D horizontal plane bridge deck model

(b) Bending moment M_F, T-beam 8 in 3D linear bridge model (Reprinted from [10])

Figure 4.9: Comparison of bending moment of the 2D linear deck model with 3D linear model obtained from T-beam 8

* x - represents the distance from the endpoint of the bridge cross-section
* a - represents the distance from the centre of the support

Table 4.6: Bending moment for T-beam 1 with a unity load F = 1000 kN at different load locations (half span length)

Distance 'a' (m)	2D Bridge deck model (kNm)	3D Bridge deck model (kNm)	Variation (%)
2	1132.66	1120	1.13
4	1482.67	1650	10.14
6	1537.39	1750	12.15
8	1310.35	1600	22.1
10	1642.65	2000	17.8
12	1737.58	2150	19.18
		Average	13.75

Table 4.7: Bending moment for T-beam 8 with a unity load F = 1000 kN at different load locations (half span length)

Distance 'a' (m)	2D Bridge deck model (kNm)	3D Bridge deck model (kNm)	Variation (%)
2	915.37	770	18.87
4	1078.95	1000	7.89
6	1065.14	980	7.99
8	723.39	600	17.05
10	1140.18	1050	8.58
12	1227.88	1200	2.32
		Average	10.45

4.3. 2D FEM approach of a single girder in vertical plane

The individual girder element built in the vertical plane is a Non-Linear Finite Element Model. The source of non-linearity introduced is material non-linearity (i.e.) the material properties are functions of the state of stress or strain to account for cracking of concrete and yielding of reinforcements. The material properties used in the non-linear girder model are explained in the section below. Also, the meshing properties and convergence criteria used for non-linear analysis of the individual girder are explained in the sections below.

4.3.1. Constitutive modeling of concrete

The material property used for the Non-Linear Finite Element Analysis of the individual girder is presented in Table 4.8 and the aspects related to constitutive modeling of concrete are explained in Table 4.9. The tensile and compressive fracture energy are calculated in accordance with RTD 1016-1 [14] and Model code 2010 [12], refer Equations 4.1 - 4.2.
The terms G_f and G_{cm} are in Nmm/mm^2, while f_{cm} in N/mm^2.

$$G_f = 0.073 f_{cm}{}^{0.18} \tag{4.1}$$

$$G_{cm} = 250 G_f \tag{4.2}$$

The mean tensile strength and Young's modulus are calculated in accordance with NEN-EN 1992-1-1 [7], see Equations 4.3 - 4.4. Both f_{ctm} and E_{cm} are in N/mm^2.

$$f_{ctm} = 2.12 ln(1 + 0.1 f_{cm}) \tag{4.3}$$

$$E_{cm} = 22[f_{cm}/10]^{0.3} x 10^3 \tag{4.4}$$

For concrete, smeared crack with the total rotating crack model is adopted [8] as recommended by RTD 1016-1 [14]. The rotating crack model is adopted instead of fixed crack model since it's less susceptible to stress-locking and results in lower bound failure. For tensile behaviour of concrete, exponential-type softening diagrams are preferred since the cracks are more localised [14]. Hordijk softening curve is used for describing the tensile behaviour in my non-linear individual girder. For defining the compressive behaviour, parabolic stress-strain diagram is used refer Figure 4.10. The

Table 4.8: Concrete FEM material properties for integrated bridge deck model (Reprinted from [10])

T-beam			
mean compressive strength	f_{cm}	87.7	N/mm^2
mean tensile strength	f_{ctm}	4.83	N/mm^2
fracture energy[a]	G_f	0.163	Nmm/mm^2
compressive fracture energy	G_c	40.83	Nmm/mm^2
Poisson ratio	ν	0.15	-
Young's modulus	E	42200	N/mm^2
Slab and cross-beam			
mean compressive strength	f_{cm}	60.3	N/mm^2
mean tensile strength	f_{ctm}	4.13	N/mm^2
fracture energy[a]	G_f	0.150	Nmm/mm^2
compressive fracture energy	G_c	37.59	Nmm/mm^2
Poisson ratio	ν	0.15	-
Young's modulus	E	36768	N/mm^2

[a] alternatively referred to as mode I fracture energy , i.e. G^I_f

parabolic stress-strain diagram is used in order to reduce the mesh sensitivity during compressive strain localistaion [14]. A reduced poisson ratio to account for damage due to cracking is adopted [10]. All the constitutive model used for modelling the non-linear individual girder FEM model is enumerated in Table 4.9.

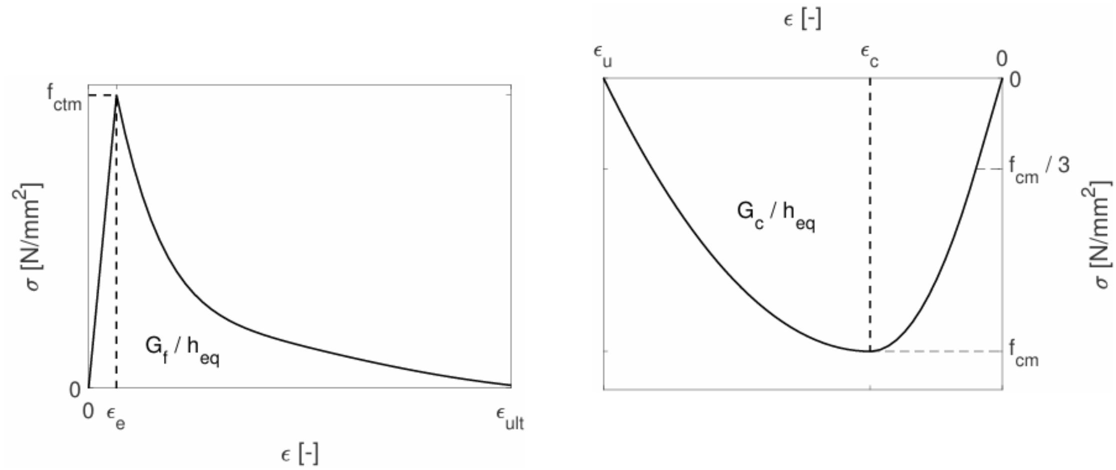

Figure 4.10: Concrete in tension and compression (Reprinted from [10])

Table 4.9: Concrete constitutive modelling (Reprinted from [10])

aspect	model used
tensile behaviour	Hordijk softening
compressive behaviour	parabolic stress-strain diagram
tension-compression interaction	Vecchio and Collins 1993
compression-compression interaction	-
Poisson's ratio	damage based
equivalent length (crack-band width)	Rots

4.3.2. Constituive modelling of reinforcements

The reinforcement and prestressing steel is modelled as embedded reinforcements. The advantage of modelling reinforcements as embedded reinforcement is that the mesh line doesn't have to

coincide with the position of the reinforcements. Also, the embedded reinforcement increases the stiffness of the mother element but does not increase the weight of the mother element. Therefore, all the reinforcements and prestressing tendons are modelled as embedded reinforcements.
The curved prestressing tendons are approximated as straight lines at an interval of 250 mm solved using the polynomial equation explained in Section 3.4. The constitute models used for defining the reinforcement and prestressing steel are enumerated in Table 4.10.

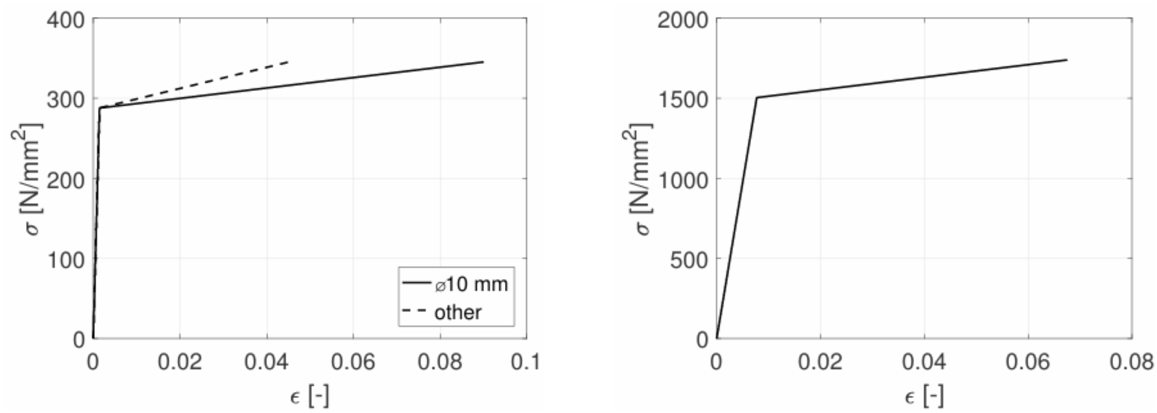

(a) Stress-strain reinforcement steel (b) Stress-strain prestressing steel

Figure 4.11: Stress-strain diagram reinforcement and prestressing steel (Reprinted from [10])

Table 4.10: Reinforcement and prestressing steel constitutive modelling [10]

aspect	model used
tensile behaviour and compressive behaviour	Von Mises plasticity
hardening hypotheis	strain hardening
bond-slip	full bond

4.3.3. Element types and sizes

Regular plane stress elements are opted for modeling the beams. Since the individual girder is modeled in 2D plane (x-y axis). For plane stress elements, the shear stresses perpendicular to the x-y direction are assumed to be zero. For 2D models, the effects in the z direction aren't considered, in other words only in-plane stresses are allowed. The variation in the cross-section of the T-girder refer 3.7 is introduced in the Finite Element Model using spatial thickness function, see Figure 4.14, Figure 4.15 and Figure 4.16.
The prestressing tendons and reinforcements are modeled using the element type 'embedded reinforcements' refer to Figure 4.18. The embedded reinforcements are used as the strains are calculated from the displacement field of the mother element ensuring perfect bonding between the reinforcement and surrounding element. Embedded reinforcement allows fine meshing as the reinforcement lines don't influence the meshing. The profile of the curved prestressing tendon is approximated by straight lines at an interval of 250 mm in the horizontal axis using the polynomial equation refer section 3.4. It is more suitable to use embedded reinforcement as finer mesh sizes are possible.
The maximum element size that can be used is 200 mm and it follows RTD 1016-1 [13]. The minimum from 24700/50 = 494 mm and 1150/6 = 191.6 mm, (i.e.) approximately 200 mm can used refer 4.11. However, there were formation of triangular elements which could cause stress concentration at these points. Hence, an element size of 50 mm is chosen refer to Figure 4.12.

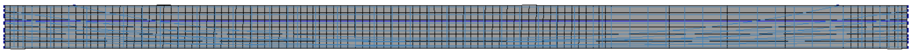

Figure 4.12: Mesh of the individual girder model in the vertical plane

Reinforced elastomeric bearing (supports)

For modelling the supports, the stiffness of the elastomeric bearing is used as an interface between the supports and the T-girder. The dimension of the elastomeric bearing are l = 306 mm, b = 206 mm and h = 15.5 mm (layer thickness). A linear support stiffness of 475 MN/m is assumed for all the analyses [10]. The shear modulus of the rubber G is equal to 0.9 N/mm^2. The support is modelled as a line interface and the corresponding stiffness in applied in vertical and horizontal directions, refer Equations 4.5 - 4.6.

$$K_{\mathsf{Y}} = \frac{K}{lb} = \frac{475 * 10^3}{306 * 206} = 7.54 N/mm^3 \tag{4.5}$$

$$K_{\mathsf{x}} = \frac{G}{h} = \frac{0.9}{2 * 15.5} = 0.029 N/mm^3 \tag{4.6}$$

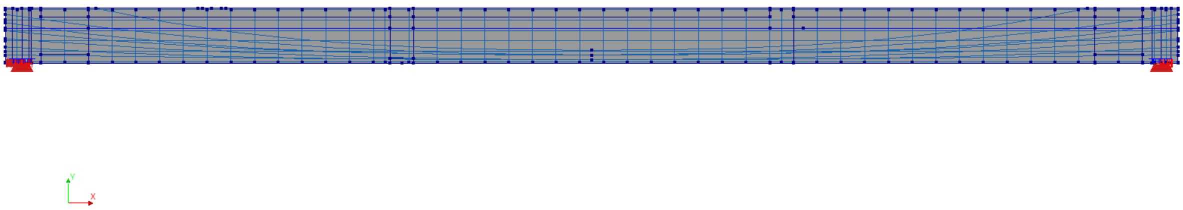

Figure 4.13: Geometry of individual girder model in the vertical plane

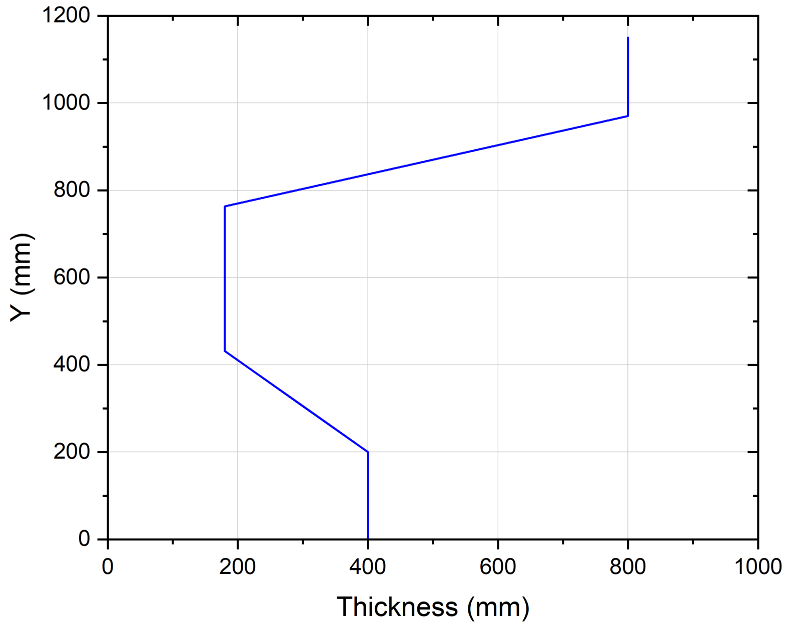

Figure 4.14: Spatial thickness function of T-beam girder

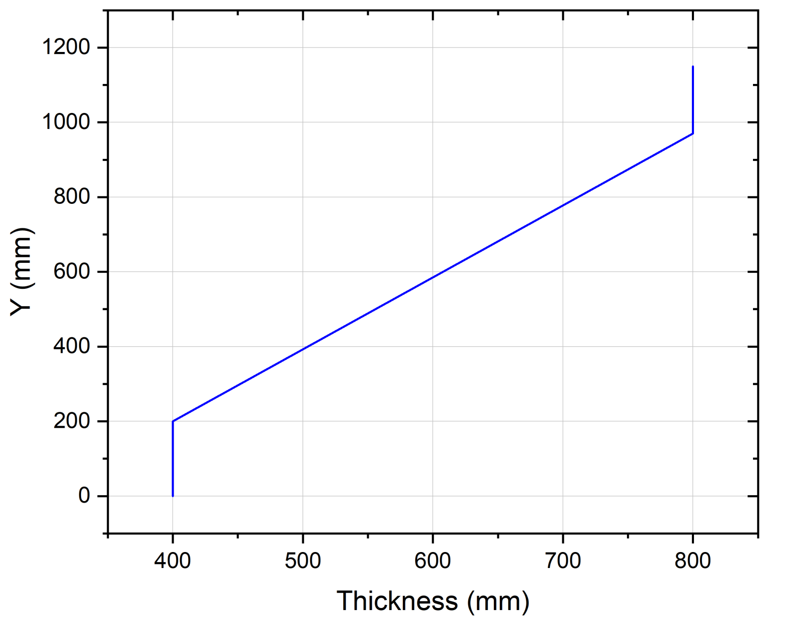

Figure 4.15: Spatial thickness function of intermediate beam

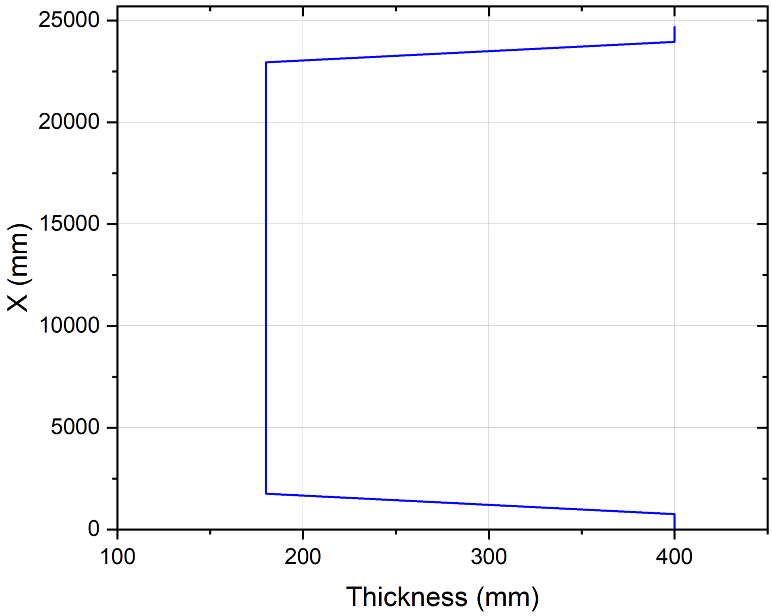

Figure 4.16: Spatial thickness function of the girder in the transition zone

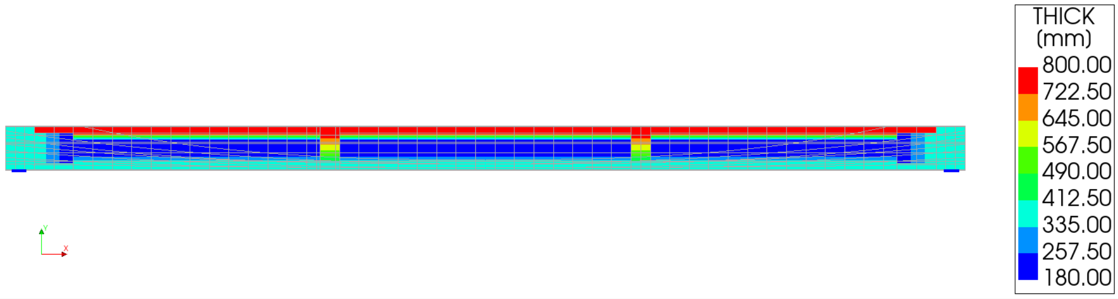

Figure 4.17: Variation of thickness along the T-girder

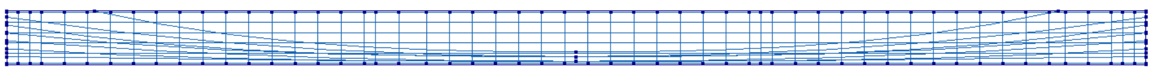

Figure 4.18: Embedded reinforcements - regular reinforcements, longitudinal and transverse prestressing tendons

Table 4.11: Maximum element size for beam structure

Beam structure	Maximum element size
2D modeling	min($l/50, h/6$)

Composed line elements

The composed line elements are mostly used for post-processing applications. Composed line elements are used for calculating the Cauchy stresses and bending moments at desired loactions. All types of elements and embedded reinforcements contribute for calculating the bending moment in the composed line elements. In the non-linear individual girder model, composed line elements are used for verifying the cross-section moment [8]. These composed line elements are modeled using line elements and are located at the centre of gravity of the T-beam (Figure 4.19) and no thickness is assigned to the composed line.

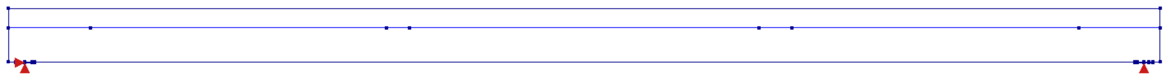

Figure 4.19: Composed line element in individual girder

4.3.4. Solution method

Non-Linear analysis is carried out for the individual girder model. In nonlinear Finite Element Analysis, the relation between the force vector and the displacement vector is not linear, this could be due to either materials or geometrical nonlinearity. Since the relation between force and displacement becomes nonlinear, the displacement mostly depends on displacement from previous step. Therefore to attain equilibrium in nonlinear analysis, an incremental-iterative solution procedure is used. For equilibrium iteration, two iterative methods are tested in the non-linear girder model - Newton-Raphson and Quasi-Newton. In Newton-Raphson method, the stiffness matrix is evaluated every iteration using the Equation 4.7 refer Figure 4.20. In the regular Newton-Raphson iteration, the stiffness equation (Equation 4.7) is recalculated at every step. This means that each prediction is based on the most recent known or predicted state, even if that state is not yet balanced.

$$K_i = \frac{\delta g}{\delta \Delta U} \tag{4.7}$$

where K_i is the stiffness matrix
δg is the change in out-of-balance force vector
$\delta \Delta U$ is the change in iterative displacement increment

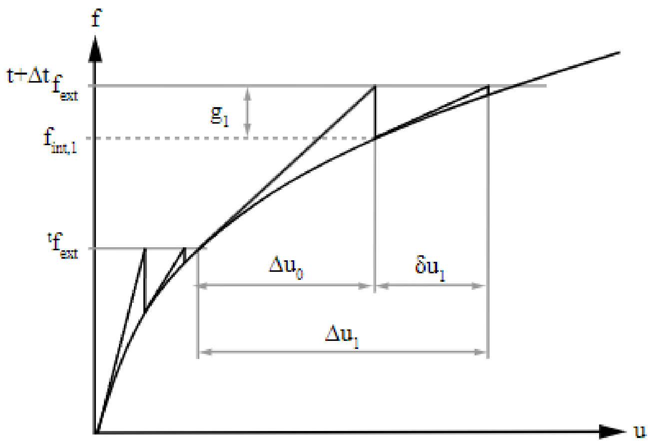

Figure 4.20: Regular Newton-Raphson iteration [8]

The Quasi-Newton or Secant methods use past solutions and force imbalances to improve accuracy. Unlike the regular Newton-Raphson method, it doesn't recalculate the stiffness matrix each time refer Figure 4.21. Instead, it uses known positions along the equilibrium path refer Equation 4.8.
The Newton-Raphson or Quasi-Newton method needs at least one criterion for equilibrium to be achieved. Therefore, certain convergence tolerance is set based on the specifications recommended

by RTD 1016-1 [14]. To attain equilibrium, it is recommended to satisfy either the energy-norm or the force-norm see Table 4.12.

$$K_{\text{i+1}} * \delta u_i = \delta g_i \tag{4.8}$$

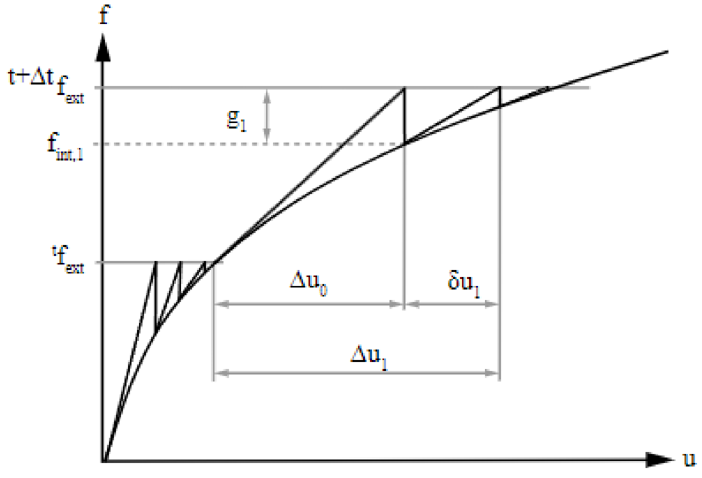

Figure 4.21: Qausi-Newton iteration [8]

In the Quasi-Newton solution method, the stiffness of the structure is determined from its positions along the equilibrium path. Where δu_i is the iterative displacement increment, and the change in out-of-balance force vector is calculated using the equation, see Equation 4.9,

$$\delta g_i = g_{\text{i+1}} - g_i \tag{4.9}$$

The line search method is adopted along with Newton-Raphson and Quasi-Newton method. Iteration methods need a good initial guess to work. If the guess is far off, especially with strong nonlinearities like cracking, they won't converge. Line Search algorithms can increase the convergence rate [8].

Table 4.12: Convergence criteria [14]

Convergence criteria	Tolerance
Force norm	0.01
Energy norm	0.001

4.4. Results from the single girder finite element model

4.4.1. Results from varying the solution method for non-linear analysis of 2D individual girder model

The number of non-convergence steps and the load versus displacement curve are checked by simulating the disconnected experimental test setup 4. The more accurate solution method that matches the disconnected experimental test setup 4 results is chosen.
The two solution methods investigated are regular Newton-Raphson and Quasi-Newton with Broyden-Fletcher-Goldfarb-Shanno (BFGS) method. The overview table of the step size and solution method is specified in Table 4.13. In phase 1, either energy norm or force norm is satisfied until the total failure load applied on the 2D individual non-linear girder. The phase 2 is extended as much as possible; either the energy norm or force norm is satisfied. The step size used for phase 1 is 0.05 while for phase 2, it is set to 0.02. The maximum number of iterations is fixed at 100. These step sizes and iteration limits are consistently applied throughout the non-linear analyses.

Table 4.13: Overview of analyses for element size and solution method

Model type	Phase	energy norm tolerance	force norm tolerance	satisfy all norms	step size	solution method
T4-50-NR-2D NLFEM	1	10^{-3}	10^{-2}	NO	0.05	Newton
	2	10^{-3}	10^{-2}	NO	0.02	-Raphson
T4-50-QNR-2D NLFEM	1	10^{-3}	10^{-2}	NO	0.05	Quasi
	2	10^{-3}	10^{-2}	NO	0.02	- Newton

* Note the element size used is 50 mm for all the Finite Element Models

From using the regular Newton-Raphson method, it can be inferred that the non-convergence of the point starts after the linear part. Also from Figure 4.23a, it can be seen that the non-convergence starts from step 13 refer Figure 4.23a. However, the load versus deflection curve from the 2D nonlinear individual girder model is comparable to the 3D nonlinear FEM model built and the experimental results of disconnected test 4, see Figure 4.22b.

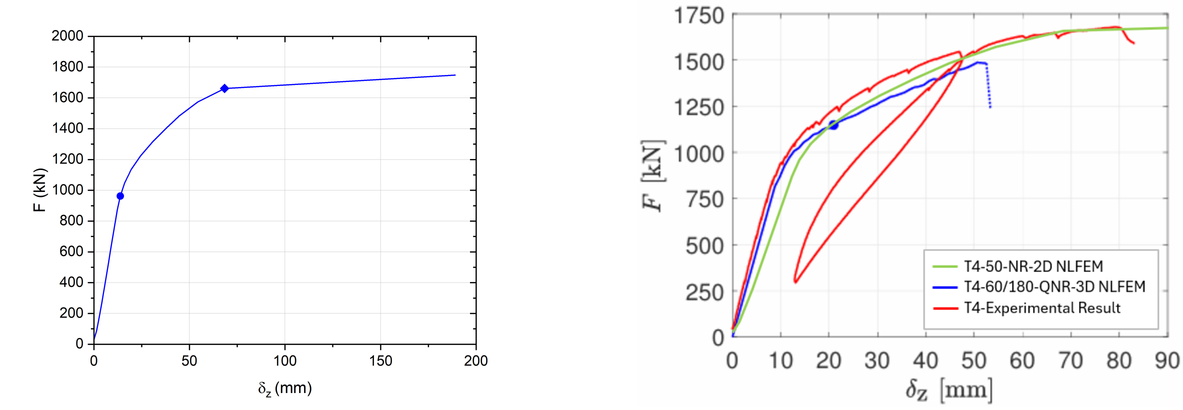

(a) Load versus deflection curve of 2D non-linear individual girder model from using regular Newton Raphson method

(b) Comparison of load versus deflection curve of test 4. Red and blue lines are reprinted from [10]

Figure 4.22: Load versus deflection curve obtained from Newton-Raphson solution method
The dot represents the last converged point and the square symbol indicates the start of phase 2

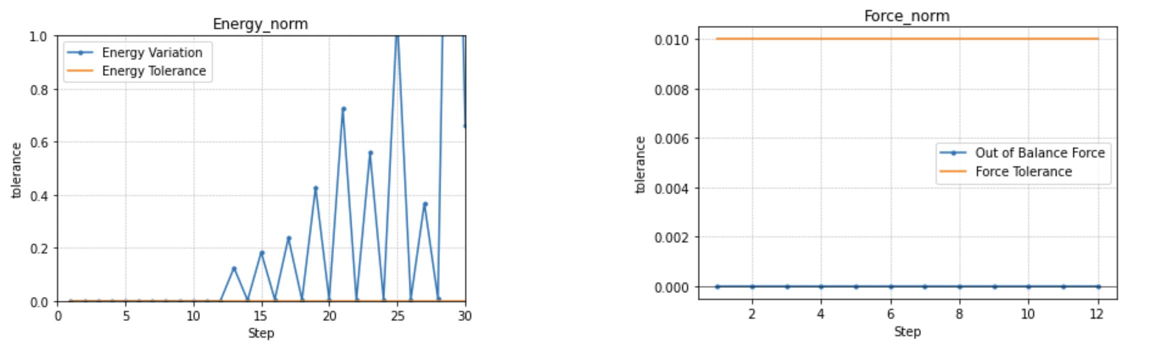

(a) Energy norm from using Newton-Raphson solution method

(b) Force norm from using Newton-Raphson solution method

Figure 4.23: Convergence Newton-Raphson solution method

The Quasi-Newton solution used for the analyses gives a similar behavior (trend of load versus deflection curve) when compared to the experimental results from disconnected test 4, see Figure 4.24b. Also, all the points converge until the failure load is reached (step 20) refer Figure 4.25a. The non-converge starts only during phase 2. It can be concluded that Quasi-Newton solution method used gives similar results when compared to the experimental result. Also, the rate of convergence is more when compared to the regular Newton-Raphson method.

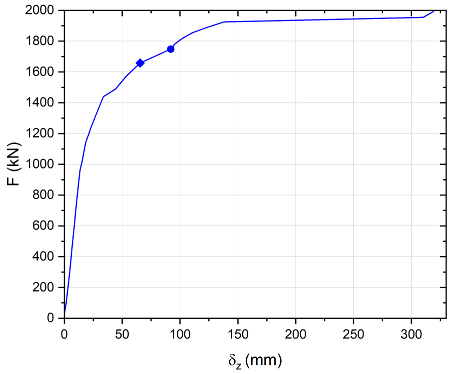

(a) Load versus deflection curve of 2D non-linear individual girder model from using Quasi-Newton method

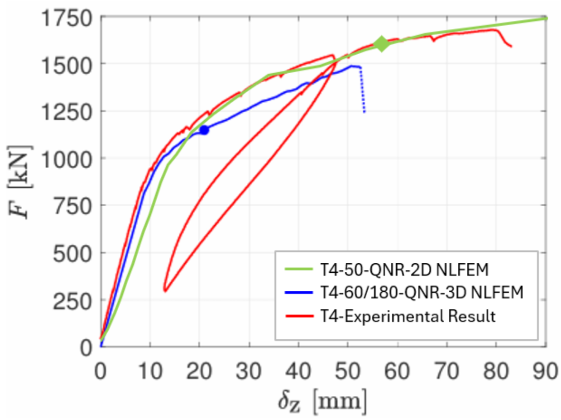

(b) Comparison of load versus deflection curve of test 4. Red and blue lines are reprinted from [10]

Figure 4.24: Load versus deflection curve obtained from Quasi-Newton solution method
The dot represents the last converged point and the square symbol indicates the start of phase 2

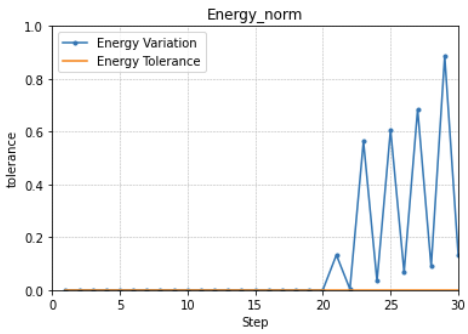

(a) Energy norm from using Newton-Raphson solution method

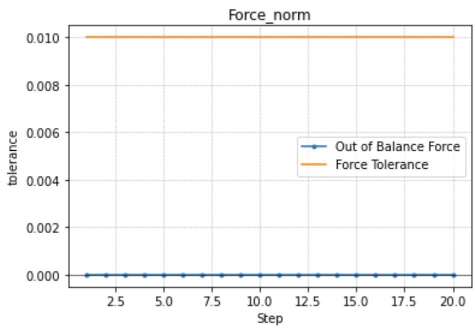

(b) Force norm from using Newton-Raphson solution method

Figure 4.25: Convergence Quasi-Newton solution method

4.4.2. Results from simulating disconnected T-beam tests

To check the Non-linear Finite Element Model of the individual girder built, the experimental test setups related to disconnected T-beam tests (tests 4, 5, 6 and 7) were simulated in the 2D non-linear individual girder model in the vertical plane refer Figure 3.9. The overview of the experimental test setup of disconnected T beams is enumerated in the Table 3.3. The overview of the FEM models used for simulating the experimental test setup is presented below.
It was also inferred from the analyses that the last converged step (step 20) from using the Quasi-Newton solution method gave the ultimate failure load when compared to the experimental test result. Hence, the load attained at the last converged step in the non-linear analysis will be considered as the maximum failure load attained from the 2D non-linear individual girder model.

Table 4.14: Overview of FEM models used for simulating experimental tests

FEM Model Used	Disconnected T-beam test	Element Size	Solution Method	Model Type
T4-50-QNR-2D NLFEM	4	50	Quasi-newton method	2D Non-linear
T4-60/180-QNR-3D NLFEM [10]	4	60/80	Quasi-newton method	3D Non-linear
T4-Experimental Result	4	-	-	Original structure
T5-50-QNR-2D NLFEM	5	50	Quasi-newton method	2D Non-linear
T5-60/180-QNR-3D NLFEM [10]	5	60/80	Quasi-newton method	3D Non-linear
T5-Experimental Result	5	-	-	Original structure
T6-50-QNR-2D NLFEM	6	50	Quasi-newton method	2D Non-linear
T6-60/180-QNR-3D NLFEM [10]	6	60/80	Quasi-newton method	3D Non-linear
T6-Experimental Result	6	-	-	Original structure
T7-50-QNR-2D NLFEM	7	50	Quasi-newton method	2D Non-linear
T7-60/180-QNR-3D NLFEM [10]	7	60/80	Quasi-newton method	3D Non-linear
T7-Experimental Result	7	-	-	Original structure

4.4.3. Disconnected beam test 4

The result from simulating the experimental test setup 4 are summarised in Table 4.15. The failure load for the analyses is chosen as the last point converged in the non-linear analysis. The ultimate failure attained from the 2D non-linear individual girder model is 98 % of the ultimate load attained from the experimental test. From observing the load versus deflection curve (refer Figure 4.24b), the curve obtained from the 2D individual girder model closely matches that of the experimental result in the plastic region when compared to the elastic region.

Table 4.15: Results from analysis of T4-50-QNR-2D NLFEM

analysis	Deflection mm	Ultimate load kN
T4-50-QNR-2D NLFEM	53.4	1658.13
T4-60/180-QNR-3D NLFEM [10]	50.6	1486
T4-Experimental Result	79	1678

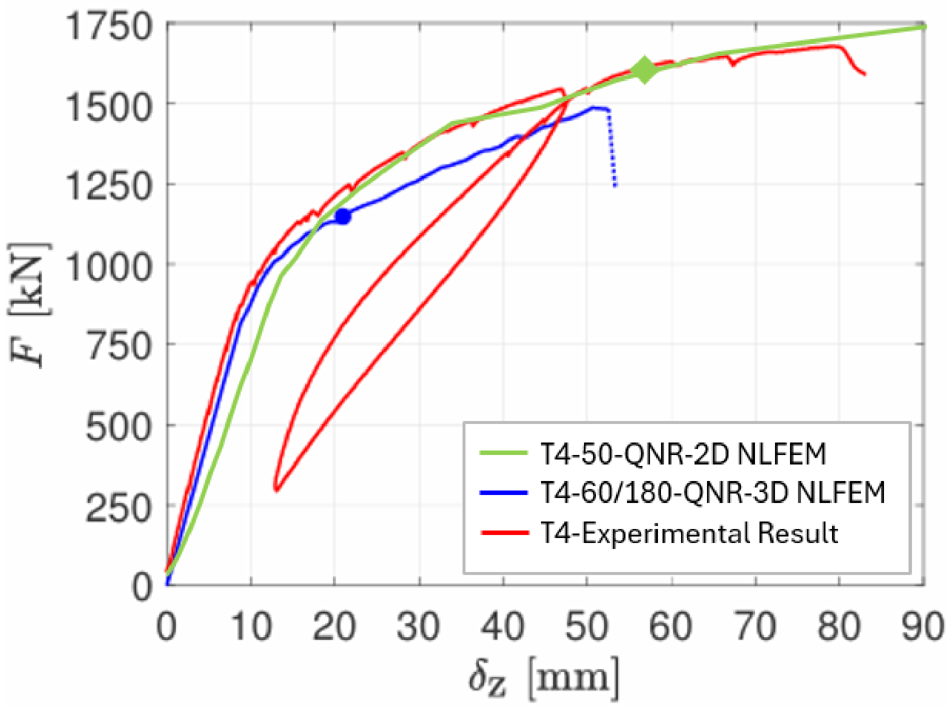

Figure 4.26: Load versus deflection curve obtained from Quasi-Newton solution method
The dot represents the start of phase 2 and the square symbol indicates the last converged point. Red and blue lines are reprinted from [10]

Cracking strains (cracking)

The cracking strains are observed at the load steps where there is a reduction in stiffness in the load versus deflection curve obtained from the non-linear analysis of the 2D individual girder model in the vertical plane. The cracks initiate from the bottom of the T-girder (flexural cracks) due to the sagging bending moment of the T-girder refer to Figure 4.27. At this load (F = 964.4 kN), a reduction in stiffness is observed from the load versus deflection curve refer to Figure 4.26. A major decrease in stiffness is observed at load F = 1439.2 kN, this is because of flexural shear crack progressing from the bottom of the beam and extending to the left support support (refer Figure 4.27b). Ultimately, the T-girder fails due to a huge flexural shear crack extending from the location of load application to the end support refer to Figure 4.31c and it is similar to that of the experimental test result of disconnected T-beam test 4, see Figure 4.28.

Figure 4.28: Flexural shear failure of T-beam test 4. Intermediate cross-beam on the left side, end support on the right side (reprinted from [10])

(a) F = 963.4 kN, δ_z = 13.5 mm, Flexural crack initiation

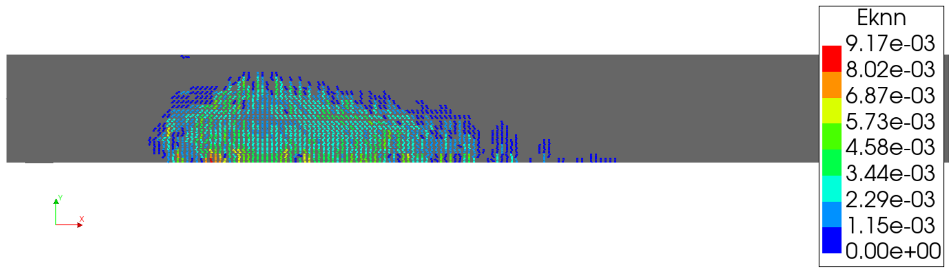

(b) F = 1439.2 kN, δ_z = 33.8 mm

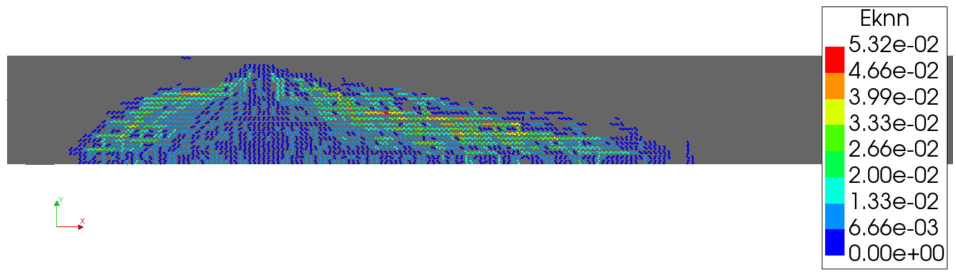

(c) F_u = 1572.3 kN, δ_u = 53.4 mm

Figure 4.27: T4-50-QNR-2D NLFEM, crack strains Ek_{nn}
(end crossbeam on the left side and intermediate crossbeam on the right side)

Yielding of reinforcement and prestressing tendons

The stresses of both regular reinforcement and prestressing steel at failure load are given in Figure 4.29. The regular reinforcements (longitudinal reinforcements) begin yielding at a load of 1140 kN at the bottom of the cross-section. The stirrups start yielding at a load of 1487 kN at the locations where flexural shear cracks form between the load application point and the support, and between the load application point and the intermediate crossbeam.
The maximum stress in the regular reinforcement S_{xx} = 305 N/mm^2 refer to Figure 4.29b. It can also be observed that the longitudinal reinforcement at the top is starting to yield due to compression.
The prestressing tendons start to yield at the bottom cross-section at the load level F = 1487 kN and the maximum stress obtained in the tendons S_{xx} = 1570 N/mm^2 at the failure load (see Figure 4.29a). There is no fracture observed in either prestressing tendons and regular reinforcements as the ultimate strain doesn't exceed 0.9 ϵ_u (see Figure 4.11).

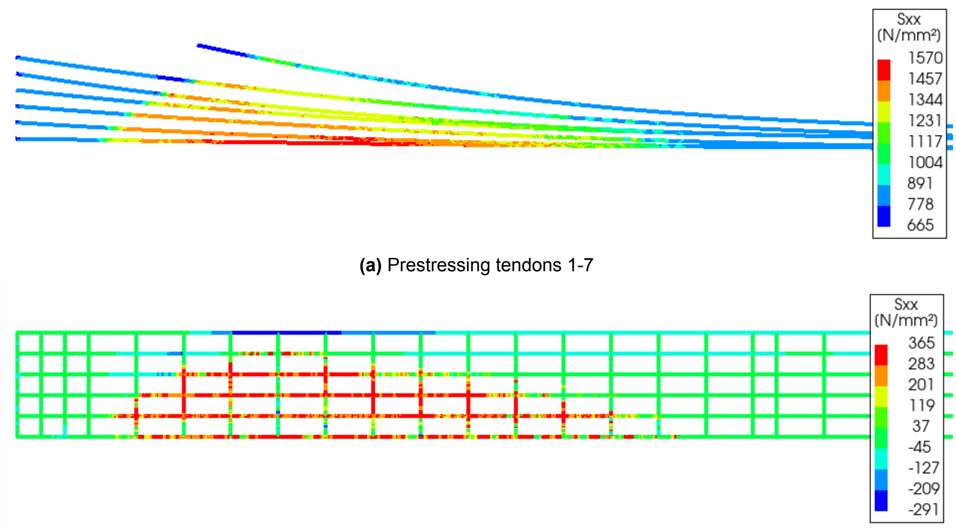

(a) Prestressing tendons 1-7

(b) Regular reinforcements

Figure 4.29: T4-50-QNR-2D NLFEM, stress S_{xx} embedded reinforcements, F_u = 1572.3 kN, δ_u = 53.4 mm (end crossbeam on the left side and intermediate crossbeam on the right side)

4.4.4. Disconnected beam test 5

The results from simulating the experimental test 5 of disconnected beam is presented in Table 4.18. The failure load calculated from the 2D non-linear girder model is 1810 kN, which is 6.28 % higher than what was obtained from the experimental result. However, the deflection attained was half that of the experimental test result obtained. The deflection from the 2D individual girder model varies significantly (50 % less) from that of the experimental result. Whereas the displacement from the 3D girder model varies by 29.7% when compared to the displacement obtained from the experimental test setup. However, the load versus deflection curve obtained from the 2D individual girder model closely follows both the 3D non-linear individual girder and the experimental result, see Figure 4.30.

Table 4.16: Results from analysis of T5-50-QNR-2D NLFEM

analysis	Deflection mm	Ultimate Failure load kN
T5-50-QNR-2D NLFEM	131.1	1810
T5-60/180-QNR-3D NLFEM [10]	53.3	1505
T5-Experimental Result	65	1703

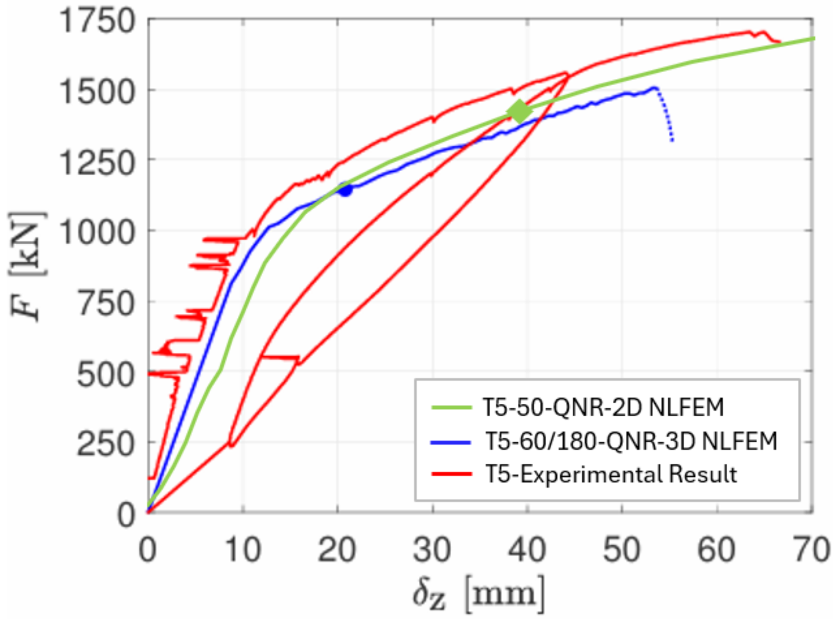

Figure 4.30: Load versus deflection curve obtained from Quasi-Newton solution method
The dot represents the start of phase 2 and the square symbol indicates the last converged point. Red and blue lines are reprinted from [10]

Cracking strains (cracking)

The cracks progress from the bottom of the T-girder at the location of the load application. The flexural/bending cracks occur due to sagging of the T-girder refer to Figure 4.31a at F = 1064kN. At this load step, the first reduction in stiffness is observed in the force versus deflection curve (see Figure 4.30). The flexural shear cracks are observed when the loading is further increased (see Figure 4.31b). Finally, the T-girder fails due to a flexural shear crack extending from the support to the location of the load applied at the ultimate failure load of 1810 kN. The failure pattern is similar to that of the experimental test result of disconnected T-beam test 5, refer to Figures 4.31 - 4.32.

Figure 4.32: Flexural shear failure of T-beam test 5. Intermediate cross-beam on the left side, end support on the right side (reprinted from [10])

Yielding of reinforcement and prestressing tendons

The longitudinal reinforcement starts yielding at the bottom cross-section at the load F = 1064 kN when the flexural crack starts to appear. The stirrups start yielding at a load F = 1419 kN at the horizontal locations between the load application point and the support, as well as between the load application point and the intermediate crossbeam, when the flexural shear crack occurs. At the ultimate load F_u = 1810 kN, the maximum stress s_{xx} obtained for the regular reinforcement is 382 N/mm^2.

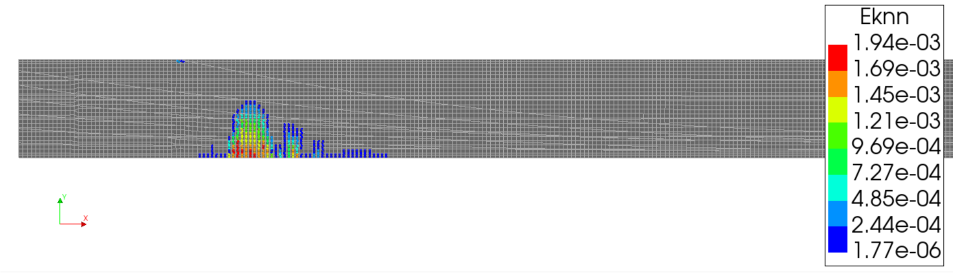

(a) F = 1064 kN, δ_z = 16.5 mm, Flexural crack initiation

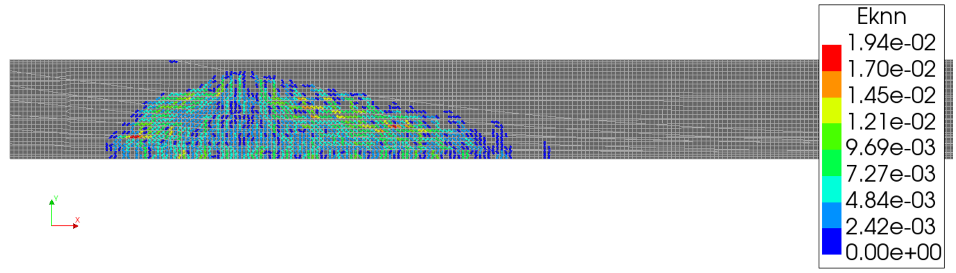

(b) F = 1419.2 kN, δ_z = 39.1 mm

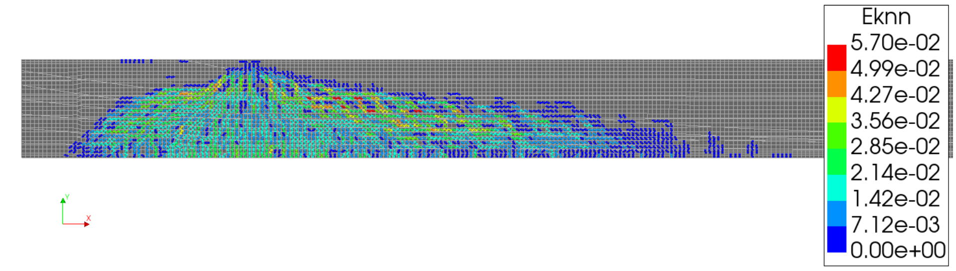

(c) F_u = 1810 kN, δ_z = 131.1 mm

Figure 4.31: T5-50-QNR-2D NLFEM, crack strains Ek_{nn}
(end crossbeam on the left side and intermediate crossbeam on the right side)

For the prestressing tendons, the tendons first start yielding at the bottom cross-section at the load F = 1597 kN due to presence of flexural shear cracks. The maximum stress attained by the prestressing tendons at the ultimate load (F_u = 1810 kN) is S_{xx} = 1576 N/mm^2. The stresses of regular reinforcement and prestressing tendons are given in Figure 4.37.
No fracture is observed in either prestressing tendons or regular reinforcements.

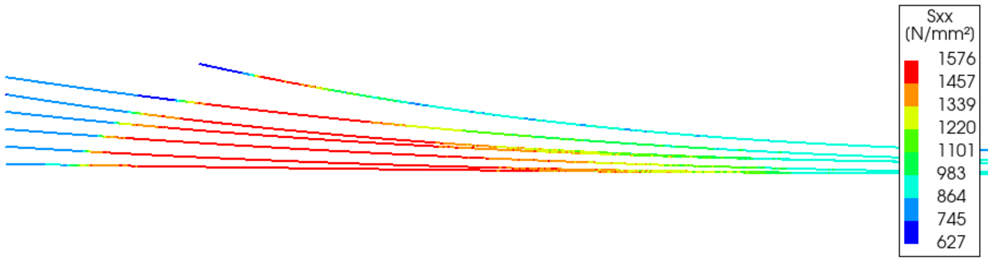

(a) Prestressing tendons 1-7

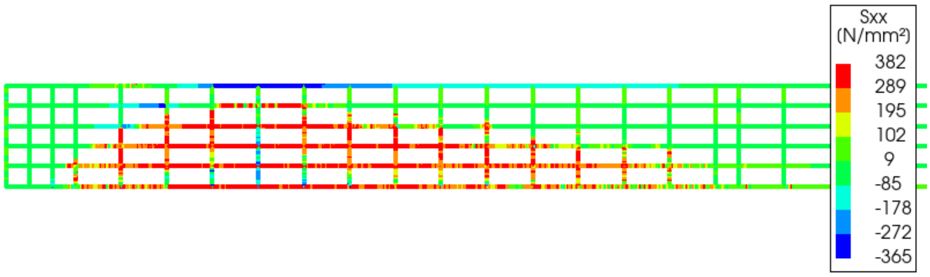

(b) Regular reinforcements

Figure 4.33: T5-50-QNR-2D NLFEM, stress S_{xx} embedded reinforcements, F_u = 1810 kN, δ_u = 131.1 mm (end crossbeam on the left side and intermediate crossbeam on the right side)

4.4.5. Disconnected beam test 6

The 2D non-linear individual girder model gave a more accurate result than the 3D non-linear girder model. The failure load attained from the 2D non-linear girder model was 80 % of the experimental test setup. Whereas the failure load attained from the 3D non-linear girder model was 84.44 % of the ultimate load attained from the experimental test 6.

Table 4.17: Results from analysis of T6-50-QNR-2D NLFEM

analysis	Deflection mm	Ultimate Failure load kN
T6-50-QNR-2D NLFEM	39.1	1663.3
T6-60/180-QNR-3D NLFEM [10]	52.0	1498
T6-Experimental Result	74	1774

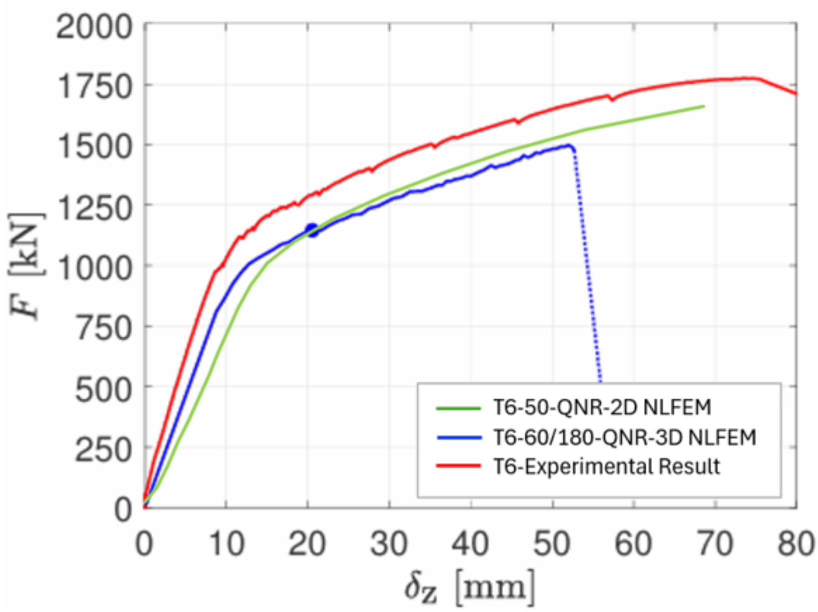

Figure 4.34: Load versus deflection curve obtained from Quasi-Newton solution method
The dot represents the start of phase 2 and the square symbol indicates the last converged point. Red and blue lines are reprinted from [10]

Cracking strains (cracking)

The progression of cracking in the individual T-girder is shown in Figure 4.35. The first cracking starts from the bottom part directly beneath the application of load refer to Figure 4.35a and there is reduction in stiffness at this load step (F = 1017 kN), see Figure 4.34. The bending crack (flexural crack) is then extended diagonally till the position of support and intermediate crossbeam, see Figure 4.35b. The T-girder fails due to a large flexural shear crack at the ultimate load of F_u = 1663 kN which is similar to that of the experimental test (refer Figure 4.35c and Figure 4.36).

Figure 4.36: Flexural shear failure of T-beam test 6. Intermediate cross-beam on the left side, end support on the right side (reprinted from [10])

Yielding of reinforcement and prestressing tendons

The regular longitudinal reinforcement starts to yield at a load of F = 1017 kN, starting from the bottom cross-section due to the sagging bending moment, consistent with the other test cases. The stirrups start yielding at a load of F = 1570kN, specifically in the diagonals between the support and load location, and between the intermediate crossbeam and load location. At the ultimate load of F_u = 1663 kN, the regular reinforcement reaches a maximum stress of s_{xx} = 365 N/mm^2 refer to Figure 4.41b. The prestressing tendons also begin yielding at F = 1570 kN, starting from the bottom cross-section, and achieve a maximum stress of 1571 N/mm^2 at the ultimate load (refer Figure 4.41a).
No fractures are observed in either the regular reinforcements or the prestressing tendons.

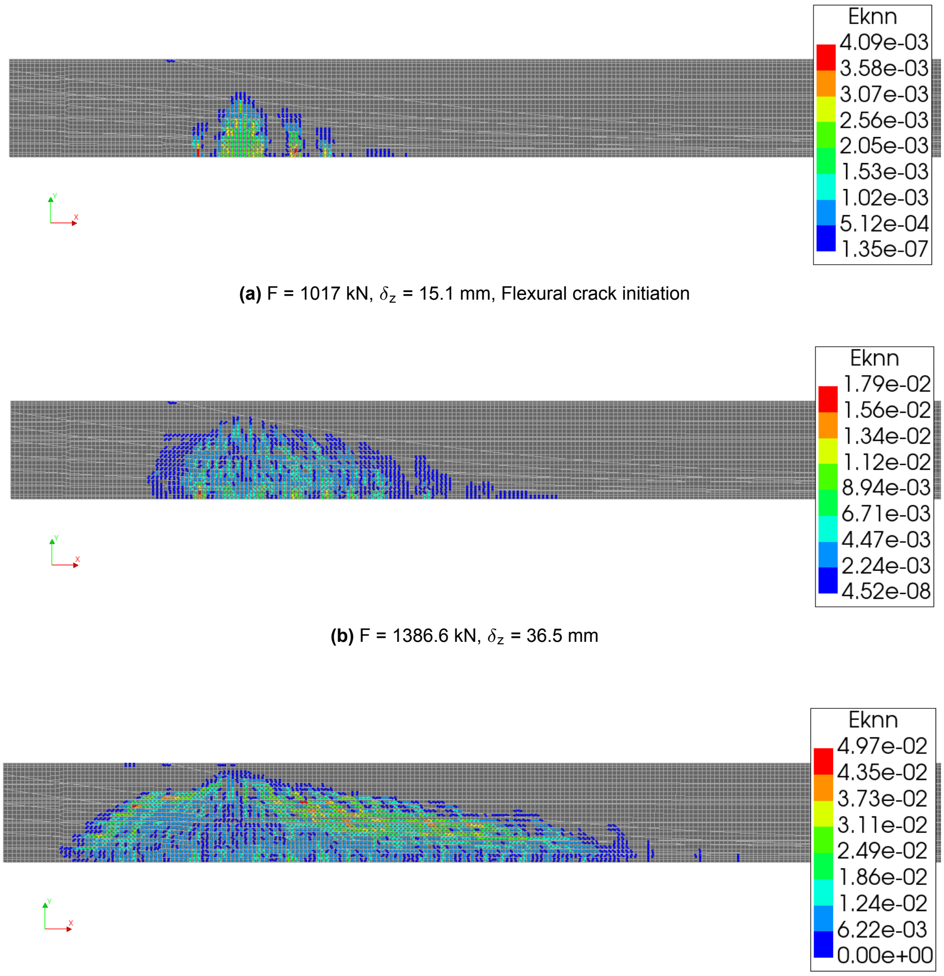

(a) F = 1017 kN, δ_z = 15.1 mm, Flexural crack initiation

(b) F = 1386.6 kN, δ_z = 36.5 mm

(c) F_u = 1663.3 kN, δ_u = 68.6 mm

Figure 4.35: T6-50-QNR-2D NLFEM, crack strains Ek_{nn}
(end crossbeam on the left side and intermediate crossbeam on the right side)

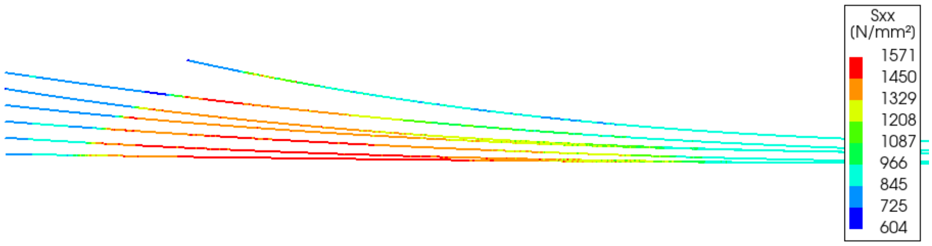

(a) Prestressing tendons 1-7

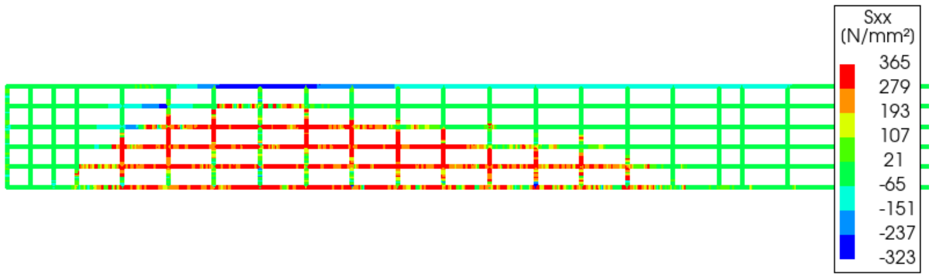

(b) Regular reinforcements

Figure 4.37: T6-50-QNR-2D NLFEM, stress S_{xx} embedded reinforcements, F_u = 1663.3 kN, δ_u = 39.1 mm (end crossbeam on the left side and intermediate crossbeam on the right side)

4.4.6. Disconnected beam test 7

From simulating the experimental test 7, it was observed that the ultimate failure load obtained from the 2D non-linear individual girder model was 6.16 % higher than the experimental test result. The failure load attained from the 3D non-linear individual girder model was 17.7% higher than the experimental failure load attained. The load versus deflection curve obtained from the 2D non-linear individual girder model follows more closely with the 3D non-linear individual girder model rather than with the experimental result, see Figure 4.38.

Table 4.18: Results from analysis of T7-50-QNR-2D NLFEM

analysis	Deflection mm	Ultimate Failure load kN
T7-50-QNR-2D NLFEM	89.4	1085
T7-60/180-QNR-3D NLFEM [10]	162.6	1203
T7-Experimental Result	132	1022

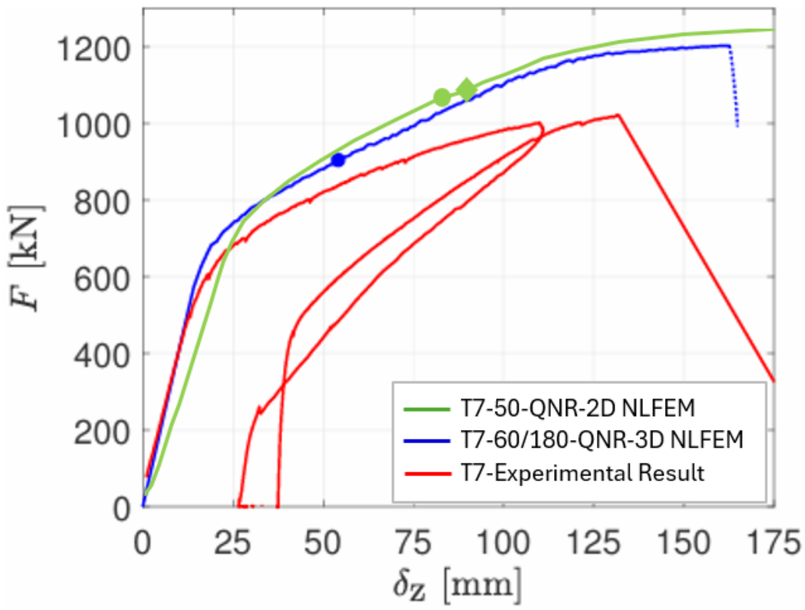

Figure 4.38: Load versus deflection curve obtained from Quasi-Newton solution method
The dot represents the start of phase 2 and the square symbol indicates the last converged point. Red and blue lines are reprinted from [10]

Cracking strains (cracking)

As observed in previous disconnected T-beam tests, cracks progress similarly, starting with flexural cracks and evolving into flexural shear cracks. The flexural cracks initiate at the bottom of the T-girder at a load of F=745 kN and progress into flexural shear cracks at F=958.7 kN. These cracks extend towards the locations of the load, supports, and intermediate crossbeam. Correspondingly, a reduction in stiffness is observed at these loads (see Figure 4.38). The failure of the T-girder is due to the formation of huge flexural shear cracks extending between the support and the point of load applied as well as between crossbeam and point of load applied (refer Figure 4.39).

Figure 4.40: Flexural shear failure of T-beam test 7. Intermediate cross-beam on the left side, end support on the right side (reprinted from [10])

Yielding of reinforcement and prestressing tendons

The longitudinal reinforcements at the bottom begin to yield at load F = 798 kN due to flexural cracks and the reduction in stiffness in the load versus deflection curve can also be observed at this load step. The stirrups start yielding at load F = 958 kN when flexural shear cracks occur. At the ultimate load F_u = 1085 kN, the maximum stress S_{xx} for regular reinforcement is 352 N/mm^2 and for prestressing steel is 1577 N/mm^2 refer to Figure 4.41.
No fracture is observed for prestressing tendons and regular reinforcements as the ultimate strain is not exceeded.

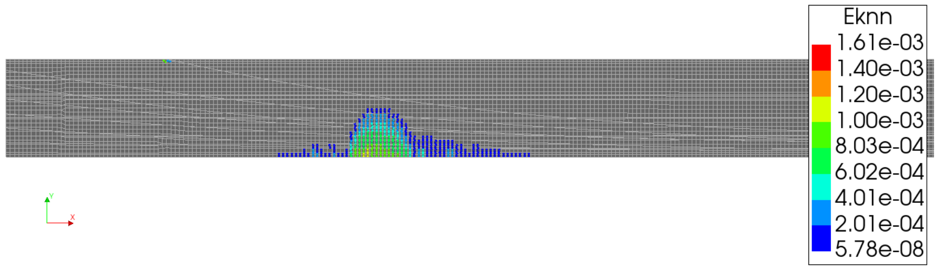

(a) F = 745.4 kN, δ_z = 27.7 mm, Flexural crack initiation

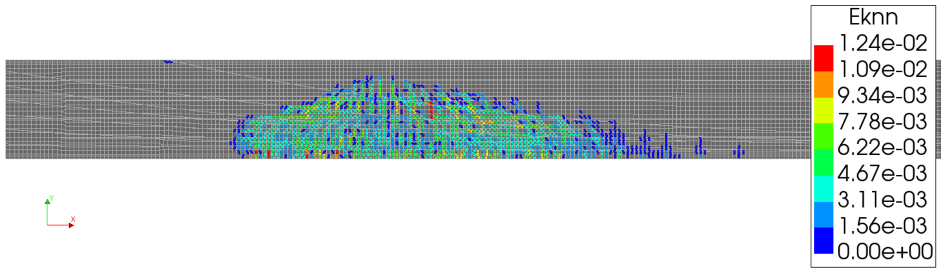

(b) F = 958.7 kN, δ_z = 58.4 mm

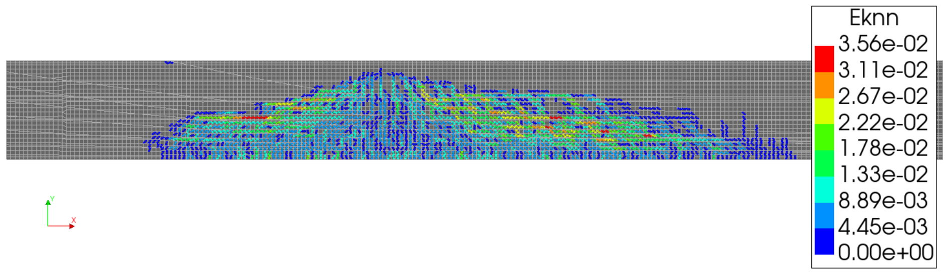

(c) F_u = 1085.1 kN, δ_u = 89.4 mm

Figure 4.39: T7-50-QNR-2D NLFEM, crack strains Ek_{nn}
(end crossbeam on the left side and intermediate crossbeam on the right side)

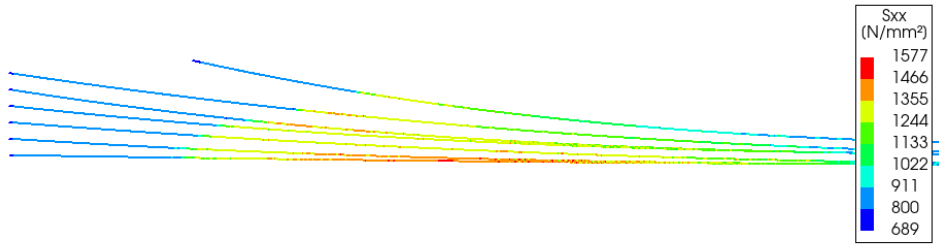

(a) Prestressing tendons 1-7

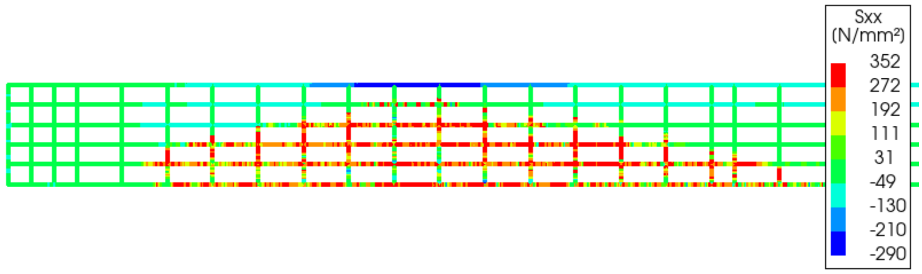

(b) Regular reinforcements

Figure 4.41: T7-50-QNR-2D NLFEM, stress S_{xx} embedded reinforcements, F_u = 1085 kN, δ_u = 89.4 mm (end crossbeam on the left side and intermediate crossbeam on the right side)

4.5. Summary and conclusion

This section summarises the modelling approach for the 2D bridge deck model and 2D non-linear individual girder model. The results from comparing the 2D bridge deck model with 3D bridge deck model, optimising solution method, and comparison of 2D individual girder model with both 3D non-linear girder model and the case study (Vecht bridge) is presented here.
Modelling of 2D bridge deck model in the horizontal plane:

- The 2D bridge deck model built using orthotopic plate element method (shape orthotropy introduced via geometrical orthotropy and not material orthotropy) behaved similar to that of the 3D linear bridge deck model [10].
- The bending moment distribution form the 2D bridge deck model varied from the 3D bridge deck model between 10.45 % - 13.75%. The 2D bridge deck model is sufficient for studying the load distribution effects alone.
- The percentage variation is acceptable and sometimes unavoidable due to the uncertainty in stiffness of the elastomeric bearing, unnoticed cracks in bridge, etc

Modelling of 2D bridge individual girder model in the vertical plane: Optimising the solution method:

- Two solution methods - Regular Newton Raphson and Quasi-Newton Raphson method is tested in the non-linear individual girder model. It was found that more points converged when Quasi-Newton Raphson method was used.
- Also, the load vs deflection curve obtained from using Quasi-Newton Raphson solution method more accurately followed the load vs deflection curve obtained from the experimental result of the Vecht bridge.

Results from the 2D non-linear girder model compared with the 3D non-linear girder model and the disconnected beam test:

- The ultimate failure load predicted by the 2D non-linear individual girder model closely matched the experimental test results, outperforming the 3D non-linear model. The variation in ultimate failure load between the 2D non-linear model and experimental data was within 10% for all disconnected T-beam tests, except for disconnected beam test 6 where the variation reached 20%. The average variation is calculated to be 9.86%.

- However, the deflection observed varied by half of that recorded in the experimental results from the disconnected beam tests for most of the cases.
- The reduction in load versus deflection observed in all the disconnected beam tests, from the non-linear analyses of the 2D individual girder, is due to the progression of flexural cracks followed by flexural shear cracks. All the individual T-girders showed failure due to flexural shear cracks forming between the end support and the load application point. This behavior is consistent with the experimental results obtained.
- It was also observed that both regular reinforcement and prestressing tendons started yielding at the locations of the cracks. However, no fracture was observed in either the prestressing tendons or the regular reinforcement, as the ultimate strains were not exceeded.

5

Correlating the individual girder model and the bridge deck model

In this chapter, the correlation of non-linear individual girder model in the vertical plane with the linear bridge deck model in the horizontal plane is studied. For this purpose, the results from the full-scale collapse test of the Vecht bridge are utilised. In particular, the experimental test setup 1 is used for comparing the results obtained. Different methods used for finding the equivalent distributed load that can be applied on the non-linear individual girder obtained from the load distribution of the bridge deck model in the horizontal plane is elaborated here. The most optimal method for correlating the individual girder model and the bridge deck model is explained in this section as well. Finally, the Non-Linear Finite Element Approach developed to assess the system behavior of the prestressed T-girder bridge is elaborated in this chapter.

5.1. Shear resistance from the 2D bridge deck model in the horizontal plane from experimental test setup 1

5.1.1. Results from linear bridge deck model from simulating experimental test setup 1

The experimental test setup 1 is simulated in the 2D bridge deck model refer to Figure 3.10 by applying the failure load at the location of 4000 mm from the support, see section 3.5.2.
The bending moment is maximum at the location of the load applied (i.e.). at 4000 mm from the support as expected refer Figure 5.1. It can be inferred that the bending moment changes from sagging to hogging at 8100 mm, this is due to the presence of an intermediate crossbeam. It can also be observed that there's a rather small spike at 16000 mm and this is due to the same reason (presence of an intermediate crossbeam) refer Figure 5.2. The shear force distribution changes from a positive to a negative value at the location of the load application (4000 mm from the support) refer Figure 5.4. Note that the bending moment distribution and shear force distribution are obtained from performing a linear analysis.

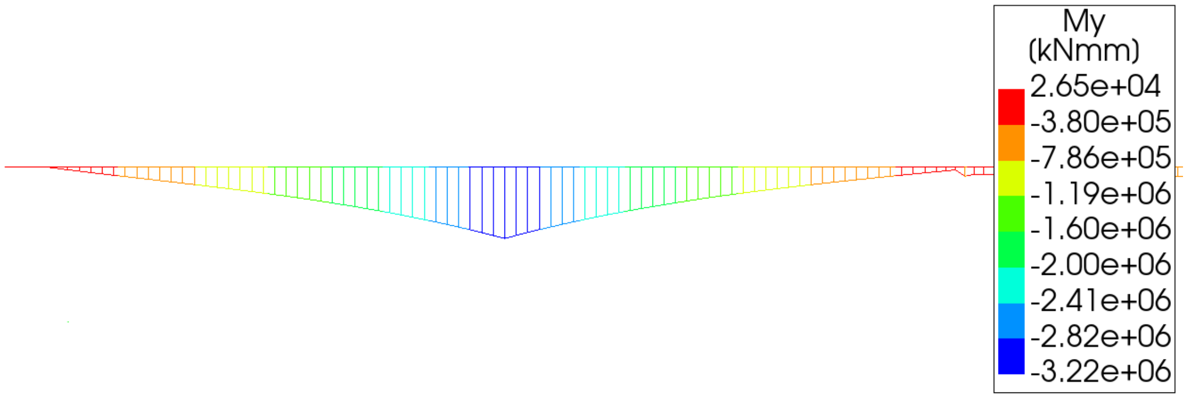

Figure 5.1: Bending moment M on T-beam 11 between the end cross-beam on the left side and intermediate cross-beam on the right side

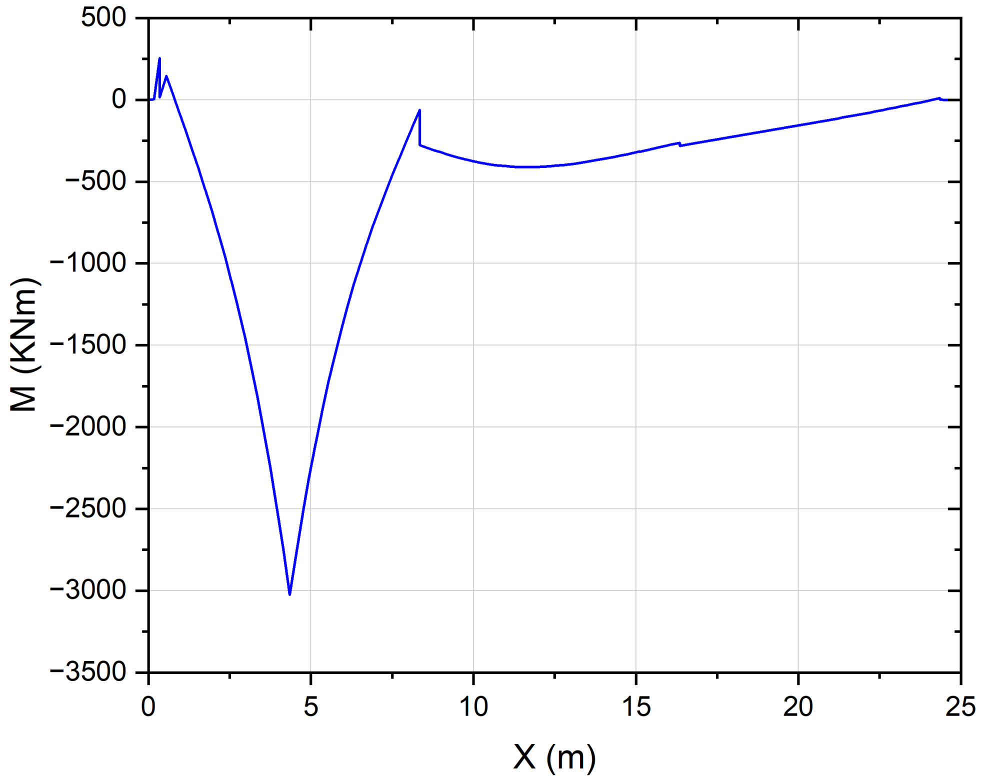

Figure 5.2: Bending moment M on the whole T-beam 11

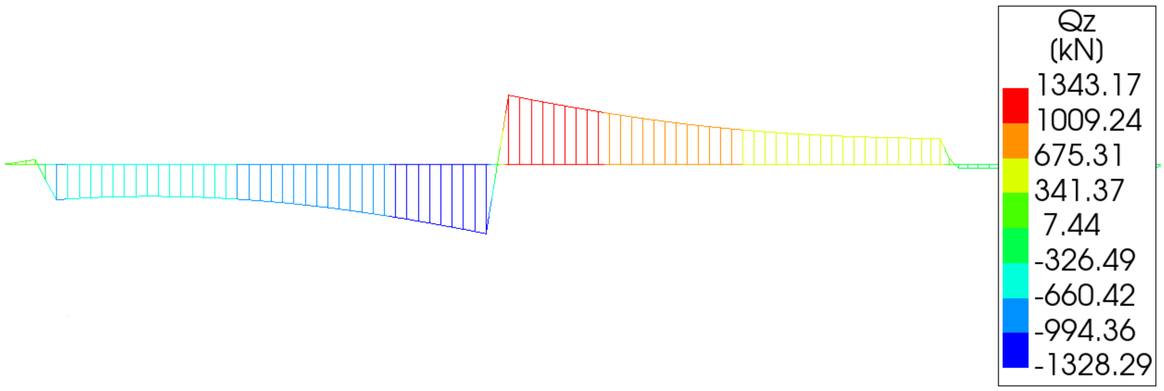

Figure 5.3: Shear force V on T-beam 11 between the end cross-beam on the left side and intermediate cross-beam on the right side

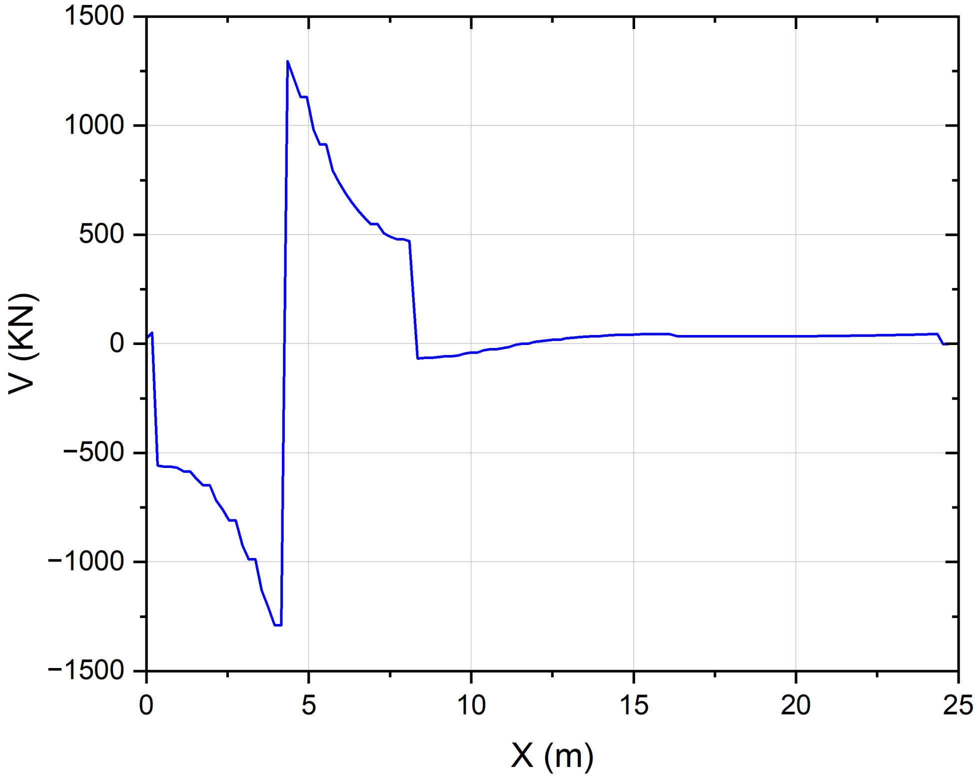

Figure 5.4: Shear force distribution V on the whole T-beam 11

5.2. Updating the equivalent loading of individual girder from bridge deck

To couple the 2D linear bridge deck model in the horizontal plane to the 2D non-linear individual girder model in the vertical plane corresponding to the loading case of experimental test setup 1. The method used for obtaining the equivalent loading follows equilibrium equation for beams in bending refer Figure 5.5.

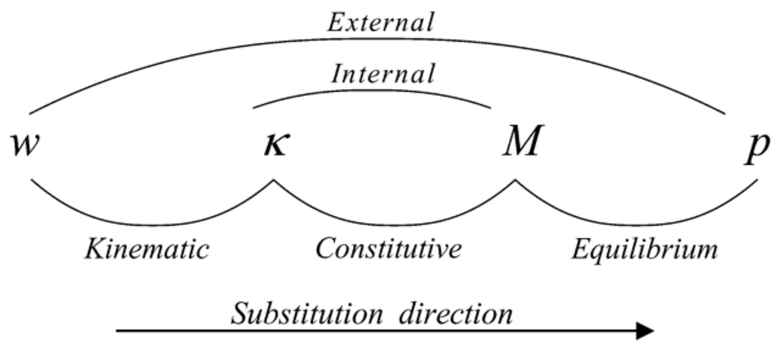

Figure 5.5: Relation scheme for bending in beams [4]

The rotation ϕ is not considered as an independent variable but as a dependent variable to the displacement 'w'. Also, the shear deformation is much less when compared to flexural deformation; hence it is negligible. Therefore, the equilibrium equation for beams in bending is opted. Then the equilibrium equation reads,

$$\frac{\partial^2 M(x)}{\partial^2 x} = -p(x) \tag{5.1}$$

The equation 5.1 is numerically solved to obtain the equivalent loading that can be applied on the non-linear individual girder in the vertical plane.
Another method used for obtaining the equivalent loading is using shear force distribution. The shear force is nothing but a derivative of the bending moment M refer Equation 5.2.

$$V(x) = \frac{\partial M(x)}{\partial x} \tag{5.2}$$

If we substitute this shear force in the equilibrium equation of 5.1, we obtain

$$\frac{\partial V(x)}{\partial x} = -p(x) \tag{5.3}$$

The equation obtained refer Equation 5.3 is then solved numerically to obtain the equivalent loading. To summarise, the two equations - Equation 5.1 and Equation 5.3 are numerically solved to find the equivalent distributed load that can be applied on the non-linear individual girder in the vertical plane.

5.2.1. Equivalent loading using bending moment distribution of the bridge deck

The idea of this method was to determine the equivalent distributed load for a bridge deck by analysing the bending moment distribution after applying a failure load (point load) of 2760 kN. The goal was to then compare the bending moment distribution, shear force distribution and total support reaction of the non-linear individual girder model after the application of the equivalent loading with that of the fully loaded beam in the bridge deck model and evaluate the differences.
First, the bending moment distribution of the bridge deck in the horizontal plane was obtained refer to Figure 5.2. Using Equation 5.1, the bending moment distribution of T-girder 11 was numerically solved to obtain the equivalent distributed load, as shown in Figure 5.6. From figure 5.6, it was observed that peaks appeared at the locations of the end cross-beams and intermediate cross-beams. These variations in equivalent loading were due to changes from hogging to sagging moments and with pronounced changes resulting from the second-order differentiation equation used. Notably, a peak occurred at 4.35m, the point load application location. Also, additional peaks occurred at 8350 mm, 16350 mm, and 24700 mm where intermediate and end cross-beams are located.
Next, the equivalent loading was applied only between the supports since reaction forces and external forces included in the equivalent loading would nullify each other. The resulting bending moment distribution, shear force distribution, and support reactions generated by the individual girder model were then compared with those from the bridge deck model.
The comparison revealed that the maximum bending moment of the individual girder differed by 16.7% from the bridge deck model. Additionally, the bending moment near the cross-beam location at

8100 mm showed a significant variation of 1900% from the bridge deck model see Figure 5.7. This large discrepancy is likely due to numerical errors and the sensitivity of the second-order differential equation for which the error is in the order of O(Δx^2).
Finally, a substantial variation of 37.91% was noted in the total support reaction between the non-linear individual girder in the vertical plane and the linear bridge deck model in the horizontal plane.

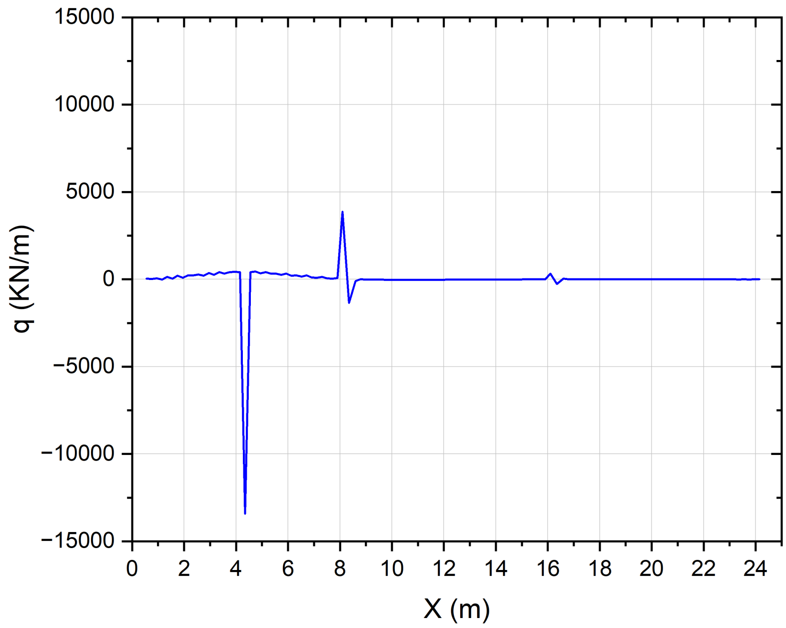

Figure 5.6: Equivalent distributed load 'q' [KN/m] obtained between the supports from moment distribution of bridge deck for experimental test setup 1

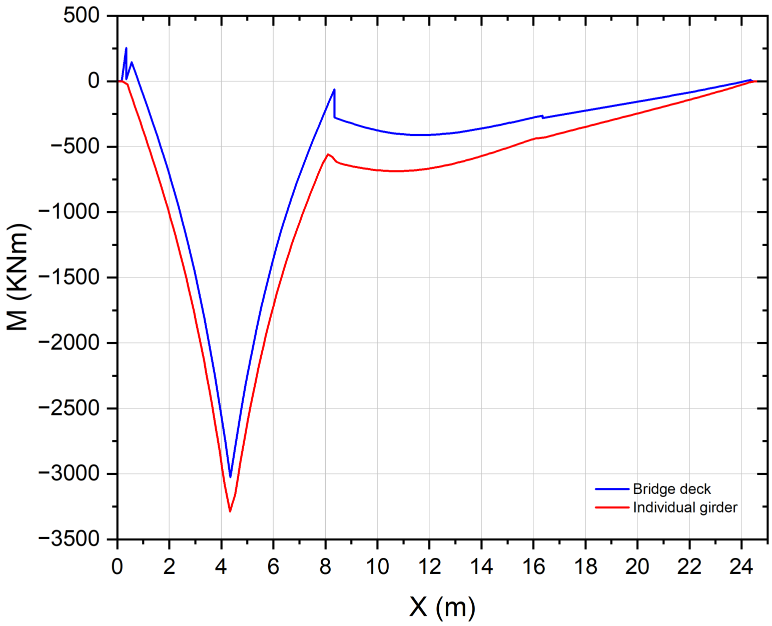

Figure 5.7: Comparision of bending moment distribution between bridge deck and individual girder model after applying equivalent loading from moment equilibrium equation

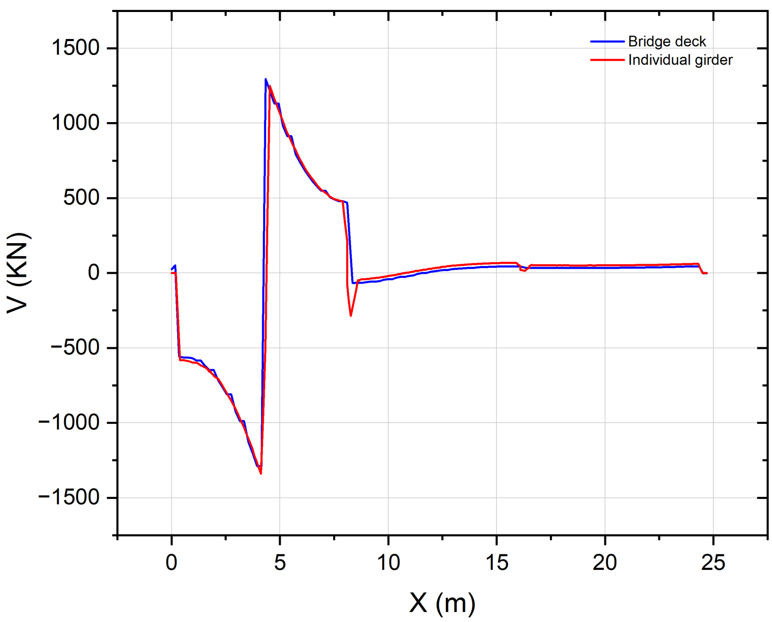

Figure 5.8: Comparison of shear force distribution between bridge deck and individual girder model after applying equivalent loading from moment equilibrium equation

Table 5.1: Comparison of support reactions between individual girder and bridge deck model after applying equivalent loading from bending moment distribution

Finite Element Model type	Left support reaction [KN]	Right support reaction [KN]	Total support reaction [KN]
2D non-linear individual girder model	580.52 (38.60 %)	60.62 (30.07 %)	641.15 (37.91 %)
2D linear bridge deck model	945.96	86.70	1032.66

5.2.2. Equivalent loading using shear force distribution of the bridge deck

The equivalent loading is obtained from the shear force distribution of the bridge deck in the horizontal plane using Equation 5.3. The objective was to apply this equivalent loading to the individual girder model and compare the results (bending moment distribution, shear force distribution and total support reaction) with the fully loaded beam in the bridge deck model.
First, the equivalent loading was derived from the shear force distribution, as shown in Figure 5.9. This loading was applied to the individual girder model between the supports. It was observed that the peaks were less pronounced at the locations of the left support and the intermediate cross-beam at 8100 m (Figure 5.9). This could be due to a lower order of numerical error (error is in the order of O(Δx)). In other words, the equivalent loading obtained from the shear force distribution is less sensitive to numerical error.
Next, the corresponding bending moment, shear force distribution, and support reactions were compared. It was found that the bending moment distribution from the individual girder closely followed that of the bridge deck model, with the maximum bending moment varying by 8.67%. The bending moment and shear force distributions obtained from the shear force-based equivalent loading were more accurate than those obtained from the bending moment-based equivalent loading. However, there was a significant discrepancy in the total support reaction obtained. The total support reaction varied by 40.69% from the bridge deck model in the horizontal plane.

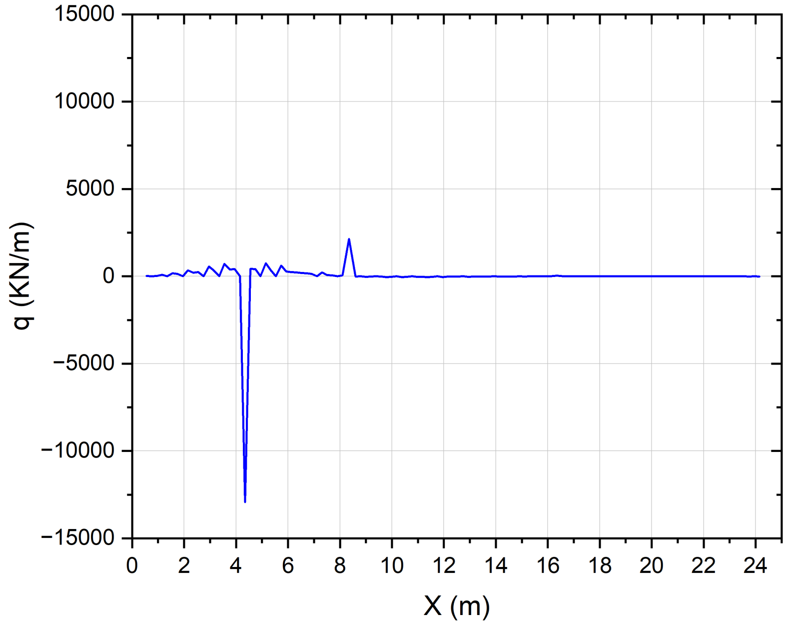

Figure 5.9: Equivalent distributed load ’q’ [KN/m] obtained between the supports from shear distribution of bridge deck for experimental test setup 1

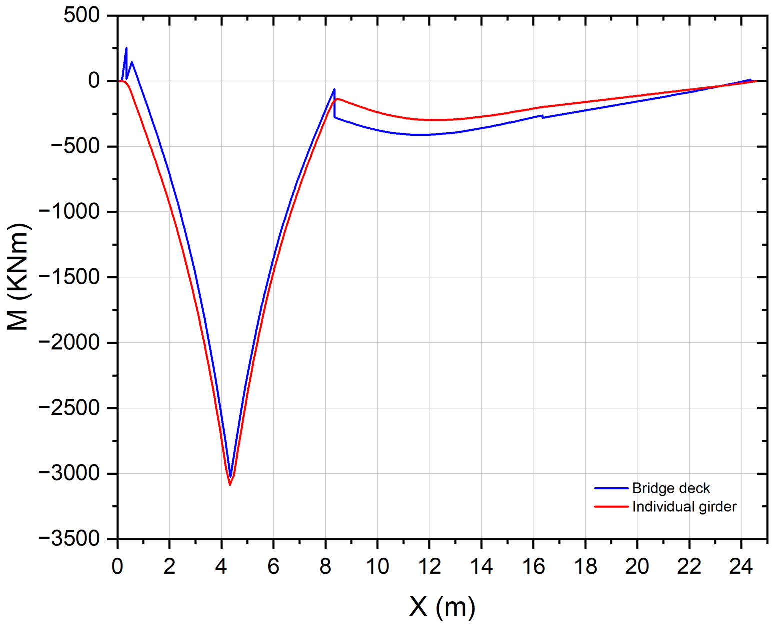

Figure 5.10: Comparision of bending moment distribution between bridge deck and individual girder model after applying equivalent loading from moment equilibrium equation

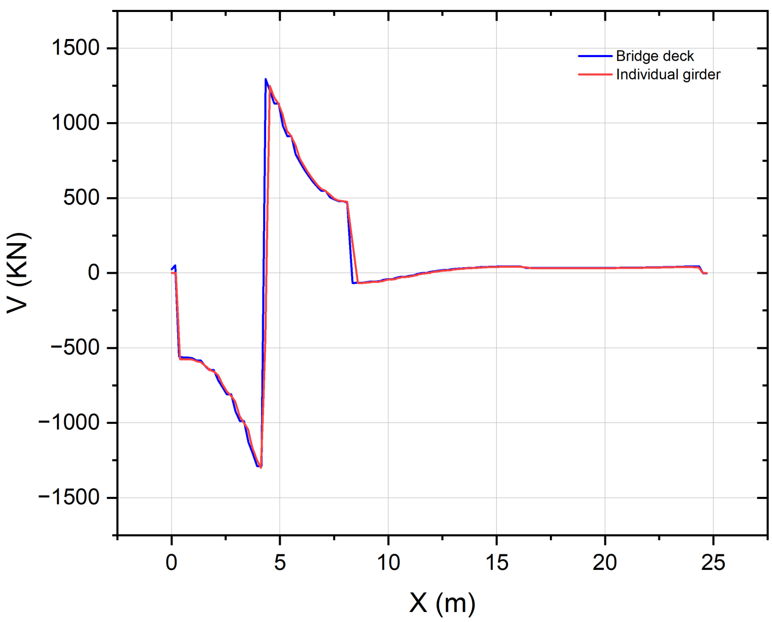

Figure 5.11: Comparison of shear force distribution between bridge deck and individual girder model after applying equivalent loading from moment equilibrium equation

Table 5.2: Comparison of support reactions between individual girder and bridge deck model after applying equivalent loading from shear force distribution equation

Finite Element Model type	Left support reaction [kN]	Right support reaction [kN]	Total support reaction [kN]
2D non-linear individual girder model	570.89 (39.65 %)	41.47 (52.16 %)	612.37 (40.69 %)
2D linear bridge deck model	945.96	86.70	1032.65

5.3. Equivalent distributed load from the uniformly distributed surface load applied

In order to figure out the discrepancies in the total support reaction obtained, a very simple loading condition is applied on the linear bridge deck model in the horizontal plane. A uniformly distributed surface load of KN/m^2 is applied to the whole integrated deck slab in the bridge deck model in the horizontal plane refer Figure 5.12. This case was chosen since all the T-girders in the bridge deck would be uniformly loaded and would behave in the same manner. The equivalent loading is derived using the same method as mentioned in section 5.2 - one from the bending moment distribution obtained from the bridge deck model and another from the shear force distribution obtained from the bridge deck model. The most optimal method for calculating the equivalent loading is chosen in such a way the relative error is less. The following equations 5.1 and 5.3.

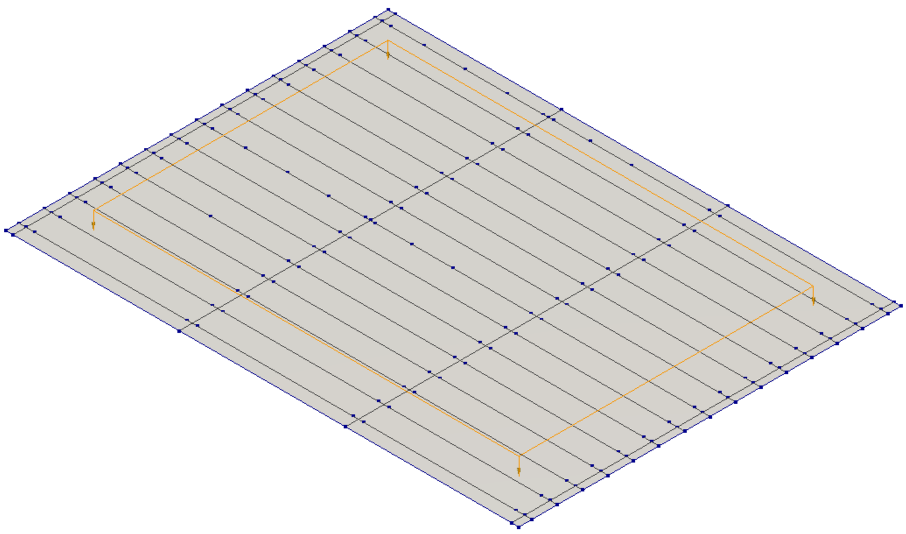

Figure 5.12: Uniformly distributed surface load applied on the 2D bridge deck model

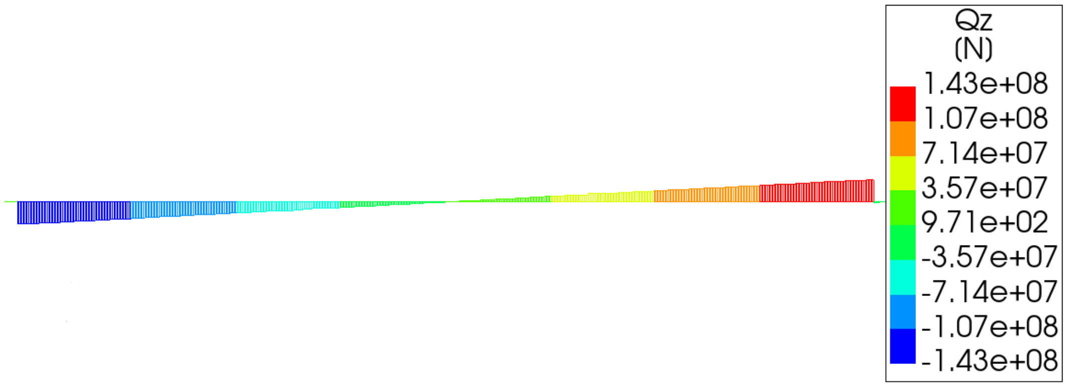

Figure 5.13: Shear force V on the T-beam after applying UDL

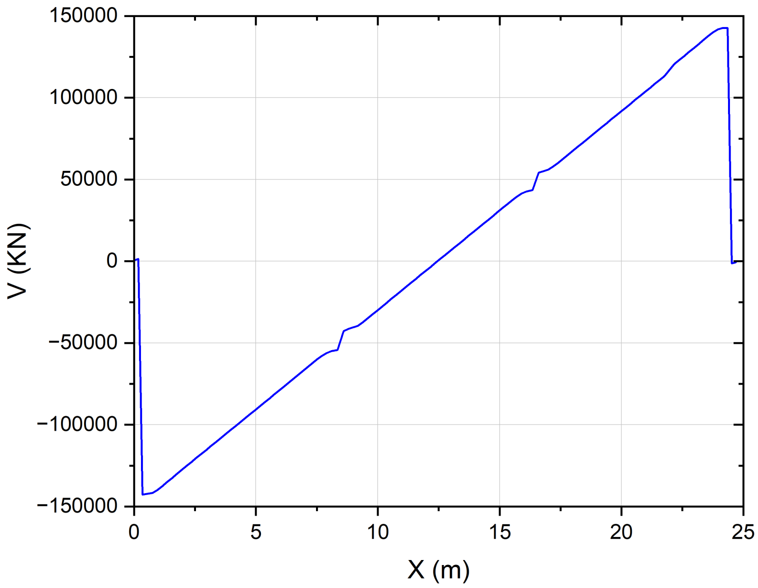

Figure 5.14: Shear force distribution V [KN]

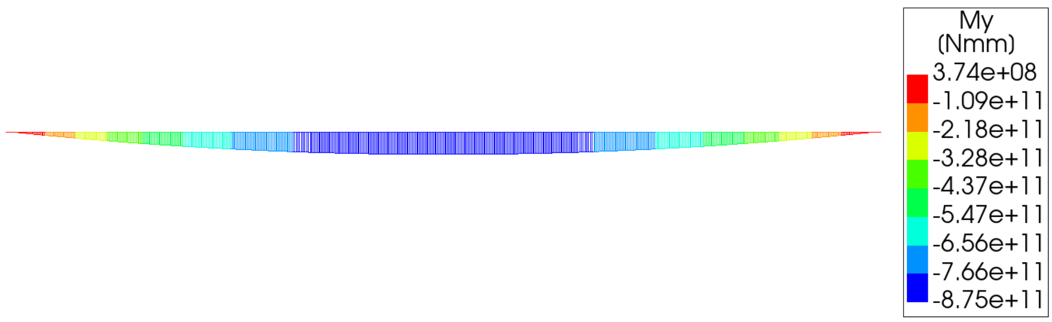

Figure 5.15: Bending moment M on the T-beam after applying UDL

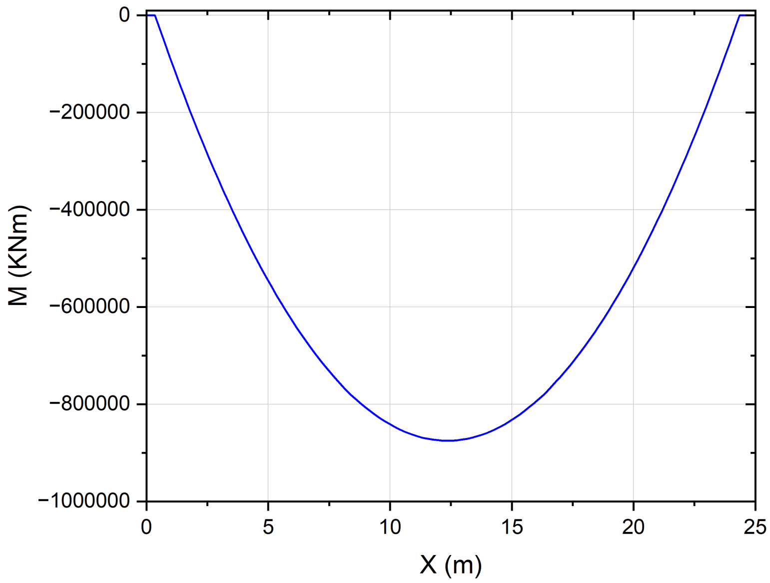

Figure 5.16: Bending moment distribution M [KNm]

5.3.1. Equivalent loading using bending moment distribution of the bridge deck

The equivalent loading to be applied on the individual girder is obtained from the moment distribution of the loaded girder namely the middle T-girder (T-girder 7) in the bridge deck model in the horizontal plane. The equivalent loading is obtained by numerically solving the bending moment distribution using the Equation 5.1. This equivalent loading refer to Figure 5.17 is then applied to the non-linear individual girder.

It can be observed that the bending moment distribution between the individual girder and the bridge deck matches accurately with very little variation (refer Figure 5.18. Similarly, the shear force distribution resulting from the equivalent loading applied to the individual girder is compared with the shear force distribution of the fully loaded bridge deck beam (Figure 5.19). Larger variations in shear force are notable at the locations of intermediate cross-beams (at 8350 mm and 16350 mm) with variations of -4.46% and 3.33% respectively.

Apart from the comparison of bending moment distribution and shear force distribution, the reaction forces were also compared. It is enumerated in the Table 5.4. It can be inferred that the total support reactions varies by 6.9 %.

In summary, under uniform loading conditions the total support reactions are nearly identical between the individual girder model and the bridge deck model. The significant variation in the total support reaction observed in previous sections 5.2.1 and 5.2.2 may be attributed to the non-uniform loading conditions from simulating the experimental test setup 1.

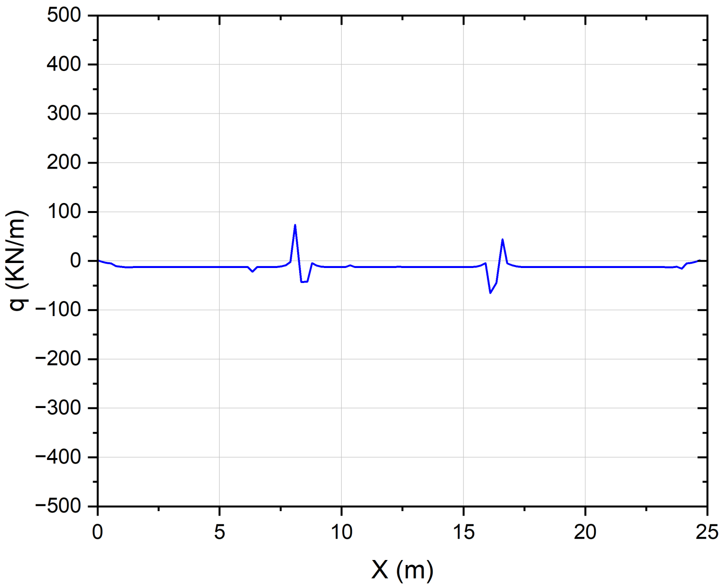

Figure 5.17: Equivalent distributed load 'q' [KN/m] obtained from bending moment distribution of bridge deck

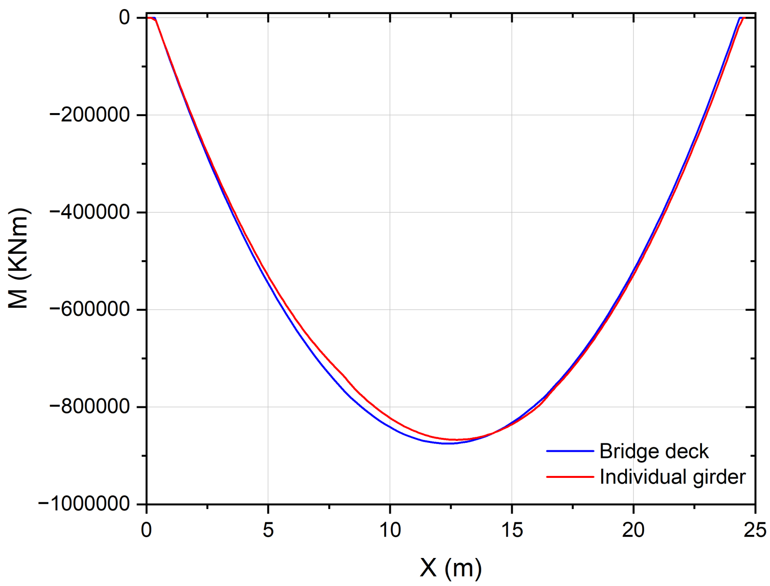

Figure 5.18: Comparison of bending moment distribution of individual girder with the fully loaded beam of bridge deck 'F_z' [KN].

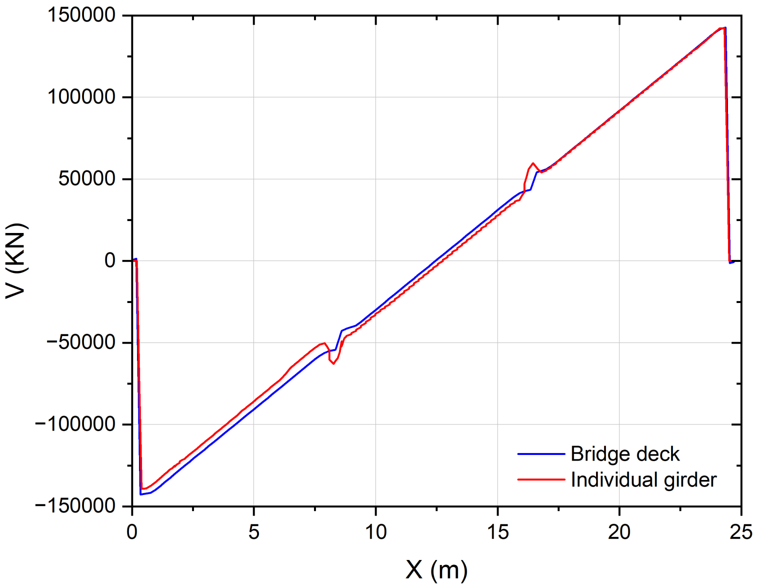

Figure 5.19: Comparison of shear force distribution of individual girder with the fully loaded beam of bridge deck 'F_z' [KN]

Table 5.3: Comparison of support reactions between individual girder and bridge deck model after applying equivalent loading from bending moment equilibrium equation

Finite Element Model type	Left support reaction [kN]	Right support reaction [kN]	Total support reaction [kN]
2D non-linear individual girder model	139259 (7.90 %)	142298 (5.90 %)	281557 (6.90 %)
2D linear bridge deck model	151232	151231	302463

5.3.2. Equivalent loading using shear force distribution of the bridge deck

Now, the equivalent loading is obtained using the shear force distribution obtained from the linear bridge deck model in the horizontal plane. The formula 5.3 is numerically solved to get the equivalent distributed load to be applied on the individual girder refer Figure 5.20. This equivalent loading is then applied on non-linear individual girder in the vertical plane and the corresponding bending moment distribution, shear force distribution and support reactions are compared with the linear bridge deck model in the horizontal plane refer Figure 5.20, Figure 5.21 and Figure 5.22. It can be inferred that the bending moment distribution and shear force distribution from the individual girder closely follow the bending moment distribution and shear force distribution of the bridge deck model. It is even more accurate when compared to the equivalent loading obtained from the equilibrium equation concerning the bending moment distribution 5.2.1. The total support reaction varies by 6.58 % from the total support reaction of the bridge deck model. It can be concluded that the equivalent loading obtained from the shear force distribution yields more accurate results when compared to the bending moment distribution. This further proves the fact that the equivalent loading obtained from shear force (single differential equation refer Equation 5.3) gives numerical error in the order O(Δx) and is more accurate. The equivalent loading obtained from bending moment distribution from the bridge deck model (double differential equation 5.1 is less accurate since the order of error is O(Δx^2)).
The total support reactions obtained from applying the equivalent loading on the non-linear individual girder in the vertical plane from both methods (bending moment distribution and shear force distribution) are comparable to the total support reactions obtained in the linear bridge deck model in the horizontal plane. Since all the beams are equally loaded there is no additional force influencing the support reactions. On the other hand, if a point load is applied on the T-beam 11 according to the test setup 1 (refer Figure 3.10), the adjacent beams namely T-beam 10 and T-beam 12 exert an additional downward force on the supports due to torsion. This could be the reason that explains why

the total support reactions obtained in the individual girder model vary from 37.91 % to 40.69 % (refer section 5.2.1 and section 5.2.2). Therefore, the effect of end crossbeam is neglected in developing the staggered 2D non-linear finite element approach for assessing the strength capacity of the prestressed T-girder bridges.

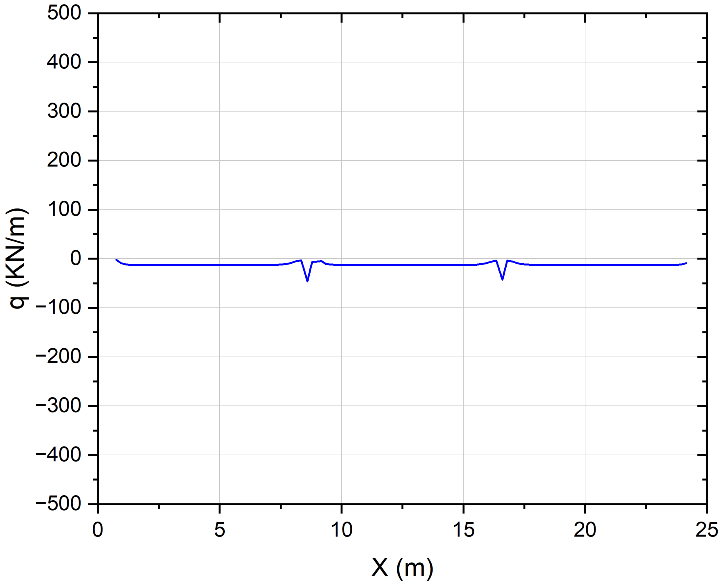

Figure 5.20: Equivalent distributed load 'q' [KN/m] obtained from shear force distribution of bridge deck

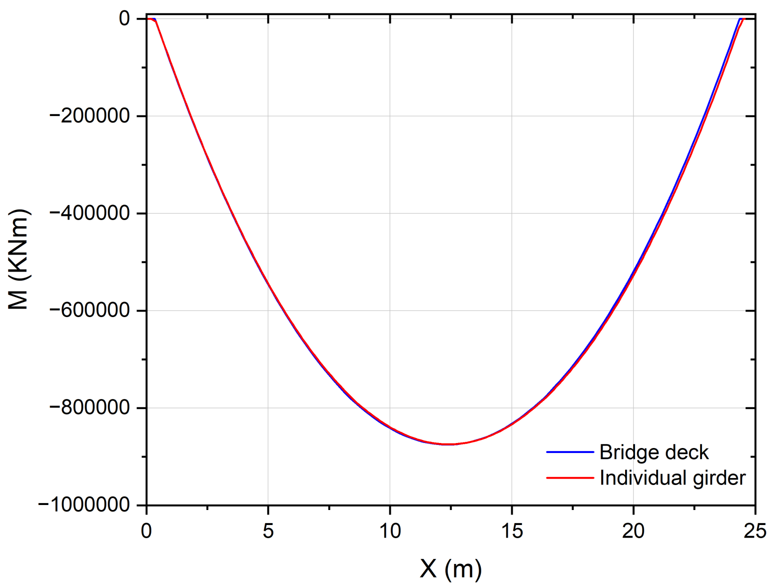

Figure 5.21: Comparison of bending moment distribution of individual girder with the fully loaded beam of bridge deck 'F_Z' [KN]

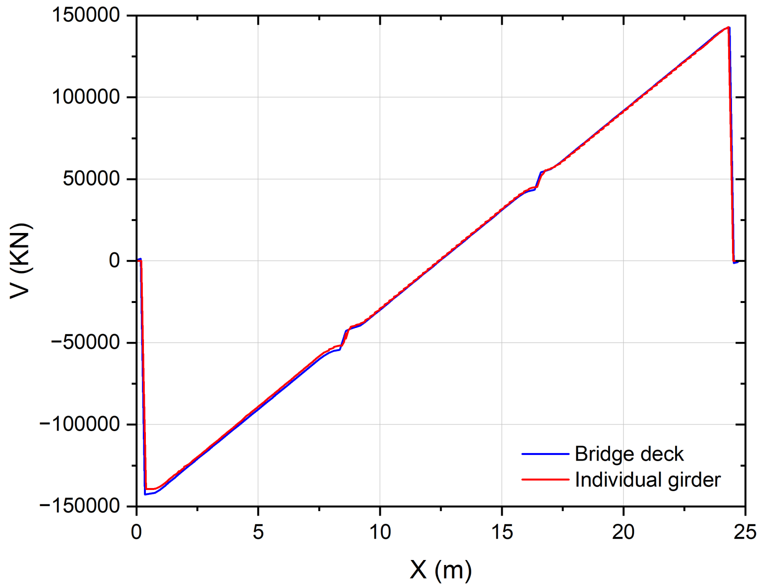

Figure 5.22: Comparison of shear force distribution of individual girder with the fully loaded beam of bridge deck ’F_z’ [KN]

Table 5.4: Comparison of support reactions between individual girder and bridge deck model after applying equivalent loading from bending moment equilibrium equation

Finite Element Model type	Left support reaction [KN]	Right support reaction [KN]	Total support reaction [KN]
2D non-linear individual girder model	139403 (7.80 %)	143150 (5.30 %)	282553 (6.58 %)
2D linear bridge deck model	151232	151231	302463

5.4. State of the art 2D staggered Non-Linear Finite Element Approach developed to assess T-girder bridge

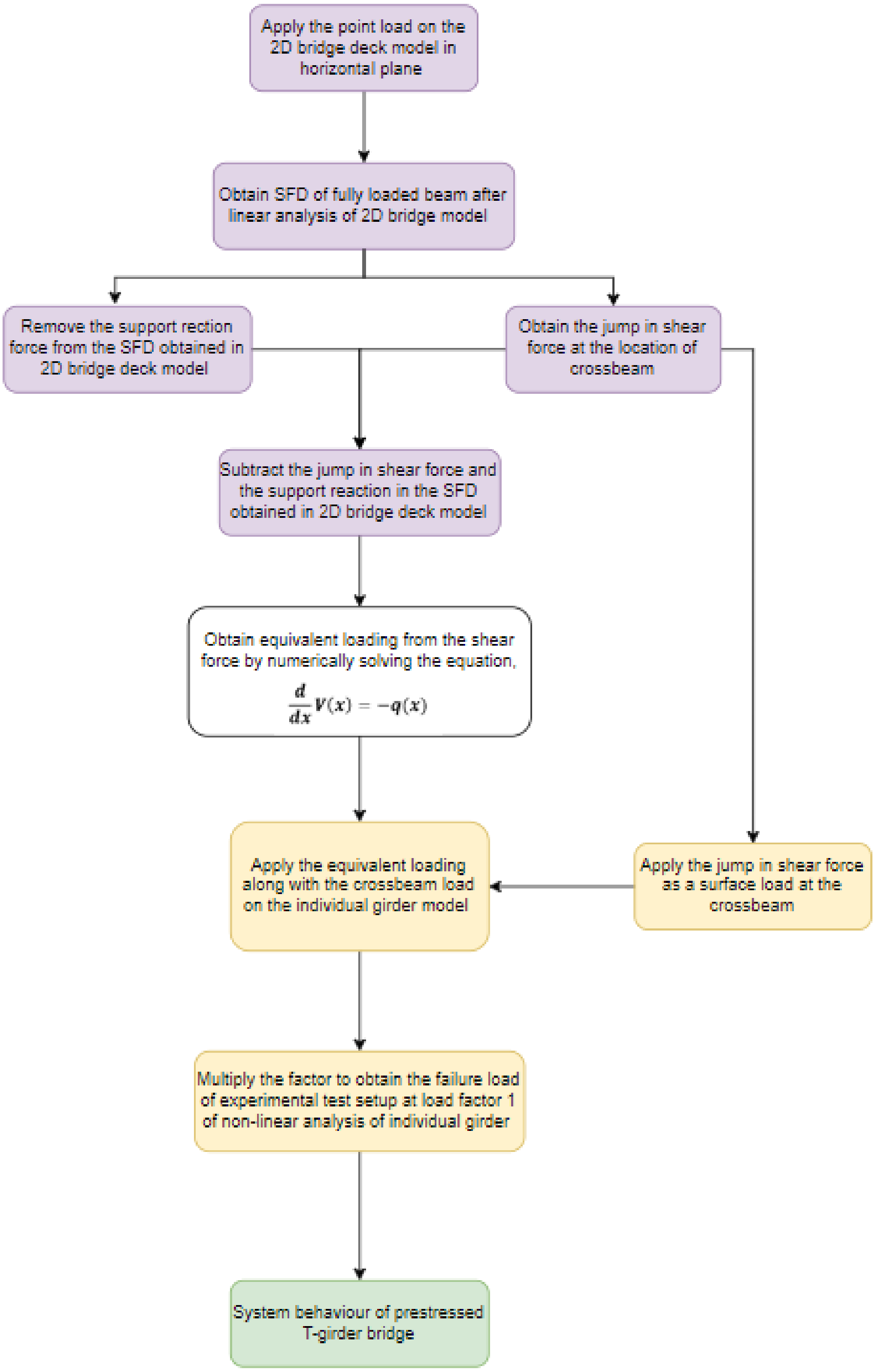

Figure 5.23: Sneha-Kostense approach 2.0
Note: The effect of end crossbeam is excluded in this approach

From section 5.3.2, it can be inferred that when an uniform load is applied on the bridge deck the support reaction from the individual girder after applying equivalent loading matched the support reaction of the bridge deck model with a variation of 6.58 %. But when the experimental test setup was simulated in the 2D bridge deck model (point load applied on the T-beam 11 refer to Figure 3.11), the support reactions from the 2D bridge deck model and the individual girder varied by 40.69 % refer Section 5.2.2. This means that the torsional moment from the adjacent T-girders is causing a downward force at the location of my support causing the reduction in my support reaction obtained in my non-linear individual girder. The torsional moment from the adjacent T-beam is transferred via the end crossbeam present, hence the end crossbeam is removed to find an accurate equivalent loading that can be applied to predict the system behavior of the T-girder bridge using just an individual girder. The process to develop the 2D simplified non-linear finite element approach developed is elaborated in the section 5.5.

5.5. Equivalent distributed load from experimental test setup 1 without the influence of end crossbeams

To translate the similar loading effect of the linear bridge deck model to the non-linear individual girder model which is comparable in terms of bending moment distribution, shear force distribution and total support reaction - three methods were opted. Firstly, an effective loading is applied using piece-wise function to mimic the experimental test setup 1. Then, the equivalent loading is applied with and without the presence of crossbeams to study the influence of the crossbeams in the behaviour of individual girder. The obtained load from the non-linear individual girder model after applying the equivalent loading is then multiplied with a Load Factor (LF) in such a way that the maximum failure load of the experimental test result is reached at the load step corresponding to load factor 1.0 when the non-linear analysis is performed for the 2D individual girder since only the load effect of the fully loaded beam from the 2D bridge deck model is translated to the 2D non-linear individual girder model. The load versus deflection curve multiplied by load factor is then compared with the connected beam test of the case study.
The overview of the FEM models used for obtaining the equivalent loading equation is presented in Table 5.5.

Table 5.5: Overview of FEM models used for simulating experimental tests

FEM model used	Equivalent Loading Method	Presence of crossbeam	Load factor applied
T1-PW-w/o_LF	Piece-wise function	-	No
T1-PW-w_LF	Piece-wise function	-	Yes
T1-w/o_CB-w/o_LF	Shear force distribution	No	No
T1-w/o_CB-w_LF	Shear force distribution	No	Yes
T1-w_CB-w/o_LF	Shear force distribution	Yes	No
T1-w_CB-w_LF	Shear force distribution	Yes	Yes

5.5.1. Effective loading using piece-wise function

The failure load from the experimental test setup 1 is applied as an effective load (33.3 % of failure load refer Table 5.7) on the non-linear individual girder model in the vertical plane. The effective load is applied as a line load of 580 mm. The 580 mm is chosen because the area of distributed load applied is 400 x 400 mm^2 and this 400 mm is extended up to the neutral axis of the integrated deck slab at an angle of 45°. The load distribution length is then, 400 + 180 = 580 mm. For modelling convenience, the line load 'q' is applied over the length of 600 mm.
From observing the load vs deflection curve referring to Figure 5.25, the failure load obtained is very conservative. Also, the stiffness of the girder by applying the load as piece-wise function is much less when compared to the actual stiffness of the existing bridge refer to Figure 5.25.

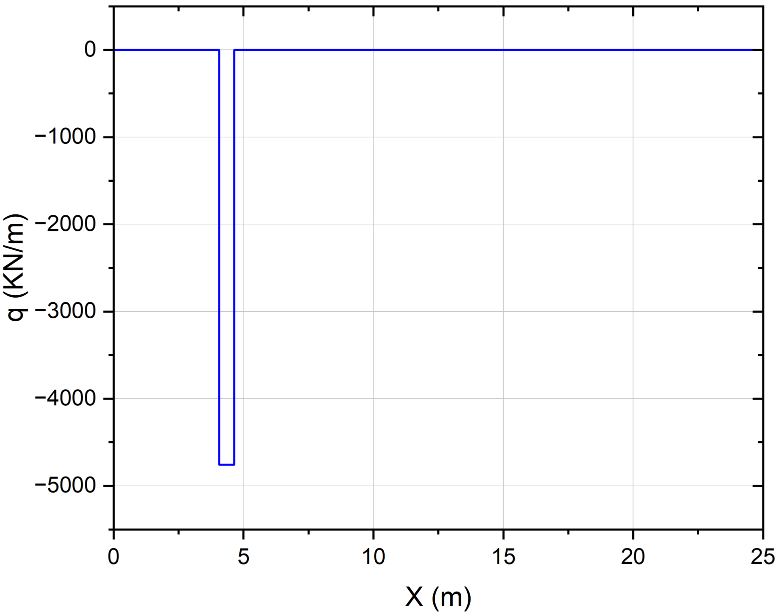

Figure 5.24: Equivalent load applied using a piece-wise function

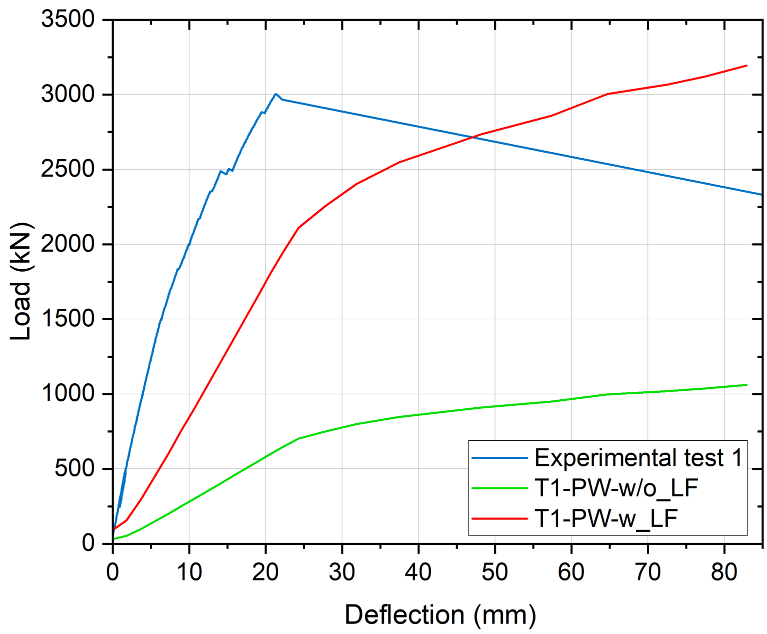

Figure 5.25: Comparison of load vs deflection curve of individual girder using piece-wise function with the experimental result of connected beam test 1. The blue line is reprinted from [10]
The Load Factor (LF) is 3.000

Cracking strains (cracking)

It can be inferred that the flexural crack initiates at the load F = 750.1 kN (see Figure 5.26a) and there is a reduction in stiffness due to the initiation of the flexural crack from the bottom of the T-girder (see 'T1-PW-w/o_LF' line from Figure 5.25). The flexural shear cracks start to appear at the load F = 910.2 kN where there is further reduction of stiffness in the load versus deflection curve. The T-girder finally fails at the ultimate load F_u = 1061.8 kN due to flexural shear cracks propagating from the end support to the position of load applied and from the intermediate crossbeam to the position of load applied (see Figure 5.26c). The crack pattern is similar to that of disconnected T-beam tests refer to Section 4.4.2. However, for the connected T-beam test, the failure is due to shear tension crack extending from the load location to the intermediate crossbeam. Just before failure, a secondary shear tension crack occurs between the supports and the loading position [11]. The piece-wise function used for equivalent loading doesn't represent the failure mechanism of the experimental test setup 1.

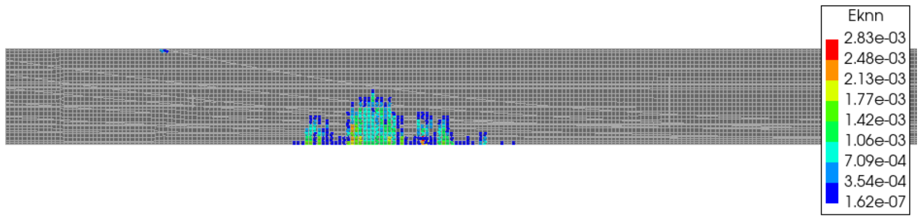

(a) F = 750.1 kN, δ_z = 27.8 mm, Flexural crack initiation

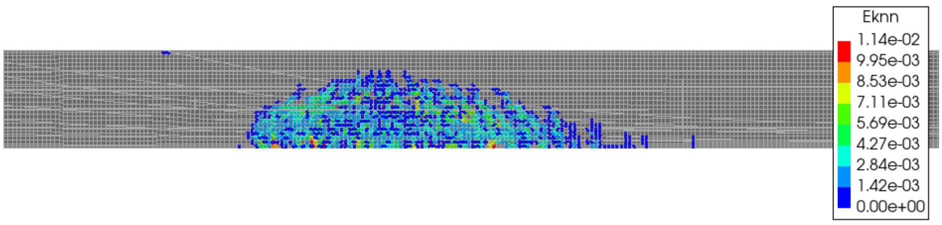

(b) F = 910.2 kN, δ_z = 37.5 mm

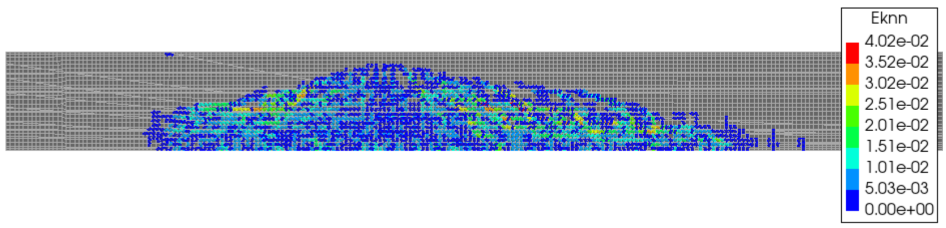

(c) F_u = 1061.8 kN, δ_u = 82.9 mm

Figure 5.26: T1-PW-w/o_LF, crack strains $E_{k\mathrm{nn}}$
(end crossbeam on the left side and intermediate crossbeam on the right side)

Yielding of reinforcement and prestressing tendons

The regular reinforcements start yielding at the bottom cross-section at the load F = 750.12 kN where the bending cracks occur. The stirrups start yielding at F = 910.21 kN where the flexural shear cracks occur. The maximum stress reached S_{xx} by the regular reinforcement is 352 N/mm^2.
The prestressing tendons start yielding at the bottom cross-section at load step F = 1020.04 kN and the maximum stress reached at the ultimate load is S_{xx} = 1562 N/mm^2.
In both prestressing tendons and regular reinforcements no fracture is observed since the ultimate strain of 0.9 ϵ_u is not exceeded (see Figure 4.11).

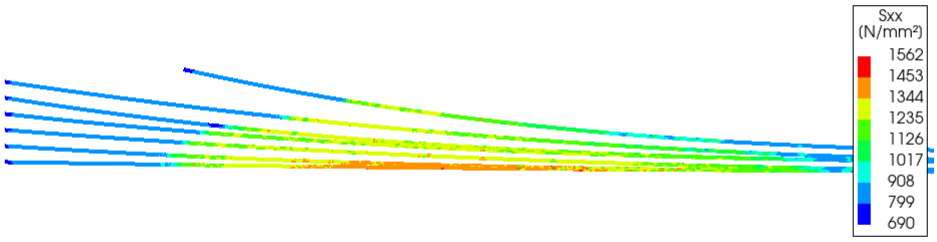

(a) Prestressing tendons 1-7

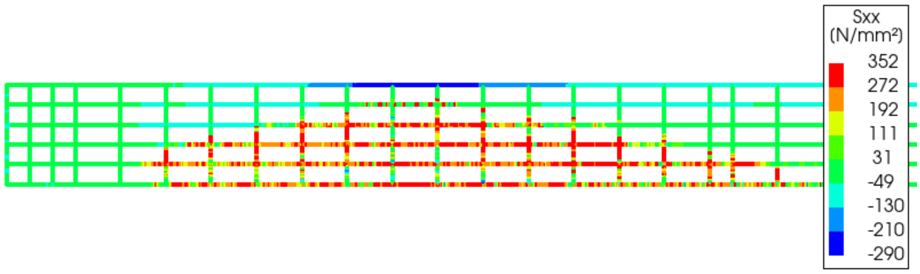

(b) Regular reinforcements

Figure 5.27: T1-PW-w/o_LF, stress S_{xx} embedded reinforcements, $F_u = 1061.8$ kN, $\delta_u = 82.9$ mm (end crossbeam on the left side and intermediate crossbeam on the right side)

5.5.2. Equivalent distributed loading without the presence of crossbeam

The equivalent loading method obtained is without the presence of crossbeam in the 2D bridge deck model in the horizontal plane. The percentage load taken up by the fully loaded beam and the adjacent beams are significantly higher than the rest of the T-beams. The load taken up by the fully loaded beam is 39.8 % and the adjacent beams are 24.7 % and 24.8 % refer Table 5.6.

Table 5.6: Amount of load taken up by the fully loaded beam and adjacent beams when no crossbeam is present

Beam number	Perctange load taken
T-beam 1	-0.8 %
T-beam 2	0.4 %
T-beam 3	0.0 %
T-beam 4	-0.1 %
T-beam 5	-0.1 %
T-beam 6	-0.2 %
T-beam 7	0.0%
T-beam 8	1.0 %
T-beam 9	5.0 %
T-beam 10	24.7 %
T-beam 11 (fully loaded beam)	39.8 %
T-beam 12	24.8 %
T-beam 13	5.5 %
T-beam 14	3.4 %
T-beam 15	-3.6 %

The shear force and bending moment diagram of the 2D bridge deck without the presence of crossbeam after applying failure load corresponding to experimental test setup 1 is presented in figure 5.28. The equivalent loading is obtained from the shear force diagram of the fully loaded beam (T-beam 11) in the 2D bridge deck model. The shear force is first corrected by removing the influence of support reactions in the bridge deck model (i.e.) subtracting the support reaction from the shear force distribution obtained and this is called as corrected shear force diagram refer Figure 5.29. The equivalent loading is obtained from the corrected shear force diagram using the equation 5.3 refer

Figure 5.30. This equivalent loading is then applied at the 2D non-linear individual girder in the vertical plane.

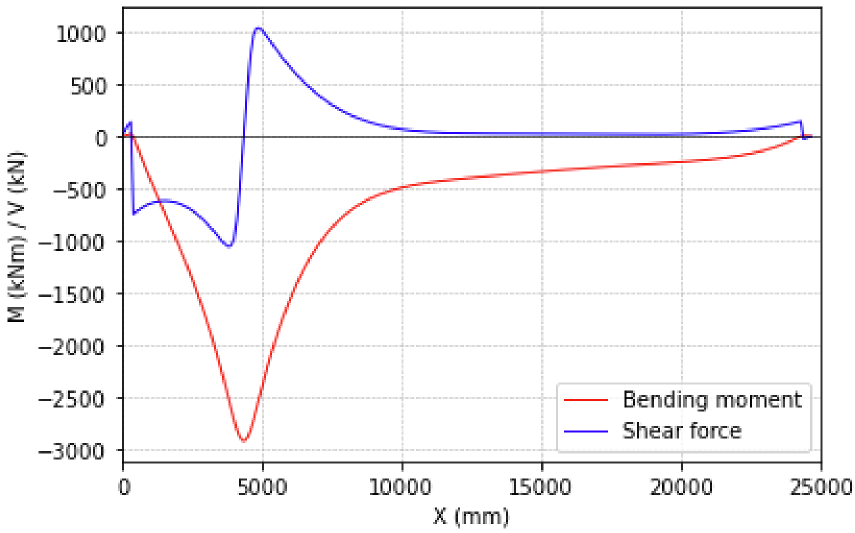

Figure 5.28: Bending moment and shear force diagram without crossbeam

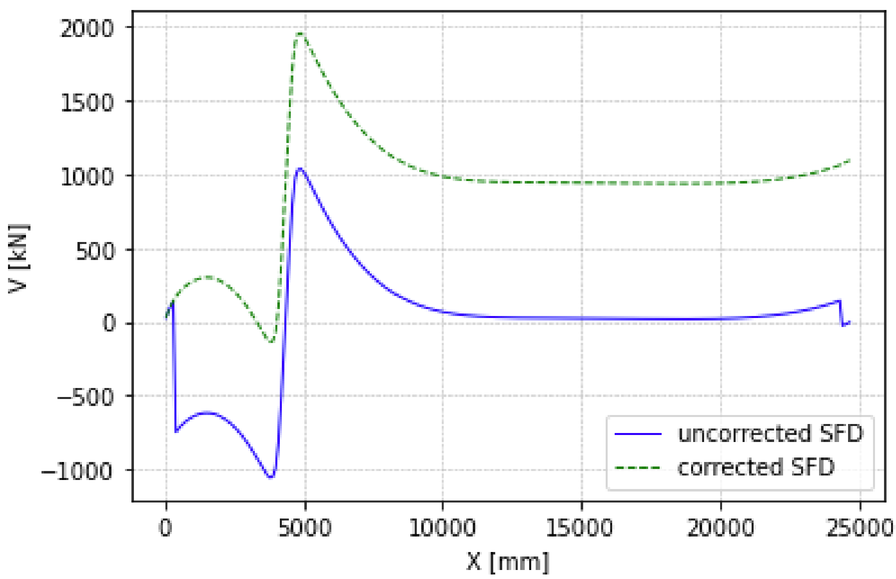

Figure 5.29: Corrected and uncorrected shear force diagram without crossbeam

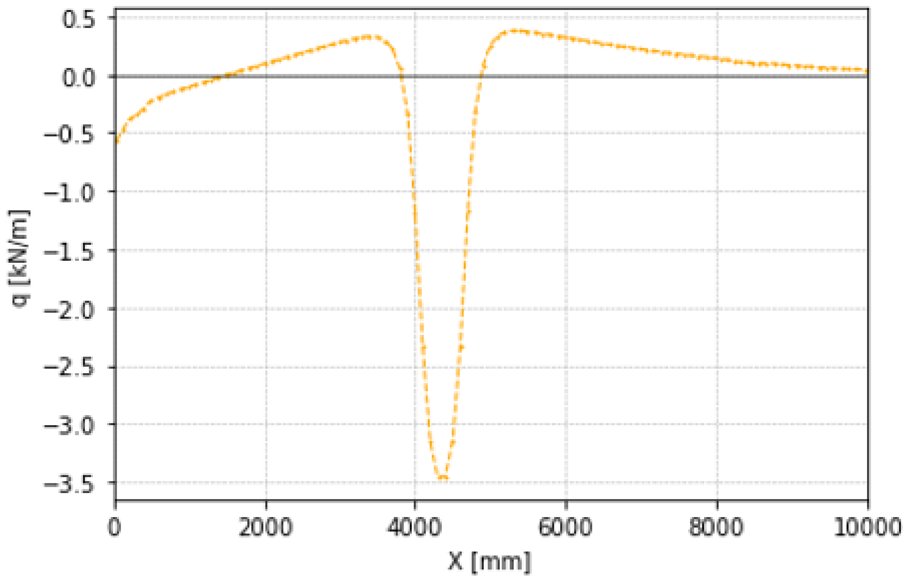

Figure 5.30: Equivalent loading to be applied on individual girder

The load versus deflection curve obtained is then multiplied with a load factor of 2.434 to get the system behaviour of the T-girder bridge. It can be inferred that load vs deflection multiplied with the load factor is comparable to the experimental test result connected beam test 1 but it is still conservative refer to Figure 5.31.

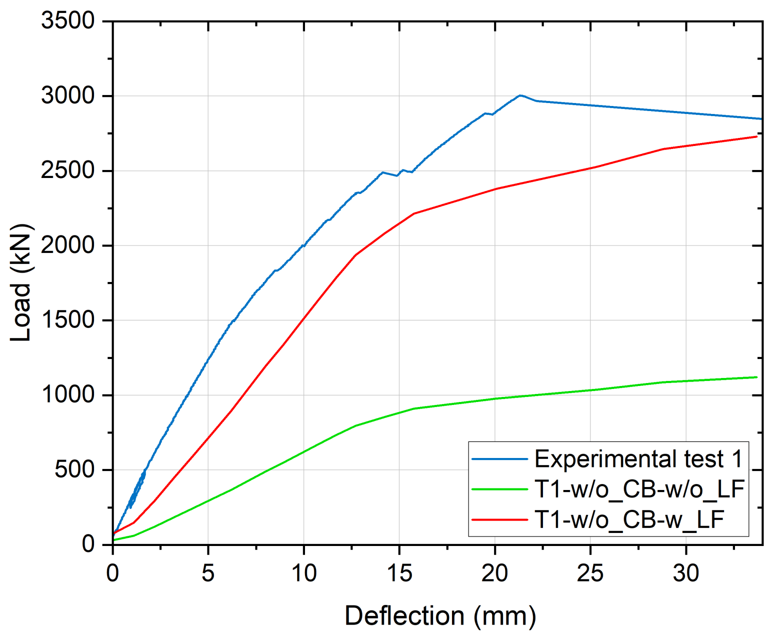

Figure 5.31: Comparison of load vs deflection curve of individual girder without crossbeam with the experimental result of connected beam test 1. The blue line is reprinted from [10]
The Load Factor (LF) is 2.434

Cracking strains (cracking)

The crack begins at the bottom cross-section of the T-girder due to the sagging bending moment of the T-girder (refer Figure 5.32b). At this load which is F = 909.8 kN, there is a reduction in stiffness (refer 'T1-w/o_CB-w/o_LF' line from Figure 5.31). As the loading increases, there is a development of horizontal crack towards the location of the intermediate crossbeam refer to Figure 5.32b. This horizontal crack is similar to the crack pattern observed in experimental test 1 [10]. However, due to the presence of a crossbeam, the shear crack propagates diagonally from the location of the applied load to the location of the intermediate crossbeam which is not the case here (see Figure 5.40).

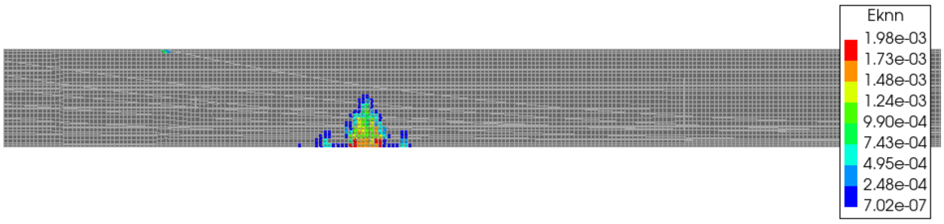

(a) F = 909.8 kN, δ_z = 15.75 mm, Flexural crack initiation

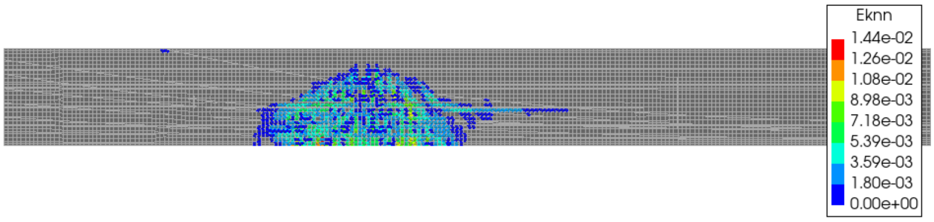

(b) F_u = 1120 kN, δ_u = 33.7 mm

Figure 5.32: T1-w/o_CB-w/o_LF, crack strains $E_{k\ \mathrm{nn}}$
(end crossbeam on the left side and intermediate crossbeam on the right side)

Yielding of reinforcement and prestressing tendons

The longitudinal reinforcement starts yielding at the bottom cross-section at the load F = 909.83 kN when the bending cracks start to develop. At this load, the first drop in stiffness is observed at the load versus deflection curve, see the 'T1-w/o_CB-w/o_LF' line in Figure 5.31. Stirrups start yielding at F = 1120.89 kN at the location where the horizontal crack develops. The maximum stress obtained by the regular reinforcement at the ultimate load is S_{xx} = 373 N/mm^2.
The prestressing tendons do not reach yielding even at failure load and the stress at the ultimate load is S_{xx} = 1410 N/mm^2. No fracture is observed at both regular reinforcement and prestressing tendons.

5.5.3. Equivalent distributed loading with the presence of crossbeam

The equivalent loading method obtained here is with the presence of crossbeam in the 2D bridge deck model. The percentage load taken up by the fully loaded beam and the adjacent beams are 33.3 %, 21.7 % and 22.2 % refer to Table 5.7. The load taken by the fully loaded beam with the presence of crossbeams is 6.5 % less than the case without the presence of crossbeams.
The bending moment and shear force diagrams obtained by the fully loaded beam is presented in Figure 5.34. To obtain the equivalent loading, the shear force is first corrected by removing the support reaction and the jump in shear force at the location of crossbeam 5.35. This sudden increase in shear force at the location of the crossbeam is applied as an upward vertical surface load at the location of the crossbeam in the individual girder model in the vertical plane refer to Figure 5.37. The figure 5.36 shows the equivalent loading with and without the presence of cross beam.

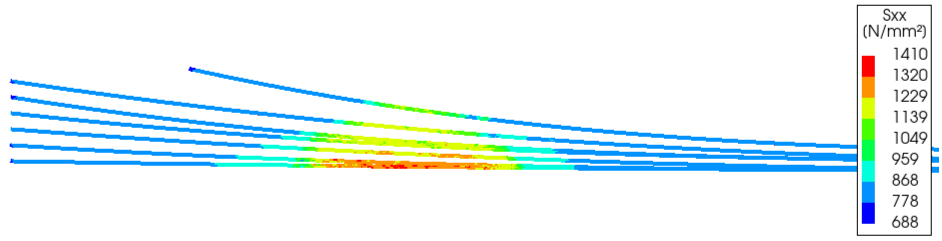

(a) Prestressing tendons 1-7

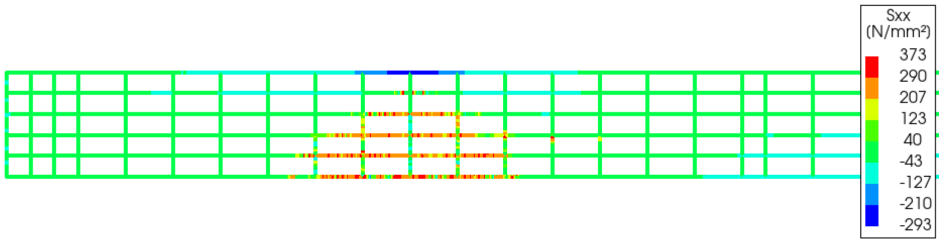

(b) Regular reinforcements

Figure 5.33: T1-w/o_CB-w/o_LF, stress S_{xx} embedded reinforcements, $F_{\mathrm{u}} = 1234.12$ kN, $\delta_{\mathrm{u}} = 39$ mm (end crossbeam on the left side and intermediate crossbeam on the right side)

Table 5.7: Amount of load taken up by the fully loaded beam and adjacent beams when no crossbeam is present

Beam number	Perctange load taken
T-beam 1	-2.0 %
T-beam 2	0.7 %
T-beam 3	0.2 %
T-beam 4	0.1 %
T-beam 5	0.3 %
T-beam 6	0.6 %
T-beam 7	1.5 %
T-beam 8	3.3 %
T-beam 9	6.9 %
T-beam 10	21.7 %
T-beam 11 (fully loaded beam)	33.3 %
T-beam 12	22.2 %
T-beam 13	7.9 %
T-beam 14	6.1 %
T-beam 15	-2.9 %

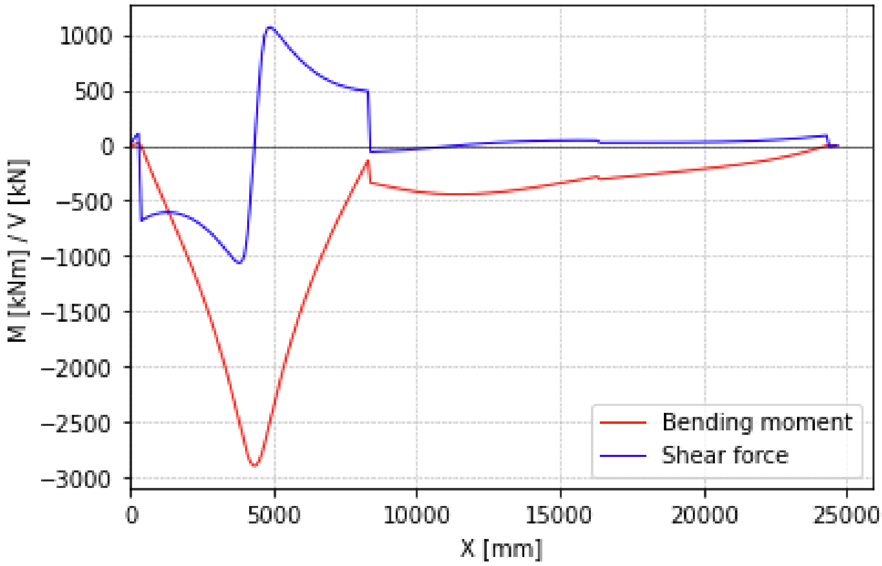

Figure 5.34: Bending moment and shear force diagram with crossbeam

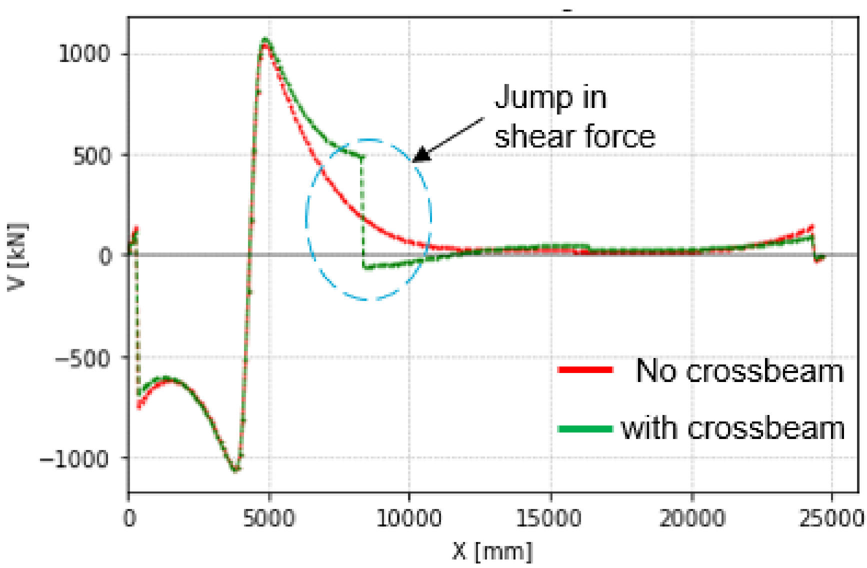

Figure 5.35: Jump in shear force at the location of crossbeam

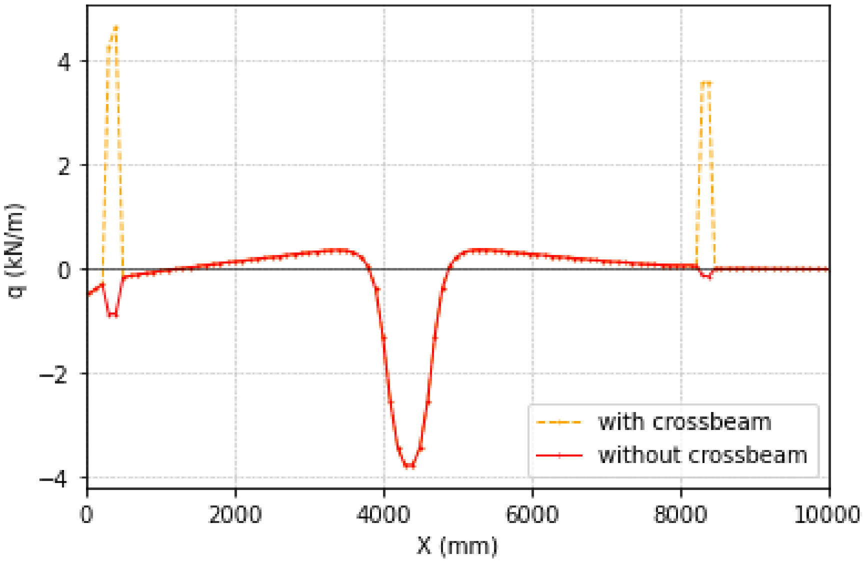

Figure 5.36: Equivalent loading with and without the effect of crossbeam

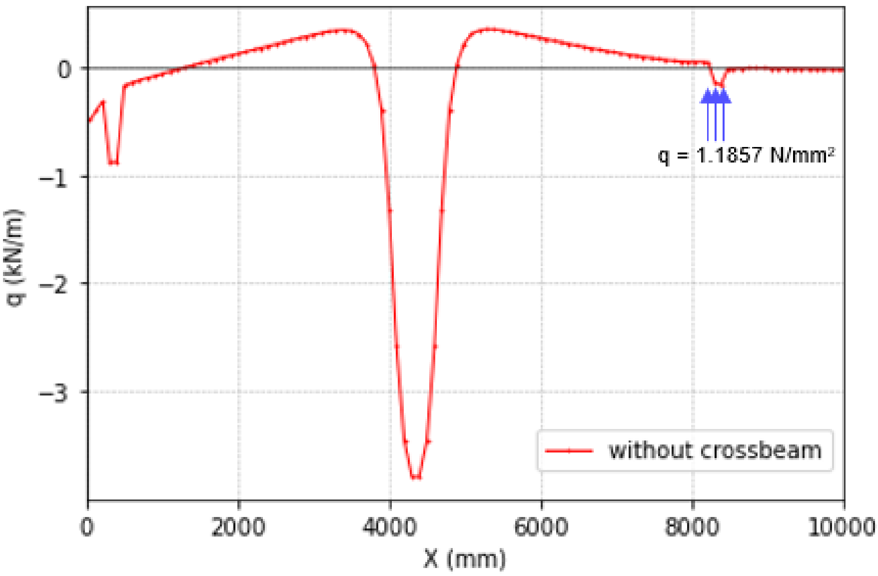

Figure 5.37: Equivalent loading with the effect of crossbeam applied as a surface load

The force versus deflection curve obtained after the application of the equivalent load on the non-linear individual girder is then multiplied with a factor of 2.589 to get the system behaviour of the T-girder bridge. It can be inferred that the equivalent loading applied from this method is accurate to that of the experimental result refer Figure 5.38. Also, the ultimate failure load predicted from T1-w_CB-w_LF is 96.5% of the failure load obtained from the experimental test setup 1 [10].

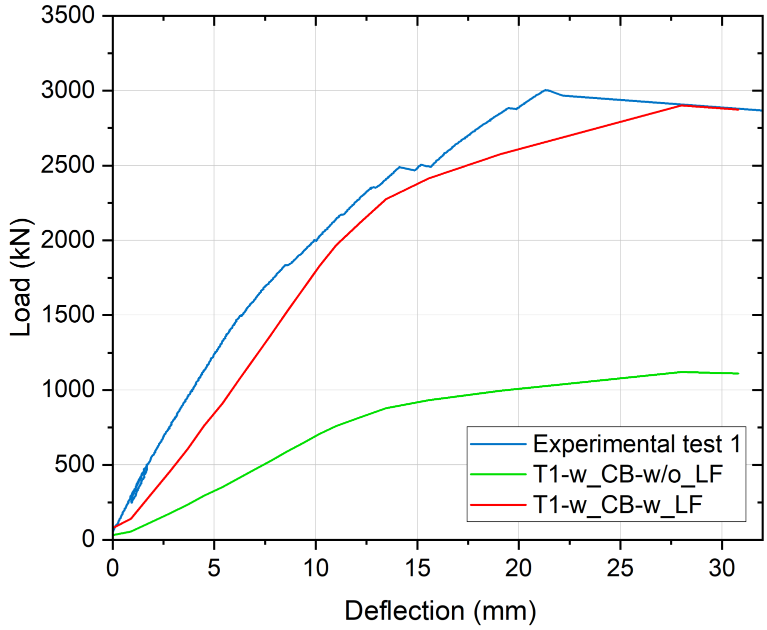

Figure 5.38: Comparison of load vs deflection curve of the individual girder with crossbeam with the experimental result of connected beam test 1. The blue line is reprinted from [10]
The Load Factor (LF) is 2.5896

Cracking strains (cracking)

Just like previous results, the first crack propagates from the bottom cross-section of the T-girder. At the initiation of the first crack (F = 820 kN), there is reduction in stiffness observed from the load versus deflection curve (refer to 'T1-w_CB-w/o_LF' line from Figure 5.38). At further reduction in stiffness at the load step F = 932 kN, there is still propagation of flexural cracks as opposed to other cases where there is progression of flexural shear cracks (refer Figure 5.39b). Ultimately, the T-girder fails due to large horizontal crack formed from the location of load applied and the intermediate crossbeam (refer Figure 5.39c. This is exactly similar to the crack pattern observed from the experimental test setup 1 refer to Figure 5.40.
From the experimental test 1, the failure was due to punching of deck through the T-girder and the web of the T-girder was severely damaged approximately 1 m from the load position towards the end position of the end support. Also, there was a large opening of shear crack in the opposite direction towards the intermediate crossbeam prior to failure [10]. The crack pattern observed from the 2D individual girder model refer to Figure 5.39c. It can also be seen that at 1 m from the load position, there are shear cracks and the T-girder fails due to the formation of large shear crack between the load position and the intermediate crossbeam (see Figures 5.40-5.41).

Figure 5.40: Shear failure of connected T-beam test 1 (intermediate cross-beam on the left side, end support on the right side [10])

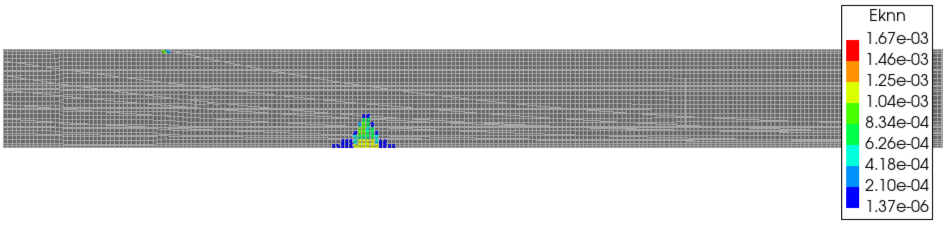

(a) F = 820 kN, δ_z = 12.2 mm, Flexural crack initiation

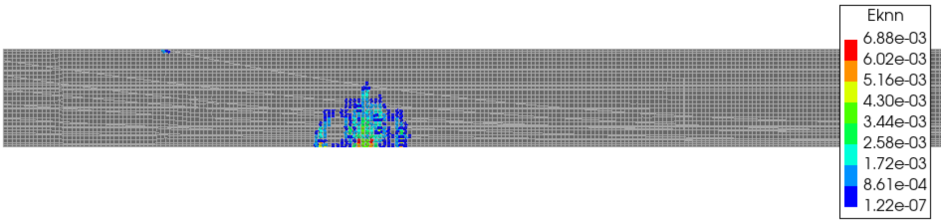

(b) F = 932 kN, δ_z = 15.56 mm

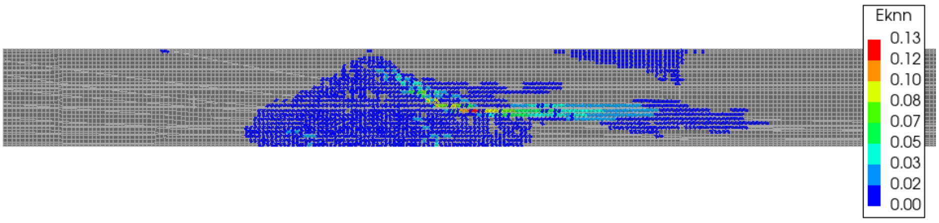

(c) F_u = 1160 kN, δ_u = 33.9 mm

Figure 5.39: T1-w_CB-w/o_LF, crack strains $E_{k\ \mathrm{nn}}$
(end crossbeam on the left side and intermediate crossbeam on the right side)

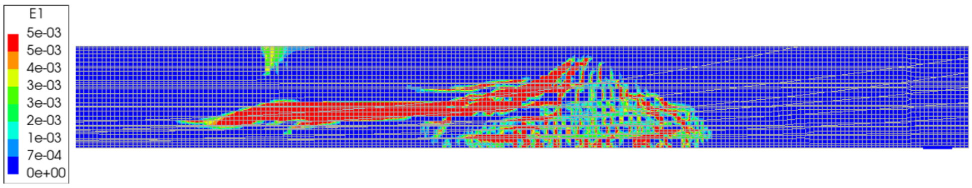

Figure 5.41: T1-w_CB-w/o_LF, maximum principal strain E1 (intermediate cross-beam on the left side, end support on the right side)

Yielding of reinforcement and prestressing tendons

The regular reinforcement starts yielding at the bottom cross-section at the load F = 879 kN and the stirrups start yielding at F = 1120 kN at the location of flexural shear crack between the load position and intermediate crossbeam. The prestressing tendons start yielding at the load step F = 1120 kN at the location of the horizontal crack between the location of the load applied and the intermediate crossbeam. No fracture is observed for both regular reinforcements and prestressing tendons since it doesn't exceed the ultimate strain.

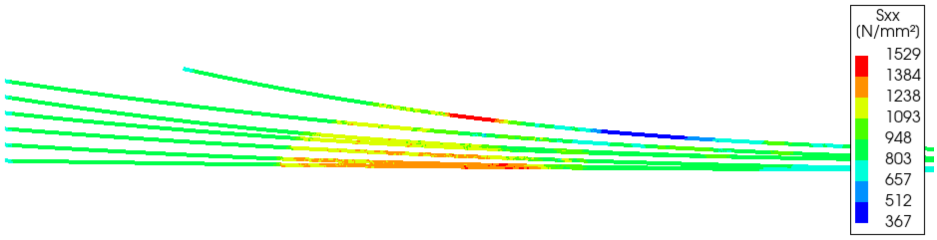

(a) Prestressing tendons 1-7

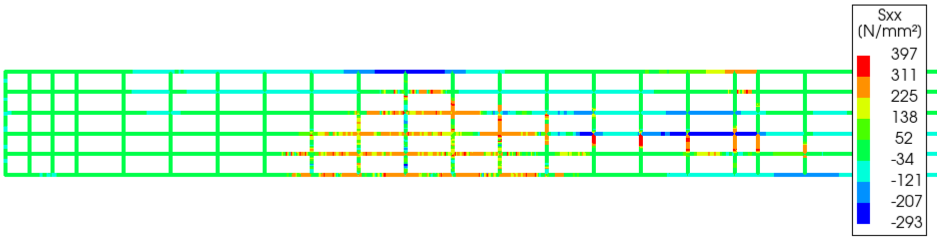

(b) Regular reinforcements

Figure 5.42: T1-w_CB-w/o_LF, stress S_{xx} embedded reinforcements, $F_u = 1160$ kN, $\delta_u = 33.9$ mm (end crossbeam on the left side and intermediate crossbeam on the right side)

5.5.4. Comparison of equivalent loading obtained using the three methods

It can be observed that the load vs deflection curve obtained using the equivalent loading method without crossbeam using shear force distribution is more precise than the one obtained using piece-wise function. However, both these methods used for obtained for getting the equivalent loading yields a conservative result. The equivalent loading obtained with the presence of crossbeam quite accurately matches the experimental result of connected beam test 1 refer Figure 5.43.

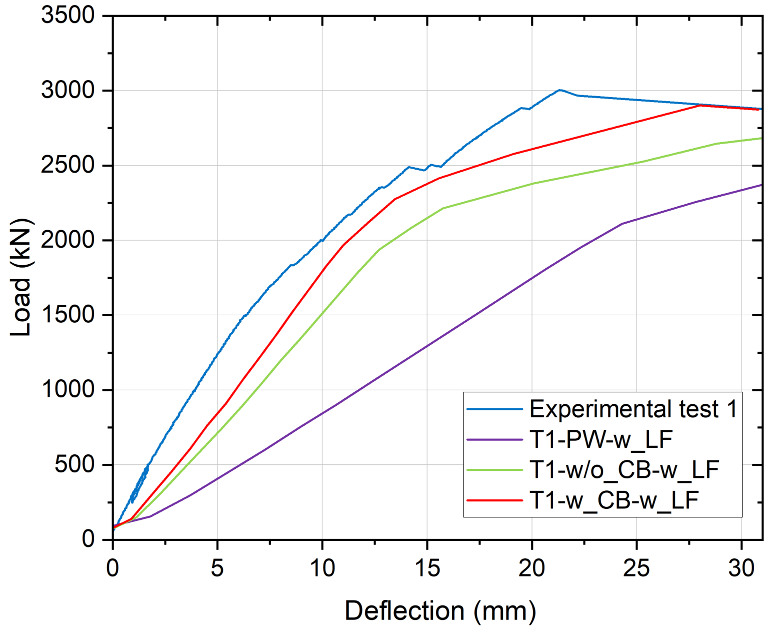

Figure 5.43: Comparison of load vs deflection curve of individual girder with crossbeam with the experimental result of connected beam test 1. The blue line is reprinted from [10]

5.6. Summary and conclusion

This section summarised how the non-linear finite element approach was developed for analysing the system behaviour of prestressed T-girder bridges.

- The support reaction obtained from applying the equivalent loading on the individual girder model from the bridge deck model built always varies between the range 44 % to 56 % using the bending moment distribution and shear force distribution of the fully loaded beam in the bridge deck model with the presence of end crossbeam.
- The equivalent loading obtained using double differentiation of the bending moment from the bridge deck model is not accurate. It is more sensitive to numerical error (i.e.), the order of error for double differentiation is proportional to second order or $O(\Delta x^2)$.
- When the load is applied uniformly in the bridge deck and is translated to individual girder through equivalent loading – the bending moment distribution, shear force distribution and total support reaction from the individual girder accurately match that of the bridge deck model.
- However, when a point load is applied in a single girder and is translated to the individual girder through equivalent loading – the bending moment and shear force distribution matched that of the bridge deck model. But the total reaction obtained was half of what was obtained in the bridge deck model.
- This huge discrepancy in the total support reaction could be due to additional downward force at the supports in the bridge deck model caused by torsional moment from the adjacent girders transferred by the end crossbeams.
- Therefore, the end crossbeam is removed in 2D bride deck model for obtaining the equivalent loading method that can be applied on the non-linear individual girder that can replicate the system behaviour of the bridge.
- The equivalent loading obtained from the peice-wise function gives a very conservative failure load and also, the stiffness of the girder is much less when compared to the experimental result.
- The equivalent loading obtained from the shear force distribution of fully loaded beam without the presence of crossbeam gives better results than the load applied as a peice-wise function.

However, it still predicts a conservative failure load of the system behaviour of the T-girder bridge.

- The equivalent loading method obtained with the presence of crossbeam from the shear force distribution of fully loaded beam gives a more accurate prediction of the system behaviour of the T-girder bridge.
- The crack pattern obtained from the equivalent loading method with the presence of a crossbeam is similar to that observed in experimental test setup 1. In contrast, the crack pattern observed in the 2D model using the piece-wise function for effective loading is similar to that of the disconnected T-beam tests.
- As expected, the regular reinforcements and prestressing tendons start to yield at the locations of the cracks. No fractures were observed in either the regular reinforcement or the prestressing tendons in any of the cases.
- It can be concluded that the staggered 2D non-linear finite element approach developed incorporating the equivalent loading method applied with the presence of crossbeam best predicts the system behaviour of the prestressed T-girder bridges.

6
Discussion

This chapter discusses the results obtained from the 2D bridge deck model developed in the horizontal plane and the 2D non-linear individual girder model built in the vertical plane, along with the considerations made in this study. It also evaluates the findings from the application of the staggered 2D non-linear finite element approach for predicting the strength capacity of prestressed concrete T-girder bridges. The results are compared with experimental data to assess the validity and efficiency of the developed staggered 2D non-linear finite element approach.

The 2D bridge deck is built by incorporating shape orthotropy using the orthotopic plate elements model. The orthotropy is introduced in terms of geometrical orthtropy and not material orthotropy. In the 2D bridge deck model built in the horizontal plane, the T-girders and the integrated deck slab connect at their neutral axis. It was inferred from the literature [3], due to Compressive Membrane Action (CMA), the integrated deck slab is not the weakest structural element but the focus is shifted to the T-girder. In the 2D bridge deck model built, the integrated deck slab just offers bending stiffness and aids in load distribution/redistribution mimicking the behaviour of the real bridge structure. However, the reduction in stiffness of the T-girder after cracking is not accounted for in the 2D bridge deck model, which may influence the load distribution/redistribution in the integrated deck slab. This aspect requires further study.

When the bending moment obtained from the 2D bridge deck model built was compared with the results from the 3D linear bridge deck model [10]. It was inferred that the average variation of the bending moment of the T-beam 1 was 13.75% (end T-girder) refer to Table 4.6. Whereas the average bending moment variation from T-beam 8 (middle T-girder) was 10.45% refer to Table 4.7. The discrepancy between the models could be attributed to differences in load distribution effects in 2D and 3D Finite Element Models, with the 3D model offering better load distribution. Despite the limitations, the variation in bending moments is comparable to the 3D linear bridge deck model, making the 2D bridge deck model sufficient for studying load effects.
Notably, there will always be a discrepancy of around 10% with either 2D or 3D finite element models compared to the real bridge structure due to uncertainties like elastomeric bearing stiffness and unnoticed cracks causing non-linear load redistribution.

In the 2D non-linear individual girder model in the vertical plane, the non-linearity is introduced through the material properties. The developed 2D non-linear finite element model of the individual girders showed a good correlation with experimental results from disconnected T-beam tests with predicted ultimate failure loads generally within 10% of the experimental values, see Section 4.4.2. However, the deflection at the failure load varied significantly from both the 3D non-linear girder model and the experimental data. This discrepancy could be because solid elements and real structures deflect differently when compared to the 2D regular plane stress elements used.

The Quasi-Newton solution method proved more efficient, providing better convergence compared to the regular Newton-Raphson method, with fewer non-converged steps and more accurate

load-deflection behavior when compared to experimental results (see Section 4.4.1). This improvement is likely due to the Quasi-Newton method's ability to update stiffness based on previous converged steps. The load versus deflection curve obtained from the 2D non-linear individual girder model closely matched the load versus deflection curves of both the 3D non-linear girder model and the experimental data. This close alignment can be attributed to the precise non-linear material properties used which were obtained from the material investigation conducted on the Vecht bridge [10] and the accurate modeling of the varying cross-section of the individual girder.
To combine the 2D bridge deck model in the horizontal plane with the 2D non-linear individual girder model in the vertical plane, an equivalent loading technique was developed. This loading technique utilised numerically solving the shear force distribution/ moment distribution of the fully loaded girder in the 2D bridge deck model. It was observed that numerically solving the shear force distribution of the fully loaded girder to obtain the equivalent loading is more accurate as it is less sensitive to numerical errors (see Section 5.2.2). After applying this equivalent loading to the 2D non-linear individual girder model and comparing it with the fully loaded girder's shear force and bending moment distributions from the 2D bridge deck model. A huge discrepancies in support reactions were observed. The support reactions varied significantly ranging from 37.91% to 40.69% (see Table 5.1 and Table 5.2). This variation was due to additional downward forces exerted on the supports of fully loaded girder by adjacent girders via end crossbeams due to torsion when point loads are applied on the 2D bridge deck model in the horizontal plane. Hence, to obtain a more accurate equivalent loading technique for the 2D non-linear individual girder model, the end crossbeams were omitted in the 2D bridge deck model in the horizontal plane. Future research should consider incorporating the effect of end crossbeam to further refine the equivalent loading technique, ensuring it accurately reflects the system behaviour of prestressed girder bridges.

In developing the staggered 2D non-linear finite element approach, three methods were explored - effective loading with a piece-wise function, equivalent distributed loading technique without the presence of intermediate crossbeams and equivalent distributed loading technique with the presence of intermediate crossbeams. It was found that the effect of intermediate crossbeams significantly influenced the stiffness and load distribution/redistribution of the bridge deck. Also, incorporating the effect of intermediate crossbeams in the equivalent loading technique resulted in load versus deflection curves that closely matched the experimental data refer to Figure 5.43, since it replicated the behaviour of the real bridge structure. Moreover, the crack strains obtained from this approach closely resembled those observed in the experimental test reults (see Figure 5.40 and Figure 5.41).

The 2D Non-Linear Finite Element Approach incorporates simplifications to enhance computational efficiency, typically achieving run time of the non-linear analyses between 18 - 21 minutes. Despite these simplifications, the developed staggered 2D non-linear finite element approach accurately predicts the system behavior and capacity of prestressed concrete girder bridges. This makes it a practical tool for conducting preliminary assessments of bridge safety.

7
Conclusion and recommendation

This chapter summarises all the main findings of the research and recommendations for future research work.

7.1. Conclusion

The conclusions related to answering the research questions are summarised in three sections namely for modelling the 2D bridge model in the horizontal plane, modelling the non-linear individual girder model in the vertical plane, and connecting the 2D individual girder model with the 2D bridge deck model using a non-linear Finite Element Approach to assess the shear capacity of the existing prestressed T-girder bridge.

7.1.1. 2D FEM approach of bridge deck in horizontal plane

1. The bridge deck is modelled using orthotopic plate elements model due it's simplicity in attaining the combination of normal forces, shear forces and bending moments of the total (section 4.1.2).
2. The integrated deck slab is modelled using plate bending element. Whereas the T-girder and the crossbeams are modelled using class I - 3D beams by inputting their orthotopic geometric properties respectively. The geometric properties are calculated from their corresponding cross-section.
3. The material property of the concrete used is linear elastic material properties because all components are considered to be uncracked due to prestressing.
4. The mesh elements size was chosen to be 100 mm to avoid the formation of triangular elements while meshing which could cause local stress concentration.
5. The bending moment obtained from the 2D linear bridge deck model varied with the 3D linear bridge deck model with a range of 10.45% - 13.75%. This is sufficient to just study the load effects such as the distribution of loads to adjacent girders.

7.1.2. 2D FEM approach of single girder in vertical plane

1. The 2D girder model built in the vertical plane is modelled with non-linear material properties of concrete, reinforcement and prestressing.
2. For modelling of reinforcements, embedded reinforcements are for the mesh line not to coincide with the location of reinforcements.
3. The curved prestressing tendons are approximated as straight lines at 250 mm intervals.
4. The elastomeric bearing (supports) are modelled using the assumption of having linear support stiffness 475 N/mm^2. If accurate linear stiffness is applied for the supports, better results could be obtained.
5. For the solution method used in non-linear analysis of individual girder model, the Quasi-Newton with Broyden-Fletcher-Goldfarb-Shanno (BFSG) method along with line search algorithm gave more accurate load vs deflection curve to that of experimental test result than the regular newton raphson method used with the line search algorithm.

6. Also, the number of non-converging points satisfying either the energy norm or force norm was much lesser for the solution method Quai-Newton with BFSG.
7. The experimental test setups of disconnected beam tests were simulated in the 2D non-linear individual girder model developed and was compared the available 3D non-linear finite element model and the experimental test results. It was inferred that the ultimate failure load obtained from the 2D was more accurate than the load obtained from the 3D non-linear FEM model. However, the deflection from the 2D individual girder model were twice as high that of the experimental results. Whereas the deflection form the 3D non-linear FEM model was comparable to that of the experimental test results.

7.1.3. Correlating the individual girder model and the bridge deck model

1. The equivalent loading obtained using the shear force distribution of the fully loaded girder in the bridge deck model was more accurate than the one obtained using the moment distribution diagram since the error for double differentiation is proportional to second order ($O(\Delta x^2)$). In other words, the equivalent loading obtained from the shear force distribution is less sensitive to numerical errors.
2. Even though the shear force distribution and bending moment distribution obtained from the 2D non-linear individual girder model after applying the equivalent loading (obtained from shear force distribution of fully load girder in the bridge deck model) matched accurately with the shear force distribution and bending moment distribution of the bridge deck model. The support reactions varied by 40.69%. This was unusual since the support reaction forces, shear force distribution and bending moment distribution are correlated (section 5.2.2).
3. To check the discrepancy in the support reactions obtained from the 2D non-linear individual girder model and the 2D linear bridge deck model, an uniformly distributed surface load was applied to the whole bridge deck model. It was found that support reaction forces, shear force distribution and bending moment distribution from the individual bridge deck model accurately matched that of the 2D bridge deck model.
4. Also, the total support reaction from the 2D non-linear individual girder varied by only 6.58% from that of the 2D linear bridge deck model when an uniformly distributed surface load was applied as opposed to the application of point load replicating test setup 1 which yielded variation in the total support reaction by 40.69% between the individual girder model and the bridge deck model. It was concluded that the torsional moment from the adjacent girders to the fully loaded girder (when point load is applied) caused an additional downward force at the location of the supports in the 2D non-linear individual girder model. The torsional moment was transferred by the end crossbeam and this effect is not translated in the 2D individual girder model. Hence, the end crossbeam is removed to develop an accurate equivalent loading technique.
5. The equivalent loading applied using a piece-wise function that is as a line load 'q' of 33.3% of the failure load of the test setup 1 over the length of 600 mm. The load versus deflection curve obtained was very conservative (i.e.) the stiffness of the bridge deck model was underestimated and it was not comparable to that of the experimental test result.
6. For the next case, the equivalent distributed load is obtained from the shear force distribution of the fully loaded beam in the bridge deck model but without the presence of crossbeam. The load versus deflection curve obtained was more accurate than the one obtained from using the peice-wise function. However, the stiffness obtained is less because the presence of crossbeams offers more stiffness and facilitates better load distribution and redistribution.
7. The presence of intermediate crossbeams is included in obtaining the equivalent distributed loading from the shear force distribution of the fully loaded beam in the bridge deck model. It was inferred that the load versus deflection curve matched even better than the case without no cross-beam. Also, it was less conservative in terms of predicting the failure load (i.e.) the load factor used for obtaining the failure load of the combined behaviour of T-girders was about 2.6%. The 2D staggered non-linear finite element approach incorporating the presence of intermediate crossbeams predicted 96.5% of the ultimate failure load of the connected T-beam test [10].
8. Overall, the simplified non-linear finite element approach can be used to predict the strength capacity of existing prestressed concrete T-girder bridges. The 2D non-linear finite element

approach developed is also computationally less costly compared to the 3D non-linear finite element models used for predicting strength capacity.

7.2. Recommendations for future research

1. The 2D bridge deck model in the horizontal plane can be improved further by updating the stiffness of concrete where it's cracked to study the non-linear load redistribution effect which can used in obtaining the equivalent distributed loading that can be applied.
2. The effect of the end crossbeam is neglected in the 2D non-linear finite element model approach developed. This needs further study because the supports can withstand more load when the end crossbeams are present, as they induce an additional downward force at the location of the supports.
3. The 2D non-linear finite element approach should be tested on prestressed concrete girder bridges with different geometries and layouts to verify the validity of the newly developed non-linear finite element approach.

Bibliography

[1] S. Alampalli et al. "Bridge Load Testing: State-of-the-Practice". In: *Journal of Bridge Engineering* 26.3 (2021).

[2] American Association of State Highway and Transportation Officials (AASHTO). *AASHTO LRFD Bridge Design Specification for Highway Bridges*. 3rd. Washington, D.C.: American Association of State Highway and Transportation Officials, 2004.

[3] S. Amir. "Compressive membrane action in prestressed concrete deck slabs". PhD thesis. Delft University of Technology, 2014.

[4] J. Blaauwendraad. *Plates and FEM*. Springer Dordrecht, 2010.

[5] C. S. Cai, M. Shahawy, and R. J. Peterman. "Effect of Diaphragms on Load Distribution of Prestressed Concrete Bridges". In: *Transportation Research Record* 1814.1 (2002), pp. 47–54.

[6] E. Canestro. "Long-Term performance of a T-shaped girder bridges by using 1D, 2D and 3D FE modelling approaches-a comparative analysis". PhD thesis. University of Surrey, 2018.

[7] CEN. *NEN-EN1992-1-1 Eurocode 2: Design of Concrete Structures - Part 1-1: General Rules and Rules for Buildings*. European Committee for Standardization. 2011.

[8] DIANA. *Diana User's Manual – Release 10.3*. 2019. URL: `http://www.dianafea.com`.

[9] M. Engen et al. "Non-linear finite element analyses applicable for the design of large reinforced concrete structures". In: *European Journal of Environmental and Civil Engineering* 23 (Nov. 2019), pp. 1381–1403.

[10] S.W.H. Ensink. "System behaviour in prestressed concrete T-beam bridges". PhD thesis. Delft University of Technology, 2024.

[11] S.W.H. Ensink et al. "Full-size field test of prestressed concrete T-beam bridge". In: *Structural Faults Repair 2018 and European Bridge Conference 2018*. 2018.

[12] fib. *Model Code 2010*. CEB-FIP, 2012.

[13] M. Hendriks, A. de Boer, and B. Belletti. *Guidelines for Nonlinear Finite Element Analysis of Concrete Structures*. report RTD:1016-1:2017. Rijkswaterstaat Centre for Infrastructure, 2017.

[14] M. Hendriks and M. Roosen. *Guidelines for Nonlinear Finite Element Analysis of Concrete Structures*. report RTD:1016-1:2019. Rijkswaterstaat Centre for Infrastructure, 2019.

[15] E. Hughs and R. Idriss. "Live-load distribution factors for a prestressed concrete, spread box-girder bridge". In: *Journal of Bridge Engineering* 11.5 (2006), pp. 573–581.

[16] NNI. *Nederlands Normalisatie-Instituut*. 2020. URL: `https://www.nen.nl/`.

[17] NNI. *NEN 1009: Gewapend Betonvoorschriften GBV 1962*. 112 pp. Nederlands Normalisatie-Instituut, 1962.

[18] NNI. *NEN 8700: Assessment of Existing Structures in Case of Reconstruction and Disapproval - Basic Rules*. Nederlands Normalisatie-Instituut. 2011.

[19] M. Qaqish, E. Fadda, and E. Akawwi. "Design of T-beam bridge by finite element method and AASHTO specification". In: *KMITL Science Journal* 8.1 (2008), pp. 24–34.

[20] B. Richard et al. "Nonlinear finite element analysis of a 50 years old reinforced concrete trough bridge". In: *Engineering Structures* 32.12 (2010), pp. 3899–3910.

[21] Rijkswaterstaat. Beeldarchief rijkswaterstaat,beeldbank.rws.nl. 2020.

[22] Rijkswaterstaat. *Richtlijnen Beoordeling Kunstwerken (RBK)*. RTD 1006:2013, Rijkswaterstaat. 2013.

[23] E. D. Sotelino et al. *Simplified Load Distribution Factor for Use in LRFD Design*. Publication FHWA/IN/JTRP-2004/20. West Lafayette, Indiana: Joint Transportation Research Program, Indiana Department of Transportation and Purdue University, 2004.

[24] N. Suksawang, H. Nassif, and D. Su. "Verification of shear live-load distribution factor equations for I-girder bridges". In: *KSCE Journal of Civil Engineering* 17 (2013), pp. 550–555.

A

Geometrical properties of T-beam Vecht Bridge

The following formulas are used for calculating the sectional properties,

$$Momentofinertiainydirection : I_{\text{yy}} = I_{\text{yy(own)}} + y'^{2}.A \tag{A.1}$$

$$Momentofinertiainzdirection : I_{\text{zz}} = I_{\text{zz(own)}} + y'^{2}.A \tag{A.2}$$

$$Momentofinertiainyzdirection : I_{\text{yz}} = I_{\text{yz(own)}} + y'.Z'.A \tag{A.3}$$

$$Torsionalmomentofinertia : I_{\text{t}} = I_{\text{yy}} + I_{\text{t}} \tag{A.4}$$

Sectional properties of T-girder with integrated deck slab used for 2D FEM model of bridge deck in the horizontal plane

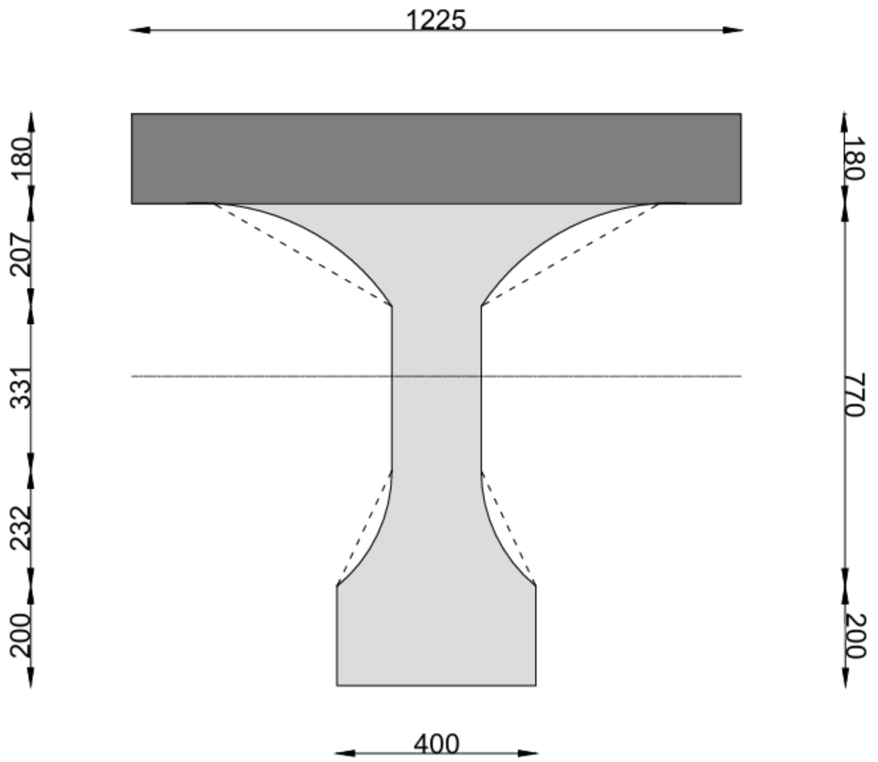

Figure A.1: T-beam with integrated deck slab

* The dotted lines represent the simplification of the cross-section of the T-girder used for calculating the sectional properties.
Cross-section area A = 506020 mm^2
Centroid y' = 432.388 mm
Centroid x' = 612.5 mm
Moment of Inertia I_y = 72468535181 mm^4
Moment of Inertia I_z = 43601894153 mm^4
Moment of Inertia I_{yz} = -1.6622e+10 mm^4
Torsional moment of inertia I^t = 1.1607e+11 mm^4

Sectional properties of End block with integrated deck slab used for 2D FEM model of bridge deck in the horizontal plane

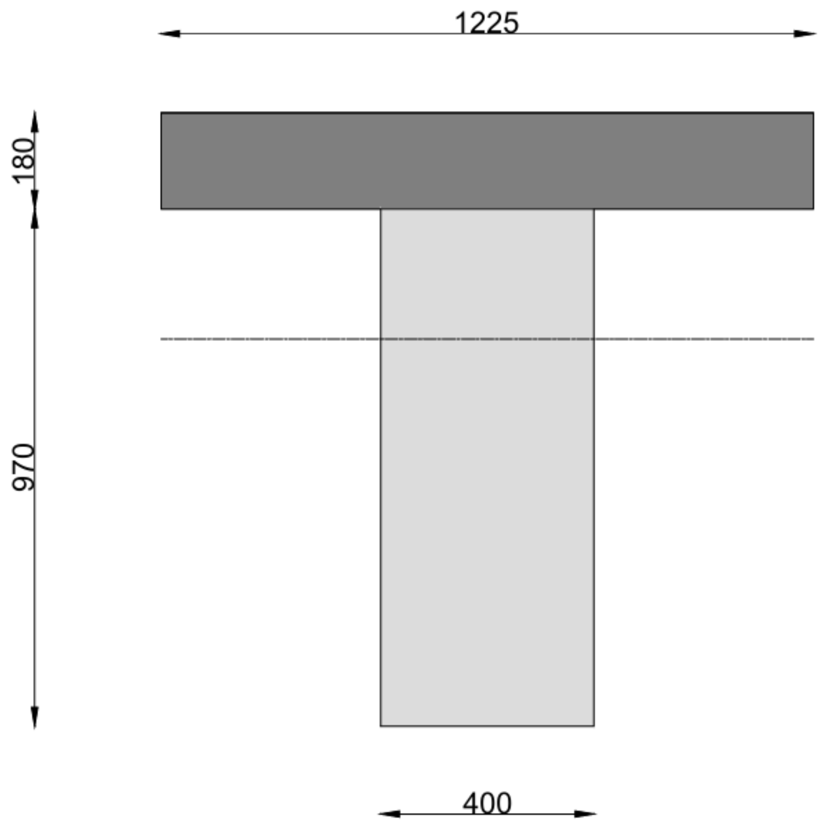

Figure A.2: End block with integrated deck slab

Cross-section area A = 608500 mm^2
Centroid y' = 424.0263 mm
Centroid x' = 612.5 mm
Moment of Inertia I_y = 78150265297 mm^4
Moment of Inertia I_z = 32747317708 mm^4
Moment of Inertia I_{yz} = 0 mm^4
Torsional moment of inertia I^t = 1.10898e+11 mm^4

Sectional properties at the location of intermediate cross-beam with integrated deck slab used for 2D FEM model of bridge deck in the horizontal plane

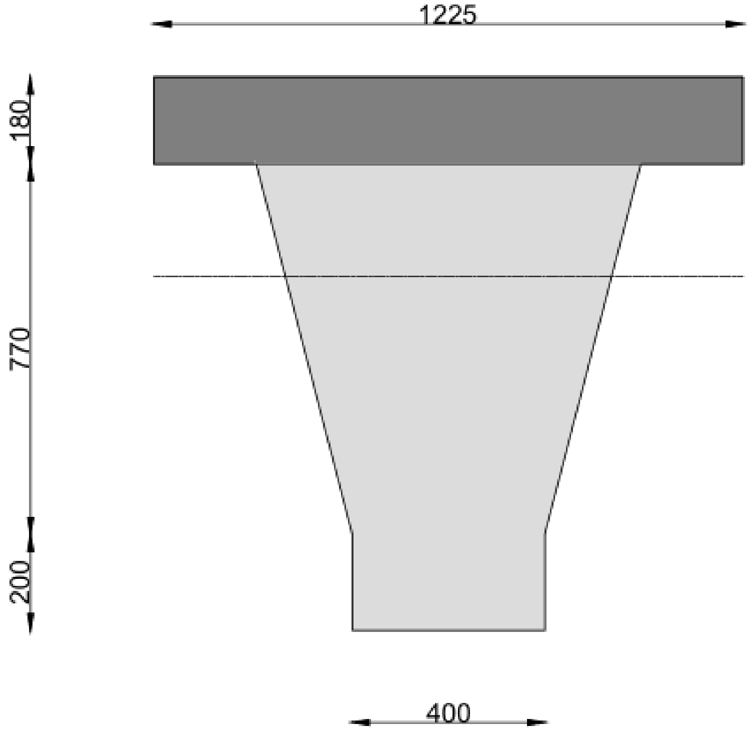

Figure A.3: Location of intermediate cross-beam with integrated deck slab

Cross-section area A = 762500 mm^2 Centroid y' = 413.6196 mm
Centroid x' = 612.5 mm
Moment of Inertia I_y = 83962179640 mm^4
Moment of Inertia I_z = 42714539931 mm^4
Moment of Inertia I_{yz} = 658777777.8 mm^4
Torsional moment of inertia I_t = 1.26677e+11 mm^4

B

Maple script used for solving tendon profile

The boundary conditions used for solving the third degree polynomial equation in Maple for the seven tendons are presented below,

For tendon 1,

```
> Y1 := A1·x^3 + B1·x^2 + C1·x + D1;
```

$$Y1 := A1x^3 + B1x^2 + C1x + D1$$

```
> gamma1 := diff(Y1, x);
```

$$\gamma 1 := 3A1x^2 + 2B1x + C1$$

```
> x := 0 : eq1 := Y1 = 340 :
> x := 8350 : eq2 := Y1 = 80 :
> x := 12350 : eq3 := gamma1 = 0 : eq4 := Y1 = 70 :
> sol := solve({eq1, eq2, eq3, eq4}, {A1, B1, C1, D1}); assign(sol);
```

$$sol := \left\{A1 = -\frac{111791}{815080240000000}, B1 = \frac{42041177}{8150802400000}, C1 = -\frac{85327577}{1319968000}, D1 = 340\right\}$$

```
>
> evalf(A1);
```

$$-1.371533679 \times 10^{-10}$$

```
> evalf(B1);
```

$$5.157918808 \times 10^{-6}$$

```
> evalf(C1);
```

$$-0.06464367091$$

Figure B.1: Boundary conditions used for solving tendon 1 profile

For tendon 2,

```
> Y2 := A2·x^3 + B2·x^2 + C2·x + D2;
```

$$Y2 := A2x^3 + B2x^2 + C2x + D2$$

```
> gamma2 := diff(Y2, x);
```

$$\gamma 2 := 3A2x^2 + 2B2x + C2$$

```
> x := 0 : eq5 := Y2 = 510 :
> x := 8350 : eq6 := Y2 = 110 :
> x := 12350 : eq7 := gamma2 = 0 : eq8 := Y2 = 70 :
> sol2 := solve({eq5, eq6, eq7, eq8}, {A2, B2, C2, D2}); assign(sol2);
```

$$sol2 := \left\{A2 = -\frac{9391}{203770060000000}, B2 = \frac{8197977}{2037700600000}, C2 = -\frac{25833177}{329992000}, D2 = 510\right\}$$

```
>
> evalf(A2);
```

$$-4.608626017 \times 10^{-11}$$

```
> evalf(B2);
```

$$4.023150899 \times 10^{-6}$$

```
> evalf(C2);
```

$$-0.07828425235$$

Figure B.2: Boundary conditions used for solving tendon 2 profile

For tendon 3,

```
> Y3 := A3·x^3 + B3·x^2 + C3·x + D3;
```

$$Y3 := A3x^3 + B3x^2 + C3x + D3$$

```
> gamma3 := diff(Y3, x);
```

$$\gamma 3 := 3\,A3x^2 + 2\,B3x + C3$$

```
> x := 0 : eq9 := Y3 = 170 :
> x := 8350 : eq10 := Y3 = 80 :
> x := 12350 : eq11 := gamma3 = 0 : eq12 := Y3 = 70 :
> sol3 := solve({eq9, eq10, eq11, eq12}, {A3, B3, C3, D3}); assign(sol3);
```

$$sol3 := \left\{A3 = -\frac{2991}{815080240000000}, B3 = \frac{6082777}{8150802400000}, C3 = -\frac{22114777}{1319968000}, D3 = 170\right\}$$

```
> evalf(A3);
```

$$-3.669577366 \times 10^{-12}$$

```
> evalf(B3);
```

$$7.462795319 \times 10^{-7}$$

```
> evalf(C3);
```

$$-0.01675402510$$

Figure B.3: Boundary conditions used for solving tendon 3 profile

For tendon 4,

```
> Y4 := A4·x^3 + B4·x^2 + C4·x + D4;
```

$$Y4 := A4x^3 + B4x^2 + C4x + D4$$

```
> gamma4 := diff(Y4, x);
```

$$\gamma 4 := 3\,A4x^2 + 2\,B4x + C4$$

```
> x := 0 : eq13 := Y4 = 850 :
> x := 8350 : eq14 := Y4 = 200 :
> x := 12350 : eq15 := gamma4 = 0 : eq16 := Y4 = 170 :
> sol4 := solve({eq13, eq14, eq15, eq16}, {A4, B4, C4, D4}); assign(sol4);
```

$$sol4 := \left\{A4 = -\frac{252173}{815080240000000}, B4 = \frac{98625931}{8150802400000}, C4 = -\frac{207643531}{1319968000}, D4 = 850\right\}$$

```
> evalf(A4);
```

$$-3.093842638 \times 10^{-10}$$

```
> evalf(B4);
```

$$0.00001210014992$$

```
> evalf(C4);
```

$$-0.1573095189$$

Figure B.4: Boundary conditions used for solving tendon 4 profile

For tendon 5,

```
> Y5 := A5·x^3 + B5·x^2 + C5·x + D5;
```

$$Y5 := A5x^3 + B5x^2 + C5x + D5$$

```
> gamma5 := diff(Y5, x);
```

$$\gamma 5 := 3\,A5x^2 + 2\,B5x + C5$$

```
> x := 0 : eq17 := Y5 = 1020 :
> x := 8350 : eq18 := Y5 = 250 :
> x := 12350 : eq19 := gamma5 = 0 : eq20 := Y5 = 170 :
> sol5 := solve({eq17, eq18, eq19, eq20}, {A5, B5, C5, D5}); assign(sol5);
```

$$sol5 := \left\{A5 = -\frac{6991}{101885030000000}, B5 = \frac{7404777}{1018850300000}, C5 = -\frac{24438777}{164996000}, D5 = 1020\right\}$$

```
> evalf(A5);
```

$$-6.861655731 \times 10^{-11}$$

```
> evalf(B5);
```

$$7.267777219 \times 10^{-6}$$

```
> evalf(C5);
```

$$-0.1481173907$$

Figure B.5: Boundary conditions used for solving tendon 5 profile

For tendon 6,

```
> Y6 := A6·x^3 + B6·x^2 + C6·x + D6;
```

$$Y6 := A6x^3 + B6x^2 + C6x + D6$$

```
> gamma6 := diff(Y6, x);
```

$$\gamma6 := 3A6x^2 + 2B6x + C6$$

```
> x := 0 : eq21 := Y6 = 680 :
> x := 8350 : eq22 := Y6 = 200 :
> x := 12350 : eq23 := gamma6 = 0 : eq24 := Y6 = 170 :
> sol6 := solve({eq21, eq22, eq23, eq24}, {A6, B6, C6, D6}); assign(sol6);
```

$$sol6 := \left\{A6 = -\frac{143373}{815080240000000}, B6 = \frac{62667531}{8150802400000}, C6 = -\frac{144430731}{1319968000}, D6 = 680\right\}$$

```
>
> evalf(A6);
```

$$-1.759004733 \times 10^{-10}$$

```
> evalf(B6);
```

$$7.688510643 \times 10^{-6}$$

```
> evalf(C6);
```

$$-0.1094198731$$

Figure B.6: Boundary conditions used for solving tendon 6 profile

For tendon 7,

```
> Y7 := A7·x^3 + B7·x^2 + C7·x + D7;
```

$$Y7 := A7x^3 + B7x^2 + C7x + D7$$

```
> gamma7 := diff(Y7, x);
```

$$\gamma7 := 3A7x^2 + 2B7x + C7$$

```
> x := 1902 : eq25 := Y7 = 1150 :
> x := 8350 : eq26 := Y7 = 350 :
> x := 12350 : eq27 := gamma7 = 0 : eq28 := Y7 = 270 :
> sol7 := solve({eq25, eq26, eq27, eq28}, {A7, B7, C7, D7}); assign(sol7);
```

$$sol7 := \left\{A7 = -\frac{261091}{549897046400000}, B7 = \frac{5689271391}{274948523200000}, C7 = -\frac{124294808133}{422997728000}, D7 = \frac{13851482591113}{8459954560}\right\}$$

```
>
> evalf(A7);
```

$$-4.747997861 \times 10^{-10}$$

```
> evalf(B7);
```

$$0.00002069213293$$

```
> evalf(C7);
```

$$-0.2938427323$$

```
> evalf(D7);
```

$$1637.299881$$

Figure B.7: Boundary conditions used for solving tendon 7 profile